Development of a First-principle Model of a Semi-batch Rhodium Dissolution Process

Norbertin Nkoghe Eyeghe

August 24, 2017

Development of a First-principle Model of a Semi-batch Rhodium Dissolution Process

by

Norbertin Nkoghe Eyeghe

A dissertation submitted in partial fulfillment
of the requirements for the degree

Master of Science (Applied Science Control)

in the

Department of Chemical Engineering
Faculty of Engineering, the Built Environment and Information Technology

University of Pretoria
Pretoria

August 2017

Abstract

First-principle modelling of chemical processes and their unit operations has been of great interest in the chemical process, as well as the control and allied industries over the past decades. This is because it offers the opportunity to develop virtual representations (models) of real process systems, which can be used to describe and predict the dynamic behaviour of those systems. These models are based on the fundamentals of the transport phenomena of fluid dynamics (involving momentum transfer), mass transfer, and energy transfer of the systems they describe.

A first-principle model of a semi-batch rhodium dissolution chemical process has been developed. It describes the dynamic behaviour of two exothermic reactions, occurring simultaneously in a semi-batch process. The dissolution of 29 kg of solid crude rhodium sponge (Rh) into 546 L of a solution of hydrochloric acid ($HCl_{(aq)}$), to produce a solution of aqueous rhodium(III) chloride ($RhCl_3.H_2O$), as well as the reaction of chlorine ($Cl_{2(aq)}$) with water ($H_2O_{(l)}$) to produce some more $HCl_{(aq)}$ in the reactor. The model was formulated as a system of explicit ordinary differential equations (ODEs), which demonstrated some good and stable qualitative tracking of the temperature and pressure data of the real reactor. The molar responses of all chemical species, as well as the heats of reactions, showed to be consistent with the description of the process, and no negative values of those variables were generated.

Estimates of the key parameters of heat and mass transfer coefficients, arrhenius constants, and activation energies of reactions were assumed and tuned to satisfaction by trial-and-error, but not optimised. This is because during simulations, the numerical solver would often fail to integrate the equations, due to the appearance of large derivatives in some model equations whenever those parameters varied, thereby stopping simulations.

Finally, the model was validated with a set of data from 45 batches. For all simulations done, the simulated temperature responses showed better prediction of data than the simulated pressure responses did, with an average percentage accuracy of 80% against 60 percent, respectively.

KEYWORDS: Rhodium dissolution, first-principle modelling, ODE formulation, model validation, stability, numerical accuracy.

Acknowledgements

I would like to acknowledge the various contributions of all those who have made this work possible.

I dearly thank my parents for their constant support and encouragement during this project and over the years. They have been my pillars of strength throughout my studies.

I would like to express my feelings of gratitude to my research supervisor, Mr. Carl Sandrock, for his insightful guidance, teaching, and availability during the project. I feel privileged to have been involved in this project as I have learned a lot from it and gained some invaluable analytical and computer programming skills.

I extend my feelings of appreciation to my colleagues: Mr. Rotimi Agbebi, for his assistance and the fruitful discussions that we have had over the project; and Mr. Carel van Dam, for his initial work of writing a model, describing a ruthenium dissolution process, which I had inherited from.

I would also like to thank Mr. Chris Steyn and Dr. Kevin Brooks for their helpful suggestions and assistance during the various meetings we have had, as well as Mr. Hermanus du Preez for helping collect critical data that was necessary for this work.

Last but not least, I would further like to thank Anglo American Platinum and BluESP (Pty) Ltd for funding the project, with the help of the Technology and Human Resources for Industry Programme (THRIP) initiative of the National Research Foundation (NRF).

Declaration of Authorship

I the undersigned, Norbertin Nkoghe Eyeghe, declare that this dissertation on the development of a first-principle model of a semi-batch rhodium dissolution process, presented in this report:

- Is the product of my own work, which started from an initial version of a mathematical model that I inherited from Mr Carel van Dam. I rewrote and further developed it in order to achieve the objectives of this project.
- Has never been submitted by myself, or anyone else, to any other university for the purpose of obtaining a degree, diploma or any other qualification.

Signed: _____

Date: August 24, 2017

Contents

List of Figures

List of Tables

Nomenclature

Abbreviations

ODE	Ordinary differential equations
FPM	First-principle model
PMR	Precious metal refinery

Chemical Species

Rh	Rhodium
Cl_2	Chlorine
H_2O	Water
HCl	Hydrochloric acid
$RhCl_3.H_2O$	Aqueous Rhodium tri-chloride

Subscripts

(s)	Solid phase
$(l-g)$	Liquid to gas
$(g-l)$	Gas to liquid
$(g-g)$	Gas to gas

(aq)	Aqueous solution
(l)	Liquid phase
(g)	Gaseous phase
CW	Cooling water
$Steam$	Steam
hx	Jacket
rx	Reactor
$(l-l)$	Liquid to liquid

Superscripts

In	Inlet
Out	Outlet
tot	Total

Greek

ρ	Molar density $(kmol/m^3)$

Constants

A	Area (m^2)
g	Gravitational acceleration (m/s^2)
h	Height of fluid in vessel (m)
R	Universal gas constant $(J/(kmol.K))$
r_{rx}	Inside radius of reactor (m)
w_{rx}	Thickness of reactor wall (m)
T_{ref}	Reference temperature (K)

V	Volume (m^3)

Parameters

E_{a_1}	Activation energy of dissolution reaction $(J/kmol)$
E_{a_2}	Activation energy of vaporization reaction $(J/kmol)$
k	Mass transfer coefficient
k_1	Arrhenius law frequency factor of dissolution reaction 1 (min^{-1})
k_2	Arrhenius law frequency factor of reaction 2 (min^{-1})
U	Overall heat transfer coefficient $(W/(m^2.K))$

Physical Properties

C_p	Specific heat capacity at constant pressure $(J/(kmol.K))$
H_v	Heat of vaporization $(J/kmol)$
M	Molar mass $(kg/kmol)$
P^{vap}	Vapor pressure (kPa)

Input Variables

$F_{Cl_{2(g)}}$	Flow rate of chlorine gas $(kmol/min)$
F_{CW}	Cooling water flow rate $(kmol/min)$
F_{Steam}	Steam flow rate $(kmol/min)$
F	Flow rate of chemical species solution $(kmol/min)$
F^{In}_{utility}	Flow rate of utility at inlet $(kmol/min)$
T^{In}_{utility}	Temperature of utility at inlet (K)

State Variables

N	Moles $(kmol)$

$T_{J_{(g)}}$	Temperature of gas in jacket (K)
$T_{J_{(l)}}$	Temperature of solution in Jacket (K)
$T_{rx_{(g)}}$	Temperature of gas in reactor (K)
$T_{rx_{(l)}}$	Temperature of solution in reactor (K)

Algebraic Variables

C	Molar concentration $(kmol/m^3)$
P	Pressure (kPa)
r_1	Rate of dissolution reaction 1 $(kmol/(m^3.min))$
r_2	Rate of reaction 2 $(kmol/(m^3.min))$
$V_{rx_{(l)}}$	Volume of solution inside reactor compartment (m^3)
H_{rx}	Heat transfered between jacket and reactor compartment $(J/kmol)$
$F_{H2O_{(l-g)}}$	Flow rate of vaporized water $(kmol/min)$
$F_{Cl_{2(l-g)}}$	Flow rate of chlorine gas dissolved into solution $(kmol/min)$
k_{r1}	Arrhenius rate constant of dissolution reaction (min^{-1})
k_{r2}	Arrhenius rate constant of vaporization reaction (min^{-1})
m	Mass, (kg)
N_{rx}^{tot}	Total moles in reactor compartment, $(kmol)$
N_{hx}^{tot}	Total moles in jacket compartment, $(kmol)$

Chapter 1

Introduction

This chapter presents the scope of the project. It gives the major motivations of the project in the form of its problem statement, then elaborates on the study objectives, and finally provides the outline of upcoming chapters of the dissertation compiled in this report.

Model development has generated major interest over recent years in the chemical process, petroleum and allied industries, as well as academic institutions. Activities in research and development cannot always experiment with new techniques or studies directly on real processes. This is because there are various constraints to be taken into account ranging from process operations, safety and environmental concerns, and ultimately financial implications. Models of real operating units and processes have shown to be a viable alternative in many ways.

This study is concerned with the development of a mathematical first-principle model (FPM), describing the dynamic behaviour of two chemical processes taking place in a semi-batch reactor. The process involves two simultaneous exothermic reactions: the dissolution of crude rhodium sponge ($Rh_{(s)}$) into an aqueous solution of hydrochloric acid (HCl), to produce a solution of aqueous rhodium(III) chloride ($RhCl_3.H_2O$), and the reaction of aqueous chlorine (Cl_2) with water (H_2O) to produce some more $HCl_{(aq)}$ in the reactor solution. The rhodium semi-batch reactor modelled is one of several reactors from the precious metal refinery (PMR) plant of Anglo Platinum.

1.1 Problem Statement

This project was motivated by the need for a virtual semi-batch reactor platform that could be used to conduct off-line experimentations and process control related studies, from which useful insight could be gained on the dynamic behaviour of the process.

Plant operators and engineers cannot always conduct dynamic testing on plant reactors, without taking the risk of destabilising the process, which in turn could affect the quality of products, with serious financial consequences. For this reason, it was required to develop a mathematical first-principle model of one of the existing batch reactors at the PMR plant. The semi-batch reactor operating the rhodium dissolution process was chosen as the prototype in this project.

1.2 Objectives

Given the problem statement as formulated above, this project was subject to the following main objectives:

- To develop a mathematical first-principle model (FPM) of a rhodium dissolution process, operated in a semi-batch reactor; and

- To assess the model performance by validating its pressure and temperature responses. This is achieved by determining how well they compare to their corresponding plant data sets that were made available to us.

1.3 Report Outline

The work conducted and compiled in this dissertation is presented in six chapters, detailing some background on the key aspects of the project, the method followed to develop the model, the major results obtained, and finally, the main conclusions drawn and recommendations made going forward.

The remaining chapters of this dissertation are presented as described below:

Chapter 2 covers a theoretical background of the key aspects of the project. It gives selected information on rhodium (Rh) and the platinum group metals (PGMs), as well as the concept of model development and the various types of models, the mathematical modelling of an ideal batch reactor, the numerical implementation and validation of mathematical models.

This chapter also presents a selective litterature review of some available recent works that have been conducted on first-principle modelling of batch and semi-batch reactors. Because litterature covers very little work on mathematical modelling of chemical processes of platinum group metals (PGMs), this section seeks to clearly emphasise that the method used for first-principle modelling of batch or semi-batch reactors is essentially the same for any chemical process operated in those reactors. This is achieved by capturing the dynamics of reactions kinetics, mass and energy of the system studied.

Chapter 3 presents the description of the process, along with the equations of the chemical reactions taking place in the semi-batch reactor system. It gives the method used to develop the first-principle model of the rhodium reactor. This is a detailed account of all steps followed in modelling the reactor, to which, the chapter gives some background of the initial version of the model which the candidate presenting this dissertation had enherited from. This is done in order to clarify the contribution that has been made to further improve the model to the final version presented in this work. The chapter further elaborates on the description of the new model by giving the key assumptions made in the reactor system, the model equations developed and the numerical integration method (solver) used to integrate those equations. In addition to that, the chapter also gives the limitations encountered in

modelling the reactor, the method used to verify the accuracy, and stability of the model and its validation.

Chapter 4 covers the results obtained from the various simulation runs of the model developed, along with their discussion. It presents two examples of some of the good simulation responses of the model, which compared well with the data sets of two batches of the real reactor runs at the plant. Though good model simulation responses were obtained, the chapter also gives an example of a poor simulation run that was obtained.

Chapter 5 draws the main conclusions of our study in terms of what was achieved according to the main objectives of the project given in Chapter 1, and the insight gained from the difficulties experienced in the mathematical formulation of the model, the numerical accuracy and stability of simulations. The chapter also presents the recommendations on this work. They are suggestions made on possible further work that could be done to improve on that which is presented in this report.

Chapter 2

Theoretical Background

This chapter covers a selected theoretical background on the key aspects of this work:

- The platinum-group metals (PGMs), their sources and common applications, followed by their extraction and selective refining.
- The concept of mathematical model development, their applications to processes occuring in batch reactors, as well as their numerical implementations and validation.

The chapter also presents a selective literature review of some recent works that have been conducted on the development of mathematical first-principle models of various chemical processes, that have occured in systems of batch and semi-batch reactors. Because literature covers very little work on the modelling of chemical processes of platinum group metals (PGMs), this review seeks to emphasise the fact that the method of capturing, from first-principle, the dynamics of reactions kinetics, as well as those of the transport phenomena of mass and energy of chemical processes, operated in batch and semi-batch reactors is essentially the same as that of any other chemical semi-batch processes, including those of PGMs.

Lastly, the chapter presents some background on the process of dissolution of gases in aqueous solutions, which has been critical in the reaction processes discussed in this work.

2.1 Platinum-Group Metals

The platinum-group metals (PGMs) consist of six exceptionally rare metal elements in the Earth's crust: platinum (Pt), palladium (Pd), rhodium (Rh), iridium (Ir), osmium (Os) and ruthenium (Ru). They often occur together in the same mineral deposits of nickel and copper and are known to share many of the same characteristics, with very similar chemical properties (Burke 1990, Crundwell et al. 2011b, Johnson Matthey 2015). Those metals are highly durable and often recycled due to their high value. Platinum and palladium are soft, malleable and ductile. They resist oxidation and high temperature corrosion. Rhodium and iridium are harder and more difficult to work with. Ruthenium and osmium are hard, brittle and have poor resistance to oxidation (International Platinum Group Metals Association 2015, Bell 2015, Kirk-Othmer 2008).

2.1.1 Sources of PGMs

Ore deposits of PGMs are scarce, they occur either as sulfides or are associated with the sulfides of copper and nickel. The ore that is mined is extremely low-grade and contains about 3 g/tonne to 10 g/tonne (0.0003-0.001%) of PGMs (Crundwell et al. 2011b). The usefulness of the metals due to their wide range of applications, along with exceptional physical and chemical characteristics, have earned them the name of precious metals. To this day, the major sources of PGMs have been found in the Bushveld Igneous Complex, covering the Transvaal Basin in South Africa. It hosts about 95 % of the world's reserves (U.S. Geological Survey 2015, Mudd 2010).

2.1.2 Applications of PGMs

PGMs have been applied in a wide variety of industries, where they have been used as catalysts to improve the efficiency of various reactions. They have also been combined with other metals to form metallic alloys of improved properties, used in the production of fuel cells as well as in the manufacturing of jewellery, amongst other uses.

2.2 Extraction of PGMs

Virtually all of the production of PGMs is from sulphide ores, which contain an average of 0.0004 % of platinum-group elements (PGEs), Crundwell et al. 2011b. The process of extracting PGEs from their copper/nickel sulphides ore, in order to produce the metals in their pure form can be divided into three majors steps,

as discussed by Crundwell et al. 2011a, Crundwell et al. 2011b, Crundwell et al. 2011c, Crundwell et al. 2011d and Gouldsmith et al. 1963:

The dry and wet treatments of the ore, by froth flotation, to produce a bulk sulphide concentrate that is rich in PGEs (0.01 to 0.02 %); the smelting and converting of the PGEs rich sulphide concentrate to produce the converter matte, with an even richer concentration of PGEs (0.2 to 0.4 %); and the refining of the PGEs from the converter matte by a series of hydrometallurgical techniques to produce the individual metals (PGMs), to a purity greater than 99.9 %. Figure 2.1 gives a generalized flowsheet of the major steps in the PGMs extraction process.

2.2.1 Dry and Wet Treatments of Ore

This is the first step of the process; the copper/nickel sulphide ore is mined and treated through some dry and wet processes, in which the ore is crushed, grinded, then passed into a froth flotation cell to produce a bulk sulphide concentrate of PGEs (0.01 to 0.02 %) and various base metals (Ni, Co, Cu and Fe). This accounts for the preliminary step that is often carried out in order to concentrate the PGMs as much as possible.

2.2.2 Smelting and Converting

In this step of the extraction process, the sulphide concentrate is then smelted (heated beyond melting points of the metals) and converted into a molten converter matte, rich in PGEs (0.2 to 0.4 %), containing some base metals impurities (metallic sulphides of Fe, Cu, Co and Ni). The produced molten converter matte is further processed by removing, as a slag, all unwanted metallic impurities (gangue materials), in order to obtain an insoluble concentrate or residue of PGMs alone. This additional upgrade of PGMs can be achieved through two process routes, as discussed by Crundwell et al. 2011a:

- Slow-cooling of molten converter matte, followed by magnetic separation to produce the PGMs concentrate; and
- Whole leaching of converter matte.

Figure 2.2 gives a generalized flowsheet of the PGMs separation process, involving the slow-cooled and magnetic concentration process (Crundwell et al. 2011a).

The slow-cooling and magnetic concentration process for separating PGMs from base metals is only used by Anglo American Platinum's refinery in Rustenburg (South Africa), which is the world's largest producer of PGMs (Crundwell

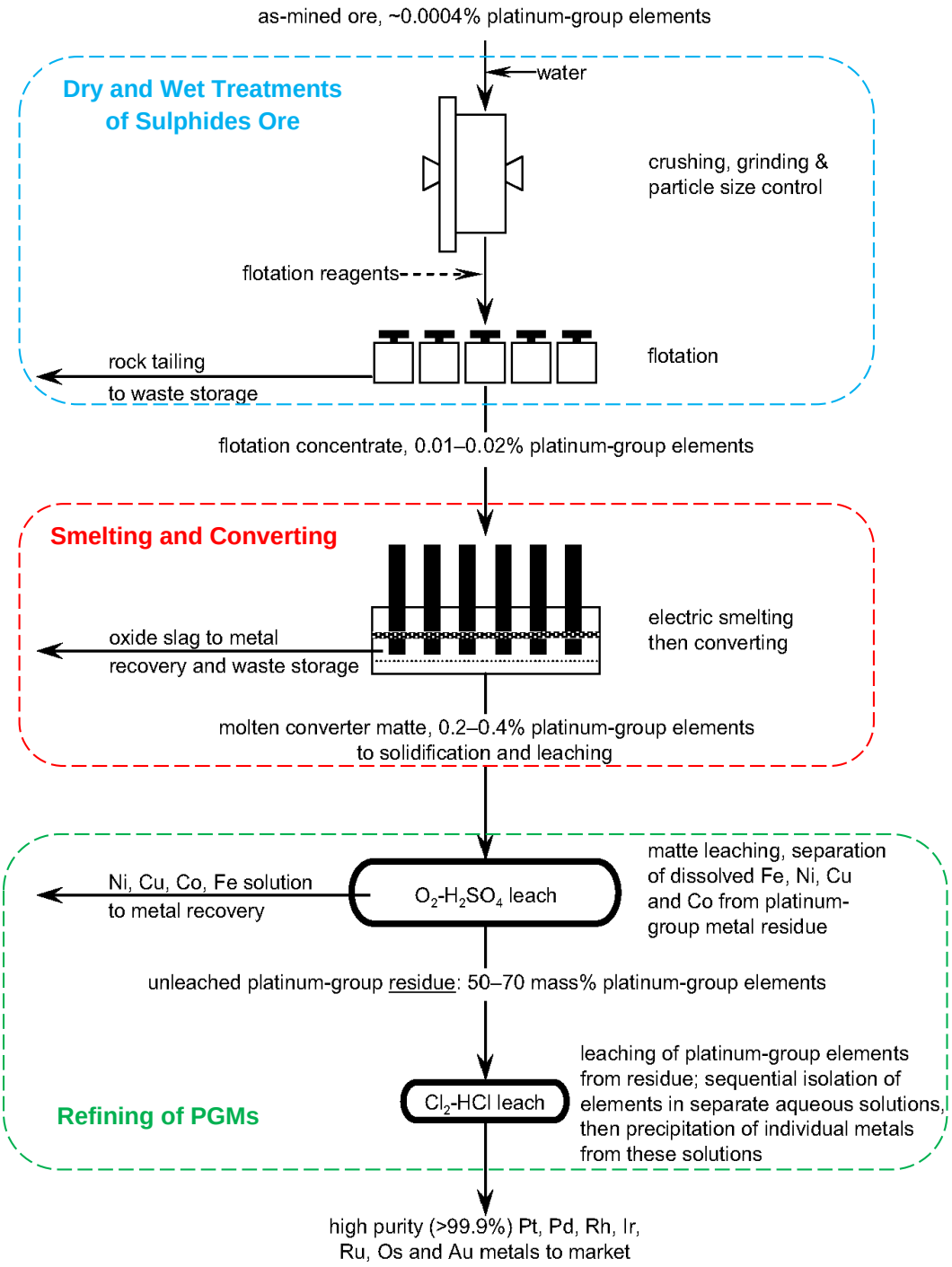

Figure 2.1: Generalized PGMs Extraction Flowsheet (Crundwell et al. 2011c)

et al. 2011a). In this process, molten converter matte is allowed to cool over several days, such that crystals of copper and nickel sulfides (Ni_3S_2, Cu_2S), as well

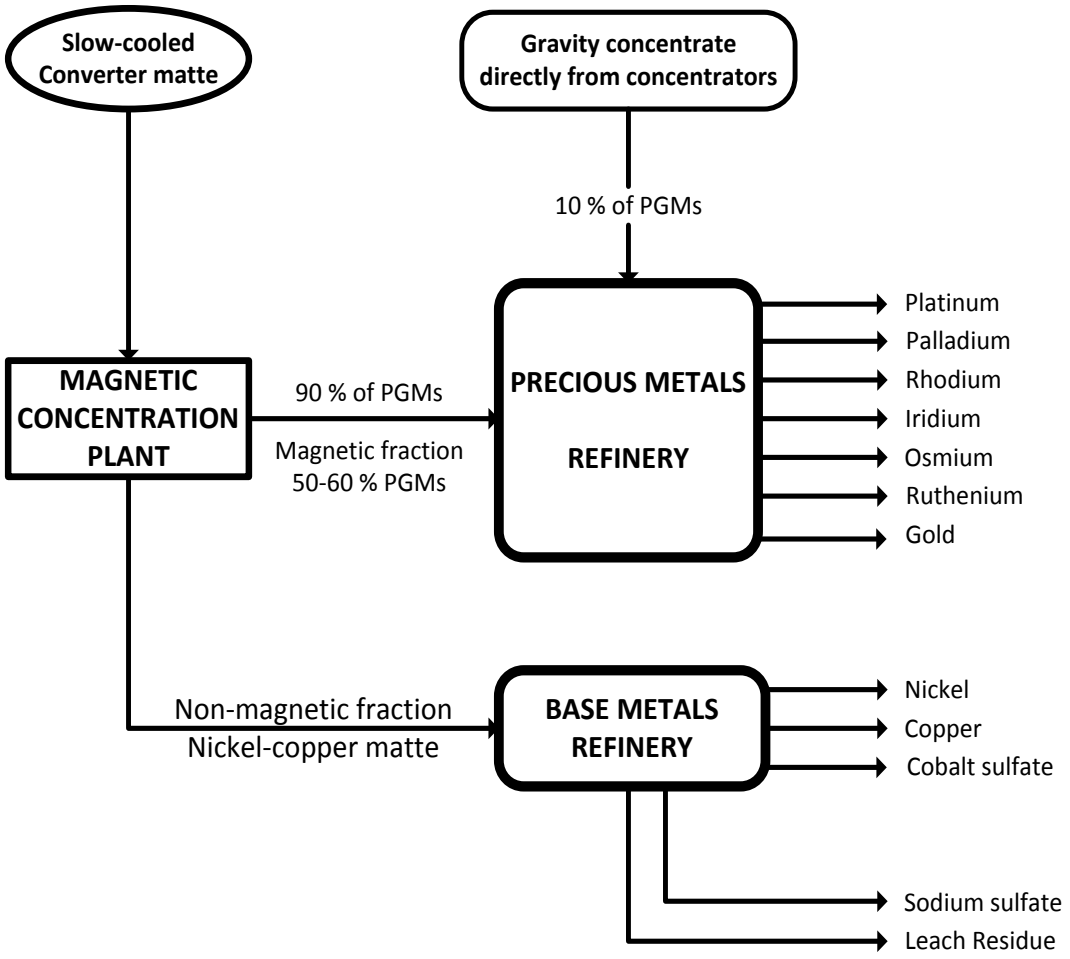

Figure 2.2: Slow-cooled and magnetic concentration process

as metal alloys can develop. Because the PGMs content of the matte concentrate is in the alloy phase, the alloys can easily be separated from the metallic sulfides to be further processed and purified at the precious metals refinery (PMR). The remaining major producers of PGMs use the whole matte leaching process.

2.2.3 Refining of PGMs Concentrate

This is the final major step of the PGMs extraction process, it takes place at the PMR. This process is described by Crundwell et al. 2011d and Crundwell et al. 2011c. At this point, separation of PGMs is achieved by sequential isolation of the metallic elements, whereby the concentrated PGMs residue is dissolved in a solution of Aqua regia, made up of strong concentrated nitric and hydrochloric acids (Moore 1911). The solution produced (the leach) containing dissolved metals of Pt, Pd, Au and the insoluble residue of Ru, Rh, Ir and Os, is further treated and

purified to concentrations greater than 99.9 %. This is done through a combination of various hydro-metallurgical techniques from precipitation, solvent extraction, ion-exchange, vaporisation or distillation and reduction.

Rhodium Refining

The complete cycle of treatment is complex and can only be briefly outlined. The separation and refining of rhodium is achieved by dissolving the PGMs concentrate, obtained from the slow-cooling and magnetic separation of the converter matte in either a solution of aqua regia or hydrochloric acid, in the presence of chlorine gas. The dissolved metals form stable complexes with chloride ions in solution (leach). The leach contains the larger quantity of platinum, palladium and traces of gold, as well as a residue of the more insoluble metals of iridium, rhodium, osmium and ruthenium. The full process involves successive stages of dissolution and precipitation of rhodium as complex aqueous salts, as well as filtration. This is followed by reduction and calcination, done under carefully controlled conditions, in electrically heated furnaces, to produce pure rhodium sponges or powders suitable for melting and further processing (Crundwell et al. 2011d, Gouldsmith et al. 1963).

Selective extraction of the remaining PGMs is achieved similarly, and all taking place in either batch or semi-batch reactors. Figure 2.3 on page 12 shows an example of the complete flow diagram of the refining process (Ssennis 2014), where the six PGMs are produced in their final form, as sponges or powders to a purity of about 99.9 % to 99.99 % (Crundwell et al. 2011d).

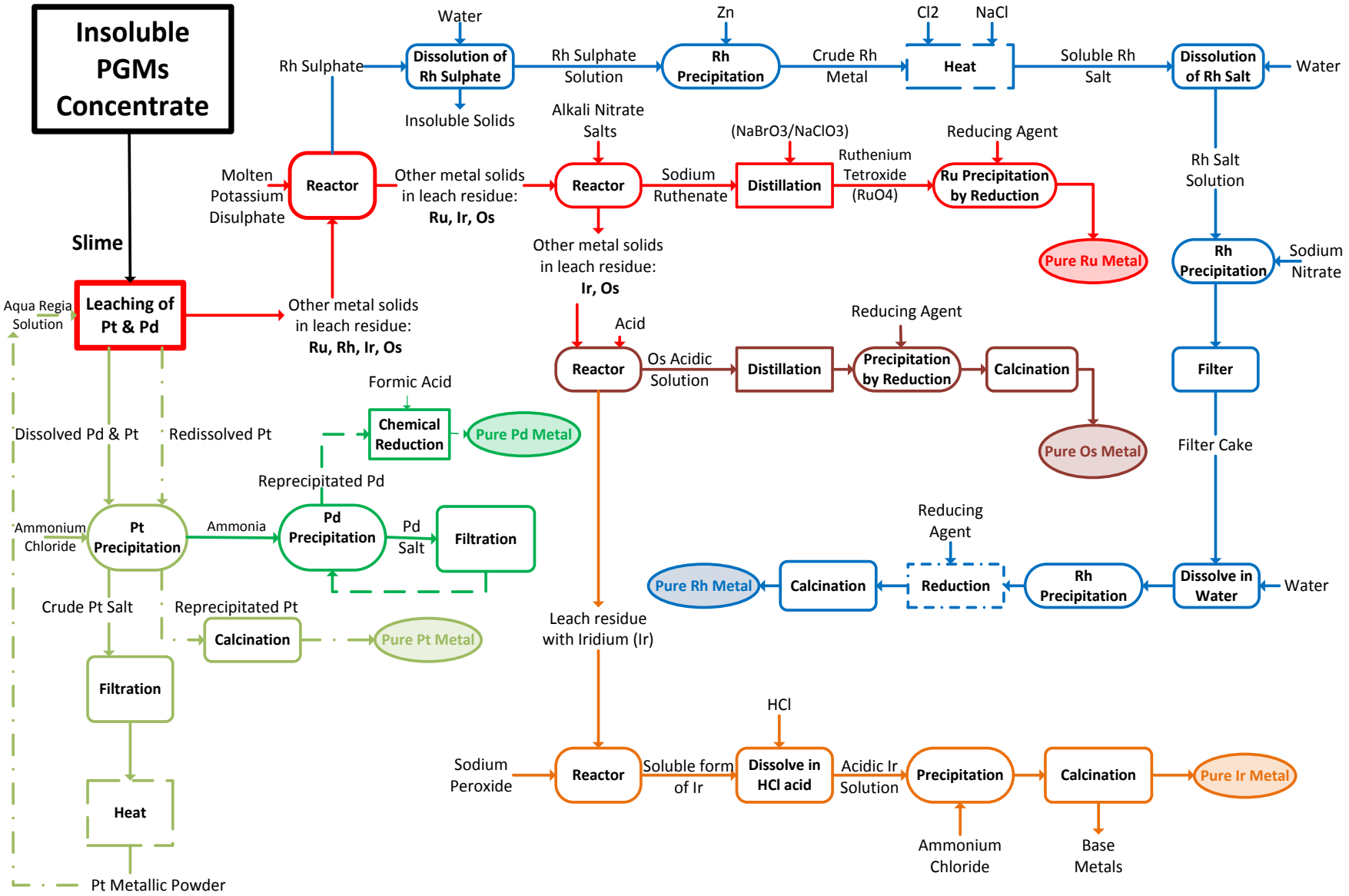

Figure 2.3: Selective refining of PGMs, (Ssennis 2014)

2.3 Chemical Batch Reactor Modelling

Modelling, or scientific modelling, is the activity whose objective is to make a particular part, feature or system of the world easier to understand, define, quantify, visualise, or simulate. It refers to the process of generating a model as a conceptual, simple and yet accurate enough representation of some phenomenon or real system (Basnet et al. 1990, Vangheluwe 2001). It is a substitute for direct measurement and experimentation. There are several types of models as a result of the various objectives of scientific modelling (Ritchey 2012).

Conceptual models. Those are made of the composition of concepts, which are used to help people know, understand, or simulate a subject the model represents.

Operational models. Those are used to operationalise or define a variable or object in terms of a process (or set of validation tests) needed to determine the model's existence, duration and quantity.

Mathematical models. Those models give a description of a system by quantifying relationships between its inputs and outputs, using mathematical concepts and language.

Graphical models. Those are probabilistic models, for which a graph denotes the conditional dependence structure between random variables.

Literature covers three types of mathematical models which have been developed for batch and semi-batch reactors of chemical processes. They are empirical models (EM), first-principle models (FPM) and hybrid models (HM) (Pierri 2006).

2.3.1 Empirical models

Empirical models (EM), also known as data-driven black box models, are models developed from a model identification platform that uses experimental data of a real system to formulate or derive its mathematical model (Pierri 2006). Empirical models may often include static and dynamic, linear and nonlinear regression models that are families of basic ARX (Auto Regressive models with exogenous inputs) or NARX (non-linear ARX) model structures (Czop et al. 2011). These models are widely used in industry for the applications of model-based control, fault detection, adaptive filtering etc. They are also commonly used for online estimation of system parameters. Czop et al. 2011 and Pierri 2006 have presented various advantages and disadvantages of empirical models.

- **Advantages of EMs:**

  They exhibit relatively low complexity, as they do not require any particular knowledge of the dynamic behaviour of systems they describe. They do not require knowledge of thermal dynamics, reaction kinetics, or key parameters of heat and mass transfer coefficients.

  They can be obtained or developed in a short space of time, with satisfactory accuracy that meets the model purpose.

  They can easily be used to develop artificial intelligence model structures of fuzzy logic, neural networks systems etc.

  They are a convenient and practical alternative for modelling a system that cannot be otherwise modelled with a rigorous mathematical description.

- **Disadvantages of EMs:**

  They require extensive sets of data in order to generate a good and accurate model.

  Purely empirical models are not very reliable for systems with significant non-linear behaviour.

  They are not adaptable to regions of variable operating conditions that are not covered by the data sets used to generate them. Any changes in system conditions will require treatment of new sets of data, hence a new model needs to be identified.

2.3.2 First-principle models

In contrast to empirical models, first-principle models (also known as white box models) are those based on physical knowledge of the system, where understanding of the system's underlying physics and chemical relations are used to derive their mathematical representation (Czop et al. 2011). Pierri 2006 has described it as the preferred approach for modelling batch reactors. It is a mechanistic approach, based on stoichiometric and kinetic knowledge. First-principle models (FPMs) use the fundamentals of the transport phenomena of energy and mass transfers to capture the dynamics of chemical systems. In a batch reactor, the kinetic dynamics describe the effect that the system's temperature and concentrations have on the rates of all reactions. The energy and mass balances relate the states (e.g. temperatures, moles, concentrations and volumes) to the system's manipulated variables (inlet streams) and possible disturbances (Pierri 2006). Like empirical models, the works of Czop et al. 2011 and Pierri 2006 have presented numerous advantages and disadvantages of FPMs.

- **Advantages of FPMs:**

  They offer great ability to predict the performance of a system because they provide profound insight into the behaviour of the system they describe.

  They can easily be adapted and rolled out to other systems of similar characteristics (e.g similar chemical processes).

  Their validity is not constrained to specific operational regions of a process since they are constructed on first-principle knowledge. Only the basic assumptions upon which they are formulated determine their validity.

  They enable system understanding and can be used for diagnostics and training simulators.

- **Disadvantages of FPMs:**

  They are expensive and difficult to build, since they may require special expertise to derive accurate equations from physical laws.

  Their derivation can be very time-consuming and unrealistic for large systems of complex dynamics and industrially-relevant reaction systems (e.g. polymerisation).

  They cannot be derived in the presence of unknown side-reactions and by-products.

  They might lead to highly complex model that cannot be useful for online applications such as real-time optimisation and control.

  They require some unknown key parameters to be determined on the basis of experimental data, or estimated either by trial-and-error, which can lead to non-optimal results, or by off-line optimisation techniques for optimal results.

2.3.2.1 Steps in First-principle modelling

The activity of developing a FPM often consists of the following steps, (Czop et al. 2011, Van Lith et al. 2002):

Basic modelling. This constitutes the inception of the modelling activity. At this point, the model is conceptualised in the form of a verbal, graphical, or other mental description involving the system to model and experiment conditions.

Model experimentation. The conceptualised model is then translated into a description of causal dependencies among defined variables. In this step, all

mathematical relations describing the dynamic effects of physical and chemical phenomena occurring in the system are analysed and presented. There may be several candidate models to formulate and choose from, depending on the purpose of the required model.

Parameter estimation. Process measurements are the most important source of information of a specific process, as they are required to identify a suitable process model. In the absence of measurements, parameter estimation can be used. This step is concerned with the parameterisation of the system, which involves finding values for certain unknown key parameters of a system (e.g. in a chemical process: reaction kinetics, heat and mass transfer coefficients). Identification methods of trial-and-error, or the more systematic linear or non-linear optimisation techniques can be used to that effect.

Expanded modelling. This step is concerned with calibrating or adjusting the model. The task allows the simplest models that are not falsified by experimental (or estimated) data to be found. The step involves fitting to the data and testing for significance. Czop et al. 2011 have described this process in two phases, where the first involves simulating the model by solving differential equations numerically, and the second involves numerical optimisation of the model's parameters with respect to an error-related objective function. The results allow uncertainty and credibility to be evaluated, and usually cause a return to the previous step.

Model validation. This step enables the model to be confronted with independent data. Those are compared to the generated outputs from model simulations. Validation should be performed in accordance with the intended use of the model (Subathra et al. 2011). If the calibrated model is more complex than the purpose required, then it must be reduced.

First-principle models are often developed as lumped parameter systems for which the physical properties of their chemical species are assumed constant, rather than distributed over some area or volume. For those systems, the dependent (output) variables of interest denoted y_k are a function of time (t) alone and are represented as $y_k(t)$. These models can be formulated as systems of ordinary differential equations (ODEs), amongst other possible mathematical formulations, and solved numerically (Bilbao et al. 2014).

2.3.2.2 Ordinary Differential Equations

This section gives a general overview of ordinary differential equations (ODEs) from which, the specific application to chemical engineering systems is given in

the following section 2.3.3, for the modelling of the ideal batch reactor.

A differential equation can be defined as a relationship between a finite set of functions and its derivatives (Ionascu 2006, Grigorian 2008, Soetaert et al. 2012), an equation containing one or more derivatives of a single unknown function of one or more variables. Differential equations involving derivatives of a function of a single dependent real variable are called ODEs (Burkard 2014, Soetaert et al. 2012).

The functions appearing in those equations depend on a single independent variable. Equations 2.1 and 2.2 give the general forms of an implicit and explicit ODEs, respectively (Grigorian 2008).

$$f(t, y, \dot{y}, \ddot{y}, \ldots, y^{(n)}) = 0 \tag{2.1}$$

$$f(t, y, \dot{y}, \ldots, y^{(n-1)}) = y^{(n)} \tag{2.2}$$

where,
f = Function
n = Maximum order of equation
t = Independent variable
y = Dependent variable
$\dot{y}$ = Derivative of y

Equation 2.1 can be reduced into Equation 2.3 to give the implicit form of a differential equation of a polynomial.

$$\frac{d^n}{dt^n} y(t) = 0 \tag{2.3}$$

where,
n = Order of equation
t = Independent variable (time)
y = Dependent variable

Equation 2.3 can also be represented as one simple function f, for which variable y is a function of t (Equation 2.4). ODEs describe the change of a state (dependent) variable y as a function f of one independent variable t.

$$\frac{d^n y}{dt^n} = f(y^n, t) \tag{2.4}$$

Equation 2.4 is called an explicit ordinary differential equation of order n. It can further be expanded to several functions (Equation 2.5), known as a system of

differential equations (Ionascu 2006) :

$$\begin{cases} \frac{d^n y_1}{dt^n} & = f_1(y^n, t) \\ \frac{d^n y_2}{dt^n} & = f_2(y^n, t) \\ & \vdots \\ \frac{d^n y_k}{dt^n} & = f_k(y^n, t) \end{cases} \tag{2.5}$$

A solution to the implicit ODE equation 2.3 would be any arbitrary function y of t with maximum oder of $n-1$ that satisfies it (Equation 2.6).

$$y(t) = a_1 t^{n-1} + a_2 t^{n-2} + \ldots + a_n \tag{2.6}$$

One can distinguish between linear and non-linear differential equations. Equation 2.7 gives the general form of a linear ODE, where function F is written as a linear combination of the derivatives of y.

$$F(t) = a_0(t)y^n(t) + a_1(t)y^{n-1}(t) + \ldots + a_n(t) \tag{2.7}$$

If the function F is zero, the equation is called *homogeneous* linear differential equation. Otherwise, it is an *non-homogeneous* linear differential equation. Any representation of a differential equation that is different from that of Equation 2.7 is termed a *non-linear* differential equation.

ODEs are often used as mathematical models of physical phenomena. Formulating ODE problems in engineering often requires the combination of conservation laws (mass and energy transfers), constitutive equations (equations of state, pressure drops, heat transfer etc) and design constraints. Implementation of those is often easier and much more efficient, by keeping the relations separate. This leads to a set of differential and algebraic equations (Biegler 2000).

2.3.3 Modelling the Ideal Batch Reactor

A quantitative analysis of the batch reactor can be obtained by mathematical modelling. The model of the jacketed batch reactor is built from the physical principles of mass balances for all species involved in the reaction and energy balances in the reactor as well as in the jacket. The resulting differential equations are mostly solved numerically. (Caccavale et al. 2011, Luyben 1990b, Donati 1999a). The modelling task can help formulate some general assessment of the reactor behaviour, depending on the complexity of the reaction kinetic schemes considered (Caccavale et al. 2011, Pierri 2006). Various works of Heinzle 2009, Luyben 1990b and Pierri 2006 have presented the modelling of the ideal batch reactor as given in the following sections.

2.3.3.1 Mass Balance

The conservation principles of mass and energy balances state that mass and energy entering a system must leave it or accumulate in it (Luyben 1990b). The mass balance in its general form must be written as:

$$\text{IN - OUT} = \text{ACC} \tag{2.8}$$

where,
IN = Mass flow into system
OUT = Mass flow out of system
ACC = Accumulation term, or time rate of change of mass inside the system

The terms IN and OUT must be positive. Equation 2.8 applies when no reaction takes place in a continuous or semi-batch system. However, when reaction occurs, the above equation can be extended to include a production or consumption term (PROD), that can either be positive or negative and is presented as:

$$\text{IN} + \text{PROD} = \text{OUT} + \text{ACC} \tag{2.9}$$

For the case of a batch system for which there are no input and output terms, Equation 2.9 reduces to:

$$\text{PROD} = \text{ACC} \tag{2.10}$$

The general equation of component mole balance for all chemical species involved in the reaction, for the batch system with variable volume, can be written as:

$$\frac{d}{dt}\int_V C_i dV = \int_V r_i dV \tag{2.11}$$

where,
V = Volume of solution in the reactor (m^3)
C_i = Concentration of a given i_{th} chemical species (mol/m^3)
r_i = Rate of reaction at which the i_{th} species is produced ($r_i>0$) or consumed ($r_i<0$), ($mol/(m^3.s)$)

In the case of a constant volume reaction, primarily in liquid phase, Equation 2.11 becomes

$$\frac{dC_i}{dt}V = \frac{d\frac{N_i}{V}}{dt}V = \frac{dN_i}{dt} = r_i V \tag{2.12}$$

The term r_i is written as

$$r_i = x_i \cdot R_r \tag{2.13}$$

where,
N_i = Number of moles of i_{th} species (mol)
x_i = Stoichiometric coefficient of the i_{th} species
R_r = Rate of reaction (mol/(m^3.s))

The rate of reaction (R_r), given in Equation 2.14, depends on the concentrations of the chemical species reacting and the reaction rate constant, which itself, is temperature dependent and calculated according to the Arrhenius law (Equation 2.15).

$$R_r = k(T) \prod_i C_i^{n_i} \tag{2.14}$$

$$k(T) = A \cdot \exp\Big(-\frac{E_a}{RT}\Big) \tag{2.15}$$

where,
k = Arrhenius rate constant (s^{-1})
T = Reaction temperature (K)
C_i = Concentration of the i_{th} reactants (mol/m^3)
n_i = Order of reaction with respect to i_{th} reactants
A = Pre-exponential (or frequency) factor of the reaction (s^{-1})
E_a = Activation energy of the reaction (J/mol)
R = Universal gas constant (J/(mol.K))

2.3.3.2 Energy Balance

Under the assumption of a constant volume and liquid phase reaction, where the density of the reactor solution is kept constant; the general energy equations of the reactor and jacket sides of a semi-batch jacketed reactor can be written as given in the following section:

Reactor Side

The energy balance for the reactor side is introduced, as in Equation 2.16:

$$\rho_{rx} C_p^{rx} V_{rx} \frac{dT_{rx}}{dt} = \rho_{rx} C_p^{rx} \Big(F_0 T_0 - F T_{rx}\Big) + Q_G + Q_c \tag{2.16}$$

where,
ρ_{rx} = Overall mole or mass density of solution in the reactor (mol/m^3)
C_p^{rx} = Specific heat capacity (kJ/(kg.K))
V_{rx} = Volume of solution into the reactor (m^3)
F_0 = Inlet volumetric flow rate of reactants (m^3/s)
F = Outlet volumetric flow rate of products (m^3/s)
T_0 = Temperature of inlet flow streams of reactants (K)
T_{rx} = Reaction temperature (K)
Q_G = Total heat generated due to reaction (J/s)
Q_c = Heat transferred between jacket and reactor compartments (J/s)

The term Q_G is either positive ($Q_G > 0$) when the reaction is heat-generating (exothermic) or negative ($Q_G < 0$), when the reaction is heat-consuming (endothermic). For a given Species i, the term Q_G can be written as

$$Q_G = -\lambda \cdot k(T_{rx}) C_i^{n_i} \cdot V_{rx} = -\lambda \cdot r_{rx} V_{rx} \tag{2.17}$$

where,
λ = Molar heat of reaction (J/mol), with λ<0 (for exothermic reaction) & λ>0 (for endothermic reaction)
r_{rx} = Rate of reaction $(mol/(m^3.s))$.
n_i = Order of reaction with respect to i_{th} reactants

The heat transferred between jacket and reactor compartments is introduced by Equation 2.18

$$Q_c = UA\Big(T_{rx} - T_{hx}\Big) \tag{2.18}$$

where,
U = Overall heat transfer coefficient (W.m^{-2}.K^{-1})
A = Area of heat transfer (m^2)
T_{rx} = Reaction temperature (K)
T_{hx} = Jacket temperature (K)

For a purely batch reactor system, Equation 2.16 reduces to Equation 2.19

$$\rho_{rx} C_p^{rx} V_{rx} \frac{dT_{rx}}{dt} = Q_G + Q_c$$

$$\frac{dT_{rx}}{dt} = \frac{Q_G}{\rho_{rx} C_p^{rx} V_{rx}} + \frac{Q_c}{\rho_{rx} C_p^{rx} V_{rx}} \tag{2.19}$$

Jacket Side

The hot and cold utilities (usually steam and cooling water) are pumped into the system through the jacket. They are used to regulate the reactor temperature. The energy balance of the solution in the jacket is given as shown in Equation 2.20

$$\rho_{hx}C_p^{hx}V_{hx}\frac{dT_{hx}}{dt} = Q_c + \rho_{hx}C_p^{hx}F_{utility}\Big[\big(T_{utility}^{in} - T_{ref}\big) - \big(T_{hx} - T_{ref}\big)\Big]$$

$$\frac{dT_{hx}}{dt} = \frac{Q_c}{\rho_{hx}C_p^{hx}V_{hx}} + \frac{F_{utility}}{V_{hx}}\Big(T_{utility}^{in} - T_{hx}\Big)$$

$$\frac{dT_{hx}}{dt} = \frac{UA}{\rho_{hx}C_p^{hx}V_{hx}}\Big(T_{rx} - T_{hx}\Big) + \frac{F_{utility}}{V_{hx}}\Big(T_{utility}^{in} - T_{hx}\Big) \tag{2.20}$$

where,

ρ_{hx} = Overall mole or mass density of solution in jacket (mol/m^3)
C_p^{hx} = Mass or mole specific heat capacity in jacket (kJ/(kg.K))
V_{hx} = Volume of solution in jacket (m^3)
$F_{utility}$ = Utility flow rates in and out of the jacket (m^3/s)
T_{ref} = Reference temperature of system (K)
T_{hx} = Jacket temperature (K)
$T_{utility}^{in}$ = Temperature of utility as it enters the jacket (K)

2.3.4 Review on FPMs of Batch and Semi-batch Processes

Literature covers a considerable amount of work that has been done on the development of mathematical first-principle models of various chemical batch and semi-batch processes, ranging from polymers production, pharmaceuticals, biochemical, biotechnological, petroleum refining etc. Regardless of the chemical process studied, the dynamics of their reactions kinetics, as well as their mass and energy dynamics were all captured similarly in order to describe the process model. A lot of interest has also been shown towards the development of hybrid models, which provide a combination of first-principle knowledge and empirical dynamic relations.

On searching, no publication could be identified in the literature that has reported on the development of first-principle models of batch and semi-batch chemical processes of PGMs. However, the work of Singh et al. 2010 has reported on a control study based on an empirical model of a batch reactor operating a PGM process. The selected review on previous works related to first-principle modelling of batch and semi-batch processes, presented below, seeks to emphasize that the method of capturing the transport phenomena of heat and mass transfers, as seen

in section 2.3.3 describing the first-principle modelling of the ideal batch reactor, can be applied similarly when modelling any chemical batch or semi-batch process, including those of PGMs.

For instance, Hvala et al. 2013 have developed a detailed dynamic FPM of a real-life industrial semi-batch vinyl acetate polymerisation exothermic reaction. The mass balance of the model was captured with a set of differential and algebraic equations, that were solved by means of iterative numerical methods. The model was used to estimate the non-measurable conditions of conversion, polymerisation rate, viscosity, and solids content inside the reactor. Those unknown conditions were further used to develop control strategies on the reactor.

Similar works on first-principle modelling of various batch (semi-batch) processes have been done, where the transport phenomena of mass and energy transfers of those processes were all captured, by deriving appropriate differential equations of batch processes (Nabi et al. 2014, Aller et al. 2014, Arora et al. 2010, Aller et al. 2009, Prokopova et al. 2009, Miteva et al. 2008b, Miteva et al. 2008a, Arora et al. 2007, Tyner et al. 2007, Nystrom 2007 and Zavala et al. 2005).

Donati 1999b has given a short review of batch reactor theory and practice, where the development of the mathematical set of equations describing the time-dependent behaviour of a batch reactor was reported. The equations were based on unsteady state mass and energy balances.

Mathematical first-principle modelling has also been applied for batch and semi-batch reactors of biochemical and pharmaceutical processes (Nystrom 2007, Edwards 2000, Le Lann et al. 1999).

In biotechnology, Zapata et al. 2010 have developed a purely mathematical FPM, describing the dynamic behaviour of limonene epoxidation with aqueous hydrogen peroxide, in the presence of catalyst PW-Amberlite. The process was a constant volume heterogeneous catalytic reaction, carried out in a batch reactor set up at laboratory scale. The model was written with three major equations. A mole balance equation describing the time rate of change (in ODE form) of limonene conversion into limonene epoxide, as well as two energy balance equations; the one describing the dynamics of the temperature of the solution in the reactor, and the other describing the dynamics of the temperature of liquid in the jacket. The proposed model was also used for optimisation work, where optimal non-isothermal temperature profiles of the system were succesfully predicted. The model was validated using experimental limonene conversion data.

In petroleum refining, Ahmed 2012 developed a dynamic FPM of a batch reactor that processed the alkylation of mono-olefins, with benzene to produce linear alkylbenzene. The model was validated against some pilot plant measurements and based on a set of nonlinear equations of mass and energy balances describing the dynamics of the batch process, where the mass balance equations described the change in concentration of mono-olefins reactant over time, and the energy equations described the dynamics of the temperatures of the reactor and jacket contents, respectively. The model was primarily developed to obtain key parameters of the system, that were then used to design tuning parameters of the adaptive self-tuning controller implemented on the reactor.

Chemical engineering processes often exhibit highly nonlinear behaviour with complex dynamics. Those properties can be difficult to capture in a purely quantitative analysis. As such, effective and practical modelling of such systems is often based on hybrid models (Nabi et al. 2014, Oliveira 2003), due to the fact that they integrate more knowledge than the classical FPMs, achieve higher accuracy with fewer iterations, and are usually cheaper and more cost-effective to develop (Oliveira 2003). Numerous hybrid models (with first-principle contribution) of chemical engineering batch or semi-batch systems have been developed (Simon et al. 2007, Van Lith 2002).

Nabi et al. 2014 has presented a structured procedure to construct hybrid fuzzy first-principles models from process data, using a simulated fed-batch bioreactor as the testing system. The model consisted of a framework of dynamic mass balance equations (introduced as ODEs), supplemented with one algebraic equation, which accounted for its first-principle contribution. It also had two fuzzy equations accounting for its empirical contribution. The first-principle part of the model described the states of the biomass, substrate and product concentrations, as well as volume and the substrate consumption rate (the algebraic equation). The fuzzy logic or empirical part of the model was used to estimate important parameters of the system.

In a similar way, Oliveira 2003 proposed a general framework of a bioreactor dynamic hybrid model that combines first-principles modelling with artificial neural networks (ANNs). It was valid for a wide class of problems applicable to bioreactor modelling of batch, semi-batch or continuous biochemical processes involving cellular catalysis. The system was described by a set of mass balance equations (ODEs), that constituted basic mechanistic knowledge, and the cell population system, represented by an adjustable mixture of neural network and mechanistic

representations.

2.4 Implementation and Numerical Integration

First-principle models require an efficient modelling and simulation language, suitable for model implementation (Czop et al. 2011). Those models consist of differential equations that must be integrated. However, for many practical applications in science and engineering, systems of differential equations cannot be integrated to give an analytical solution. Rather, they need to be solved numerically (Soetaert et al. 2010, Czop et al. 2011, Soetaert et al. 2012). For that reason, modelling and simulations are often done in numerical languages such as MATLAB & Simulink, Python etc. Models can also be developed independently from such platforms as Modelica, which is a language that enables creation of open code that can be executed in numerous third party simulation environments like CATIA Systems, Dymola, LMS Imagine.Lab AMESim, JModelica, MapleSim, MathModelica, OpenModelica, SCICOS, SimulationX (Czop et al. 2011). Explicit and implicit integration methods are commonly used to find numerical solutions of first-principle models (Soetaert et al. 2012).

2.4.1 Explicit methods

Explicit integration methods are those that involve explicit calculation of solutions of differential equations at every time step with no iteration (Luyben 1990b, Soetaert et al. 2012). This is done by numerical integration of differential equations, where the system's derivatives are evaluated at the current time (t) and new values of variables are predicted at the next step in time ($t+\Delta t$). This process is repeated at every time step of the simulation, with constant or variable incremental step size Δt (Soetaert et al. 2012, University of Colorado 2014a).

Explicit methods are known under various names in the engineering literature. They have been referred to as step-by-step, Initial-value, Marching, Purely Incremental or Predictor-only methods (University of Colorado 2014b). This is because they make no attempt to correct the accuracy of the converged solutions. Those methods are commonly used for dynamic analysis of linear and/or non-linear computationally intensive systems (Soetaert et al. 2012).

Although there is a large number of different explicit methods (algorithms) with various levels of complexity in the literature, two are very popular, self-starting and easy to use. They are the first-order Euler and the fourth-order Runge-Kutta methods (Soetaert et al. 2012), of which only the Euler algorithm is recalled below:

Euler Algorithm

This has been reported as the simplest numerical integration and the most useful algorithm to use (Luyben 1990b, Soetaert et al. 2012). It is represented in its general form as given in Equation 2.21.

$$\begin{cases} x_{n+1} & = x_n + f_{(x_n,t_n)} \cdot \delta t \\ t_{n+1} & = t_n + \delta t \end{cases} \tag{2.21}$$

where,
f = General differential function
x = State variable
t = Time
n = Current time step
δt = Integration step size

Advantages and disadvantages

Explicit methods present many advantages. For instance, they are useful when solving systems of complex dynamics, they can offer accurate results and are not computationally intensive. However, a big disadvantage is that they are prone to numerical instability, because the computed solutions can diverge from correct values if small enough step sizes are not taken. As a result of that, it is often necessary to use very small step sizes, such that systems of processes containing both fast and slow dynamics in their equations can be correctly integrated numerically. Such systems are known as systems of stiff differential equations. They slow down the computational speed of integration methods, with a possibility of generating inaccurate results (Luyben 1990b, Soetaert et al. 2012).

2.4.2 Implicit methods

Implicit integration methods are those involving the use of algorithms that result in implicit equations that must be solved for the new values at the next time step (Luyben 1990b). These methods are also known as Corrective, Predictor-corrector, or Incremental-iterative methods. They work in much the same way as their explicit counterpart to predict new values of variables at the next time step $t+\Delta t$, except for the fact that they use Newton-Raphson iterations as the corrective action of the algorithm, in order to enforce the computation of correct solutions. This is achieved by adjusting the computed solutions as they drift away from correct values, even when large integration step sizes are taken. At each

time step, the incremental formula of the algorithm operates as a predictor that provides a starting point for the corrective iteration action. The purpose of this iteration is to eliminate (or at least reduce) the error contained in the converged solution (Soetaert et al. 2012, University of Colorado 2014a).

The first-order explicit Euler algorithm (Equation 2.21) can be modified for an implicit formulation as given in Equation 2.22 (Luyben 1990b.

$$\begin{cases} x_{n+1} & = x_n + f_{(x_{n+1},t_{n+1})} \cdot \delta t \\ t_{n+1} & = t_n + \delta t \end{cases} \tag{2.22}$$

where,
f = Differential function
x = State (dependent) variable
t = Time
n = Current time step
δt = Step size

The difference between Equation 2.21 and Equation 2.22 is that, in the latter, the differential function f (or derivative) is evaluated at the next step in time (t+δt) where the value of variable x_{n+1} is not known. Therefore, the unknown variable x_{n+1} appears on both sides of the equation. The implicit formula solves for the unknown x_{n+1} based on itself and on the current value x_n.

Advantages and disadvantages

Implicit integration methods offer various advantages and disadvantages. The biggest advantages are that, they do not become numerically unstable regardless of the value of step size chosen; the possibility of choosing larger step sizes with little effect on stability allows for faster computation of solutions than with explicit methods; they are very useful for stiff systems of differential equations. However, the disadvantages are that they are more complicated to program and debug when implemented in numerical platforms, and they become slower and more difficult to use with large systems of hundreds of differential equations. This is a common occurrence in most engineering systems and models with non-linear dynamics (Luyben 1990b).

2.4.3 Stiff Differential Equations

There is no unique nor universally accepted definition of stiffness in the literature (Shampine et al. 2007), where various definitions have been proposed.

In Weierstrass Institute 1995, systems of stiff differential equations have been presented as those characterised by the existence of both slow (smooth) and fast (transient) changing solutions, when certain initial conditions are applied to it. That is, in solutions of differential equations describing the system, there exist some components which decay faster than others. Many of such are common in chemical engineering systems that handle reactions processes. In those systems, the reacting components of faster dynamics arrive in a very short time to their equilibrium state, whereas the slowly changing components are more or less fixed in comparison to the former, hence they are termed stiff.

Lambers 2009 has defined an ODE as a stiff differential equation if its exact solution $y(t)$ includes a term that decays exponentially to zero as t increases, but whose derivatives are much greater in magnitude than the term itself. Hairer et al. 1999 has also presented stiff systems of differential equations as those characterised by the fact that the numerical solution of slow movements is considerably perturbed by nearby rapid solutions.

Brydon et al. 1998 has defined stiff differential equations as those for which two or more disparate time scales are important. Systems of those equations are governed by enormously varying time scales, for which existing methods, though specially developed to integrate them, are inefficient, and produce spurious solutions.

2.4.4 Numerical solvers

There is a number of general-purpose numerical solvers that are available in the MATLAB Software. They each have various specific capabilities and can be used to integrate systems of differential equations. Solver ode15s was used in the work presented in this dissertation.

Solver Ode15s: This is a multi-step and variable-order solver based on the numerical differentiation formulas (NDFs), of which the simplest form is known as the Newton's difference quotient (seen in Equation 2.23).

$$\frac{f(x+1)-f(x)}{h} \tag{2.23}$$

It optionally uses the backward differentiation formulas (BDFs) that are usually less efficient, and first-order through fifth-order optimisation algorithms to solve systems of equations, converging to solutions with low to medium order of accuracy (Mathworks 2015a). It is suitable for solving systems of stiff differential algebraic equations (DAEs) and ODEs (NC State University 2015, Mathworks 2015b).

2.5 Dissolution of Gases in Aqueous Solutions

The concept of gas dissolution in aqueous solutions was of particular importance to this project. This is because the dissolution of $Cl_{2(g)}$ in the reactor solution had a significant effect on the dynamics of the modelled reactor pressure. This will be further discussed in section 3.1 of Chapter 3, describing the chemical process studied in this work.

The dissolution of gases into aqueous solutions is a chemical process that is well described by Henry's law (Sander 2015). It gives a direct relationship between the concentration of a chemical species in an aqueous solution, the partial pressure of that chemical species in the gaseous phase under equilibrium condition with the aqueous solution, and the appropriate Henry's law constant corresponding to the system considered. There are many variants of Henry's law constants which can all be classified into two fundamental types (Sander 2015): Henry's law solubility constant and Henry's law volatility constant, given by Equations 2.24 and 2.25 respectively.

$$H^{CP} = \frac{C_i}{P_i} \tag{2.24}$$

where,
H^{CP} = Henry's law solubility constant (kmol/(m^3.kPa))
C_i = Concentration of species i dissolved into aqueous solution (kmol/m^3)
P_i = Partial pressure of gaseous species i under equilibrium condition (kPa)

$$K_H^{PC} = \frac{P_i}{C_i} = \frac{1}{H^{CP}} \tag{2.25}$$

where,
K_H^{PC} = Henry's law volatility constant (m^3.kPa/kmol)

Equations 2.24 and 2.25 can be re-arranged to express the solubility of a chemical species in terms of the partial pressure of that species in the gas phase. Under the assumption that the gas in a system displays ideal behaviour, the total pressure of the gas can be derived from the Ideal gas law.

2.5.1 Ideal Gas Law

The ideal gas law, given by Equation 2.26, describes the mathematical relationships between the properties of pressure, volume, moles and temperature of gases. It can be used to calculate the pressure of a gas in a closed system when all the other

properties are known. Under certain operating conditions, gases for which those properties are accurately described by the ideal gas law are said to exhibit ideal behaviour (College 2015).

$$PV = nRT \tag{2.26}$$

where,
P = Pressure of gas (kPa)
V = Volume of gas (m^3)
n = Moles of gas (kmol)
R = Universal gas constant (kJ/(kmol.K))
T = Temperature of gas (K)

The ideal gas law applies well under conditions of low pressures (typically below 1 atm) and high temperatures (above 1000 K), for which gases are said to approach ideal behaviour. However, this is very often not the case under conditions of high pressures and low temperatures, for which significant deviations from ideal gas behaviour do occur (College 2015).

2.5.2 Deviation from Ideal Gas Law

A modified gas law known as the van der Waals equation has been introduced as given by Equation 2.27 (College 2015). It accounts for the non-ideal behaviour observed for many gases, at relatively high pressures and low temperatures, for which the relationships between pressure, mole, volume, and temperature are not accurately described by the Ideal Gas Law.

$$PV = nRT \rightarrow \left(P + \frac{an^2}{V^2}\right)\left(V - nb\right) = nRT \tag{2.27}$$

where,
a = Strength of attraction between molecules of a particular gas.
b = Size of the molecules of a particular gas.

Values of the van der Waals constants "a" and "b" are often determined experimentally. The term "$\frac{an^2}{V^2}$" added to the pressure in the ideal gas law is the correction for molecular attraction, and the term "nb" subtracted from the volume in the ideal gas law is the correction for volume of gas molecules.

Chapter 3

System Description and Modelling

This chapter presents the description of the process, along with the equations of the chemical reactions taking place in the semi-batch reactor system. It gives the method used to develop the first-principle model of the rhodium dissolution process. This is a detailed account of all steps followed in modelling the process, to which, a background is also given of the initial version of the model we had inherited from. This is to clarify what we have contributed to this modelling work, from the initial version of the model as inherited from Mr. Carel van Dam, to the final version of the developed first-principle model of the rhodium dissolution process, presented in this dissertation. The chapter further elaborates on the description of the model by giving the key assumptions made in the reactor system, the model equations developed and the numerical integration method (solver) used to integrate those equations. Also given are the limitations encountered with the model, the method used to verify the accuracy, and stability of its simulated responses and their validation.

3.1 System Description

The system is a jacketed semi-batch reactor in which two exothermic reactions take place simultaneously in the presence of chlorine gas. They are the dissolution of some crude rhodium sponge ($Rh_{(s)}$) in an aqueous solution of hydrochloric acid (HCl), to produce a solution of aqueous rhodium(III) chloride ($RhCl_3.H_2O$) and the reaction of $Cl_{2(aq)}$ with water (H_2O) to produce some more $HCl_{(aq)}$ and some hypochlorous acid ($HClO_{(aq)}$), (Hsia 2015, Sherrill et al. 1931). $Cl_{2(aq)}$ is formed from $Cl_{2(g)}$ that partly dissolves into the reactor solution during the reaction phase. Equations 3.1 and 3.2 show the chemical reactions of the process, believed to be taking place in the semi-batch reactor system, shown in Figure 3.1 below.

$$Rh_{(s)} + 3HCl_{(aq)} + H_2O_{(l)} \rightarrow RhCl_3(H_2O)_{(aq)} + 3H^+_{(aq)} + 3e^- \tag{3.1}$$

$$Cl_{2(aq)} + H_2O_{(l)} \leftrightarrow HCl_{(aq)} + HClO_{(aq)} \tag{3.2}$$

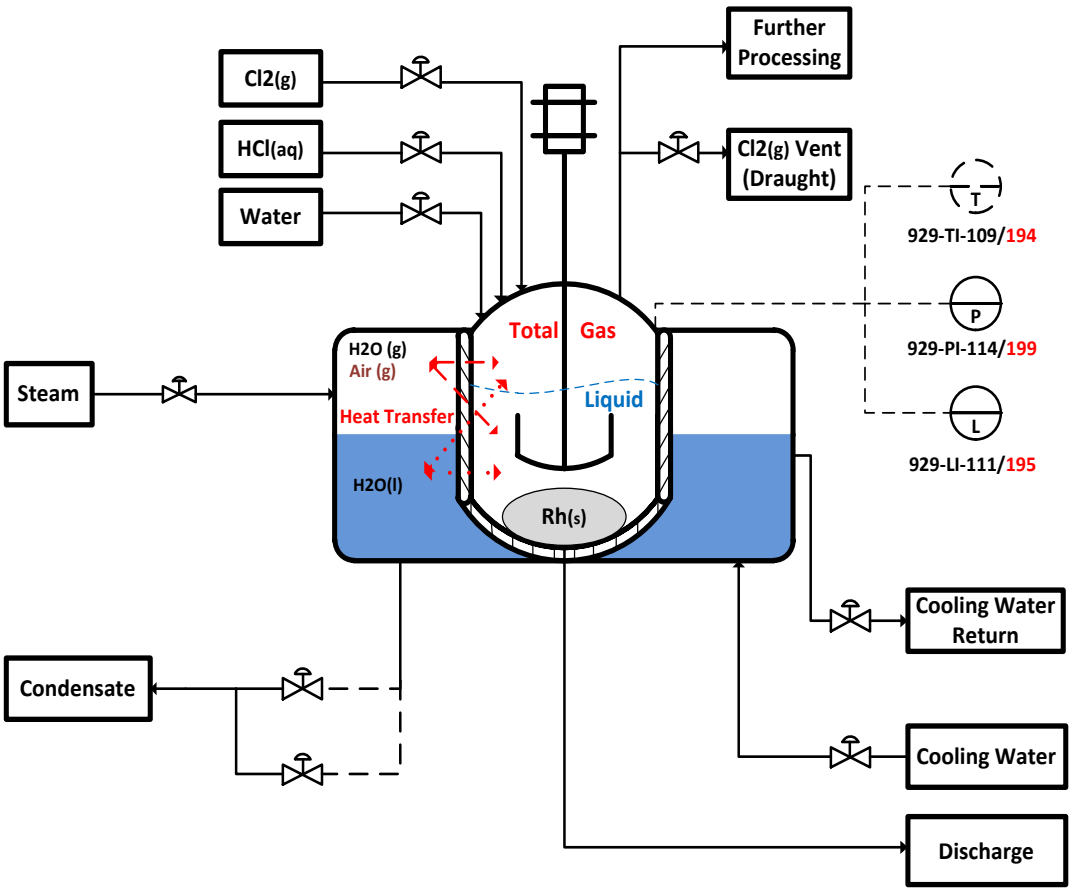

Figure 3.1: Semi-batch reactor of rhodium dissolution

It should be clearly noted that we do not know the exact chemistry of this process, in the form of the correct equations of the chemical reactions taking place in the reactor. This is because no documentation clearly providing that information was available to us. However, we gained some good understanding of the process from information provided in the operational procedure document of the plant reactors that was made available to us, as well as some more references (Crundwell et al. 2011b, Crundwell et al. 2011c, Crundwell et al. 2011a, Crundwell et al. 2011d) which have provided a more general description of the PGMs reaction processes. In all documentation at our disposal, only information of the chemical species used as reactants is known with no clear specification of what the products are, other than the fact that a liquor of rhodium compound, whose chemical content is unclear to us, is formed after reactions. Therefore, Equation 3.1 was written according to the general descriptions given the above-mentioned references and Equation 3.2 was written as given by Alkan et al. 2005 and Hsia 2015.

In this process, the hot and cold utilities of steam and cooling water were the input variables used to regulate the reactor temperature, whilst the flowrate of $Cl_{2(g)}$ pumped into the reactor was the input variable used to regulate the pressure requirement inside the reactor. There is no knowledge of possible side reactions occuring or gaseous substances produced. The reaction process taking place in the semi-batch reactor can be described over five operational phases.

The first phase of the process involves loading the reactor with all the reactants, composed of 29 kg of crude rhodium sponge ($Rh_{(s)}$) and 546 L of an aqueous solution of hydrochloric acid (HCl) at a concentration of 11.5 kmol/m^3. Crude rhodium sponge is a solid and porous form of rhodium metal, with a purity greater than 99.98 % of rhodium (Crundwell et al. 2011d). Those initial quantities of reactants correspond to some molar amounts of 0.27 kmol of $Rh_{(s)}$ and 6.28 kmol of $HCl_{(aq)}$.

The second phase is the chlorination, whereby an initial amount of $Cl_{2(g)}$ is pumped into the reactor, in which some of it dissolves into solution to form some $Cl_{2(aq)}$. During this phase, $Cl_{2(g)}$ is added until the reactor reaches an initial gauge pressure of 150 kPa.

The third phase involves an initial temperature control where steam is pumped into the jacket until the reactor temperature reaches 40 $^{\circ}C$, at which point steam is cut off, the reactor temperature controller is set to a target of 50 $^{\circ}C$. From this, minor reactions starts and cooling water is activated when the reactor temperature reaches the controlled target of 50 $^{\circ}C$.

Fourth is the reaction phase. It involves simultaneous temperature and pressure control in the reactor. During this phase, more $Cl_{2(g)}$ is pumped until the reactor pressure rises to a gauge pressure of 300 kPa (equivalent to 400 kPa absolute). $Cl_{2(g)}$ serves to maintain the reactor at the required absolute pressure of 400 kPa during this phase. At this point the exothermic reactions fully proceed, steam and cooling water are activated alternately into the jacket in order to regulate the temperature of the dissolution reaction at around 50 $^{\circ}C$ until its completion.

The fifth phase is the depressurisation (de-chlorination) during which, after the dissolution reaction has completed, some plant air is sparged into the reactor solution to remove $Cl_{2(aq)}$ and to depressurise the reactor by displacing $Cl_{2(g)}$ out of it until the end of the batch.

At the end of each batch, $Cl_{2(g)}$ contained in the reactor is vented and directed to a scrubbing column for further cleaning. The reactor is then discharged safely, decommissioned and recommissioned for the next batch.

3.2 Modelling Method

This section presents the method followed to model the chemical process, which we refer to as the reactor model from this point onward. It covers the key assumptions made in the model, the size of the developed model (number of equations), the numerical method (solver) used to integrate those equations and the limitations encountered during simulations. It also presents how the model was validated, as well as the method used to verify the accuracy and stability of its responses.

The modelling work was entirely done in version 7.10.0.499 (R2010a) of the MATLAB computational environment. The process was taken as a lumped parameter system, for which the physical properties of its chemical substances were only a function of time, and not spatially distributed throughout the reactor volume (see section 2.3.2.1 of Chapter 2). The simulations were run on a computer, with the processor specifications of Intel(R) Core(TM) i5-3337U CPU, 1.80 GHz and an installed memory (RAM) of 6 GB.

This section is presented in two main parts that aim at clarifying the contribution made to this modelling work by the candidate presenting this dissertation:

- The first part gives a background of the initial model that was developed as a system of fully-implicit differential algebraic equations (DAEs), which the candidate presenting this dissertation work had inherited from. Of particular importance discussed in this part are, the initial objective of the work, the

chemical process modelled, the mathematical formulation and size of the model, and finally the major limtations encountered with this model version.

- The second parts elaborates on the work that has been done to solve the various limitations encountered in the initial model, and the efforts made to significantly improve the consistency of the model. The fully-implicit DAEs model had been revised by simplifying the description of the reactor system, correcting the equations and explicitly rewriting the sets of equations in an equivalent system of Ordinary Differential Equations (ODEs).

3.2.1 Model of Fully-implicit DAEs

Initial Objective of Project

The initial orientation of this work was to develop a generic model of a semi-batch reactor that could be used to describe any chemical process of PGMs dissolution. To that end, Mr. Carel van Dam had initially done some work on the modelling of dynamic systems with known data, using a simple tank system, for which he had proposed an object-oriented modelling platform as a proof of concept. That platform was to investigate how optimization problems of parameter estimation could be integrated in modelling languages (van Dam et al. 2012). In order to meet the objective of developing a generic model, he then attempted to refocus his work to the development of a first-principle model of a semi-batch reactor operating a ruthenium dissolution process, as requested by the project's industrial partners. However, his work was incomplete since it had not successfully generated any meaningful simulations and was therefore subject to significant improvement.

Chemical Process Modelled

The initial model described the simultaneous exothermic reactions of dissolution (Equation 3.3) of ruthenium ($Ru_{(s)}$) in a solution of $Cl_{2(aq)}$ to produce an aqueous solution of ruthenium tri-chloride ($RuCl_{3(aq)}$). And the evaporation (Equation 3.4) of $RuCl_{3(aq)}$, in the presence of sodium chlorate ($NaClO_{3(aq)}$), used as the oxidizing agent, to produce ruthenium tetroxide ($RuO_{4(g)}$) as the main product, with sodium chloride ($NaCl_{(aq)}$) and hydrochloric acid ($HCl_{(aq)}$) as by-products.

$$2Ru_{(s)} + 3Cl_{2(aq)} \rightarrow 2RuCl_{3(aq)} \tag{3.3}$$

$$2H_2O_{(aq)} + 2RuCl_{3(aq)} + 2NaClO_{3(aq)} \rightarrow 4HCl_{(aq)} + 2RuO_{4(g)} \ldots + Cl_{2(g)} + 2NaCl_{(aq)} \tag{3.4}$$

Mathematical Formulation and Model Size

This reactor was modelled as a system of fully-implicit differential algebraic equations (DAEs), with a total of 150 differential algebraic equations describing the dynamic behavior of 150 process variables (25 states and 125 algebraic relations). Equation 3.5 gives the mathematical formulation of the fully-implicit DAEs model.

$$Model\ of\ Fully-implicit\ DAEs: \begin{cases} f_1(t, y_1, \dot{y_1}) & = 0 \\ f_2(t, y_2, \dot{y_2}) & = 0 \\ & \vdots \\ f_{150}(t, y_{150}, \dot{y}_{150}) & = 0 \end{cases} \tag{3.5}$$

where,
t = Independent variable (Time)
y = Process variable
$\dot{y}$ = Derivative of y
f = Function f, or differential algebraic equation of y

Major Limtations of Model

Upon inheriting the model, the new candidate presenting this work had invested significant efforts to troubleshoot and correct the model equations. The model displayed the following major limitations as observed:

- Consistent initial conditions for all 150 variables of the model equations could not be found. This was necessary to ensure that equations would all be fully satisfied at least at the initial time step (t_0) of the simulation.
- There was significant modelling errors in some model equations as many thermodynamic and reactions dynamics were incorrect. For instance, reactor and jacket temperatures did not respond at all to hot and cold utilities inputs.
- The nonlinearity combined with the presence of stiffness in model equations (as discussed in section 2.4.3 of Chapter 2) would cause the fully-implicit DAE solver used, ode15i, to often break and prematurely stop simulations.
- It was believed that the size of the model and its fully-implicit DAE formulation made it rather difficult for the only fully-implicit solver ode15i, available in the MATLAB version used, to correctly integrate all 150 DAEs of the system. This is because model responses still showed some inconsistency since many numerically integrated solutions were still incorrect. The 150 solutions

of all equations had to be iterated, all at the same time and at every time steps, until they would eventually converge towards correct solutions that would fully satisfy the statement of Equation 3.5, that every model equation must be equal to zero at every time steps of the simulation. This was difficult to achieve, especially during phases of dynamic changes in the model inputs variables of flowrates of utilities and $Cl_{2(g)}$.

3.2.2 Model of Explicit ODEs

As a result of the various difficulties encountered with the initial fully-implicit DAE model of the ruthenium process, a decision was made to simplify the model to a form that would make it a lot easier to solve and simulate. To that effect, the model was revised and many parts of it rewritten. The size of the ruthenium model was reduced to fewer process variables and the model equations corrected and rewritten as an explicit system of ordinary differential equations (ODEs), whose mathematical formulation is given by Equation 3.6.

$$Model\ of\ Explicit\ ODEs: \begin{cases} \frac{d^n y_1}{dt^n} & = f_1(y_1^n, t) \\ \frac{d^n y_2}{dt^n} & = f_2(y_2^n, t) \\ & \vdots \\ \frac{d^n y_k}{dt^n} & = f_k(y_k^n, t) \end{cases} \tag{3.6}$$

where,
t = Independent variable (Time)
y = Process variable
n = Order of equation
$k = k^{th}$ equation
f = Function f, or ordinary differential equation of y

The greatest benefit of the ODE mathematical formulation in contrast to the DAE formulation is that, systems of ODEs can only become zero when the process they describe is at steady state. Therefore, it is only at steady state that one can have a good appreciation of the extent of errors existing in model equations. This is because, at steady state, process variables are expected to be reasonably constant with negligeable dynamics over the simulation time span. However, during the transient phase of the system, considerable dynamics of process variables can be seen as their ODEs cannot be constrained to zero.

Later on, another suggestion had been made from one of the project industrial partners to rather convert the model from the ruthenium to the rhodium dissolu-

tion process, for which more plant data of process inputs variables (utilities and $Cl_{2(g)}$ flowrates) and outputs variables (temperature and pressure) were readily available for the validation task. The first-principle model of the rhodium reactor was then rewritten as an explicit system of ODEs from the chemical reactions given in equations 3.7 and 3.8.

$$Rh_{(s)} + 3HCl_{(aq)} + H_2O_{(l)} \rightarrow RhCl_3(H_2O)_{(aq)} + 3H^+_{(aq)} + 3e^- \tag{3.7}$$

$$Cl_{2(aq)} + H_2O_{(l)} \rightarrow HCl_{(aq)} + HClO_{(aq)} \tag{3.8}$$

3.2.2.1 Model Assumptions

The model developed was subject to the following assumptions:

- The reactor solution was perfectly mixed.
- There was negligible heat loss to the surroundings.
- The thermal resistance of the reactor wall, separating the jacket and reactor compartments, was neglected in order to allow direct energy transfer between the jacket and reactor compartments of the reactor. This was done because it was observed that the energy equation of the wall displayed the same exact dynamics as that of the jacket temperature. Therefore, it did not add any useful contribution to the model, but was simply an additional equation with little dynamic effect. This reduced the number of equations of the model, hence the number of function evaluations during numerical integrations.
- The solutions were ideal in the model. That is, the chemical substances in solution obeyed Equation 3.9 of Raoult's Law (Luyben 1990a), for which the properties of the solutions were expressed in terms of molar concentrations or partial pressures instead of activity coefficients.

$$P = \sum_{j=1}^{NC} x_j P_j^S \tag{3.9}$$

  where
  P = Total pressure of gas.
  P_j^S = Vapour pressure of pure j_{th} component.
  x_j = Mole fraction of j_{th} component in solution.

- Ideal behaviour of gases, for which the gaseous chemical species obeyed Equation 3.10 of Dalton's Law (Luyben 1990a).

$$P_j = P \cdot y_j \tag{3.10}$$

where
P = Total pressure of gas.
P_j = Partial pressure of j_{th} component in the vapour.
y_j = Mole fraction of j_{th} component in gaseous phase.

3.2.2.2 Size of Model

The reactor was modelled by keeping track of 10 counts of elements taking part in the reactions. The reactor side of the system contained a total of seven elements of which, a solid element (Rh), two in the gas phase (H_2O and Cl_2) and four in the aqueous solution (HCl, H_2O, Cl_2 and $RhCl_3.H_2O$). To simplify the model, hypochlorous acid ($HClO_{(aq)}$) was not taken into account because it was considered to be a by-product of the reactions.The jacket side of the system contained three elements, water and air in the gas phase and only water in the liquid phase. Figure 3.2 below shows the chemical species (in their various phases) captured in the model.

The model was therefore written with a total of 92 equations and variables, of which 14 differential equations described the dynamic behaviour of all state variables and the remaining 78 equations, described the algebraic equations of the system.

3.2.2.3 Model Limitations

The major limitations encountered during the modelling process were as follows:

Consistent initial conditions of model variables. It was difficult to come up with a stable method of automatically computing consistent initial conditions for all 14 state variables of the model. This is because it was found that the actual molar amounts of reactants, loaded into the reactor at the begining of each batch, were not all solutions of the model's 14 differential equations during numerical integrations. Those were necessary to ensure that the integration of all equations was starting from known initial values of correct solutions, which would fully satisfy all model equations at t_0.

Stiffness in model equations. There was presence of stiffness (discussed in section 2.4.3 of Chapter 2) in some of the model's differential equations, which created both fast and slow dynamic changes in those equations at various time steps during numerical integrations.

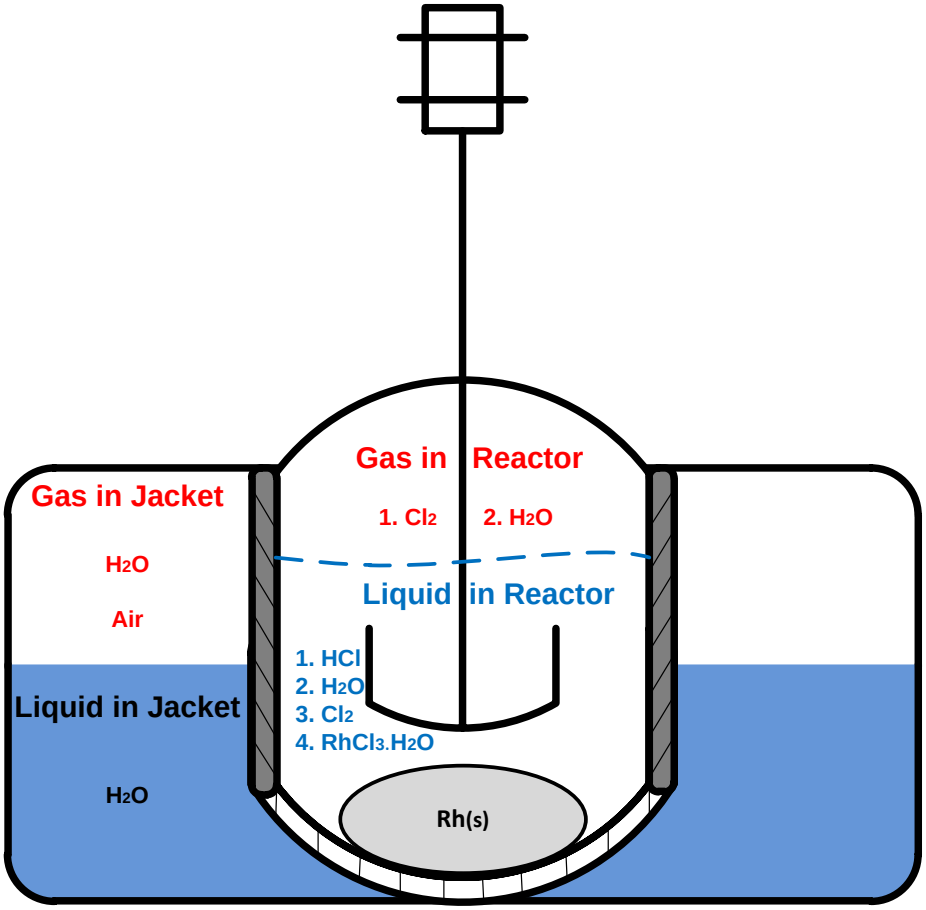

Figure 3.2: Chemical Species in the Model

Stiffness was a consequence of the nonlinearities in the model. It would often cause solver ode15s to fail and prematurely stop numerical integrations, at certain time steps during simulations with certain batches. This is because the appearance of fast dynamics would often generate large derivatives in the equations, which in turn would require the solver to take infinitesimal integration step sizes, in order to successfully integrate those large derivatives. The problem with solver ode15s taking very small step sizes was that, at certain time steps during simulations, those small step sizes would violate the solver's minimum allowable integration step size (tolerance). However, numerical solvers cannot violate their step size tolerance when integrating equations. When that happens, the solver fails to integrate the equations and the simulation prematurely stops. This problem was constantly occuring during simulations and was a serious inconvenience, since no meaningful model responses could be obtained.

3.2.2.4 Model Equations

The full set of model equations written as a system of ODEs and algebraic equations can be seen in Appendix A. The equations were numerically integrated using MATLAB solver ode15s.

The mathematical model presented in this work was written from first-principle as an attempt to capture the essential dynamic behaviour of the chemical, thermodynamic and major transfer phenomena taking place in the real semi-batch reactor system. The simulated responses of the model's temperature and pressure were of particular importance in this study. This is because those were the only output variables for which real plant data was available for model validation.

Computation of Consistent Initial Conditions

In the effort to correctly integrate the model differential equations, ensure that simulations started from correct initial solutions of the equations and that good model performance could be achieved; it was necessary to find consistent initial conditions for all states (derivative) variables of the model. That is, values of all states variables that were true solutions of the model differential equations at the initial time step t_0 had to be found. To that end, the MATLAB solver FSOLVE (The Mathworks 2017) was used to compute consistent initial conditions of the model variables. It finds a solution x for a system (function) of nonlinear equations such that Equation 3.11 applies.

$$F(x) = 0 \tag{3.11}$$

where
F = A function or system of nonlinear equations that returns a scalar value or a vector of values
x = A solution value or a vector of solution values

In our experience writing this model, it was found necessary to constantly conduct trial-and-error adjustments of certain key options, used as input arguments to the FSOLVE routine, in order have it converge towards such values that were true solutions (consitent initial conditions) of the model equations. This task was critical towards achieving good model performance. The following options were interacted with (The Mathworks 2017):

1. **Algorithm:** The optmization algorithm "trust-region-reflective" was used amongst the other two available choices of "levenberg-marquardt" and "trust-region-dogleg".

2. **DiffMaxChange:** A positive scalar selected as the maximum change in variables for finite-difference gradients.
3. **DiffMinChange:** A positive scalar selected as the minimum change in variables for finite-difference gradients.
4. **MaxFunEvals:** A positive scalar selected as the maximum number of function evaluations allowed.
5. **MaxIter:** A positive scalar selected as the maximum number of iterations allowed.
6. **TolFun:** A positive scalar selected as the termination tolerance on the function value.

While searching for consistent initial conditions for a set of equations variables, FSOLVE can stop for the following reasons among others (The Mathworks 2017):

- FSOLVE converged to a solution.
- Change in integration step size is too small.
- Change in residual norm of function evaluation is too small.
- Computed search direction is too small.
- Too many function evaluations or iterations.
- Converged to a point that is not a solution.
- Line search of the optimization algorithm failed.

Default settings of FSOLVE options did not always help obtain good model performance. As a result, they had to be adjusted continuously until good initial conditions were obtained. Whenever consistent initial conditions were not found, the model showed poor simulations performance, and at times, solver ode15s completely failed to integrate the nonlinear equations as it stopped simulations. This task having been done by trial-and-error, better model performance could still be achieved with better tuning of FSOLVE options.

Model of Reactor Pressure

Of critical importance to this model was the mathematical description of the pressure exerted by the total gas in the reactor system, which we refer to as reactor pressure. Ideal behaviour of the total gas (consisted of $Cl_{2(g)}$ and $H_2O_{(g)}$) in the reactor was assumed in this work, from which the reactor pressure was modelled according to the Ideal Gas Law (Equation 3.12).

$$PV = nRT \tag{3.12}$$

where
P = Pressure of reactor model (kPa)
V = Volume of total gas in reactor model (m^3)
n = Total moles of gas in reactor model (kmol)
R = Universal gas constant (kJ/(kmol.K))
T = Temperature (K)

As presented in Section 3.1 describing the chemical process in the reactor system, it was understood that $Cl_{2(g)}$ was pumped into the reactor to maintain its pressure to the required value of 300 kPa (gauge) during the reaction phase. As $Cl_{2(g)}$ was added into the reactor, some of it dissolved into the reactor solution of $HCl_{(aq)}$ to form some $Cl_{2(aq)}$, which in turn reacted with $H_2O_{(l)}$ to produce some more $HCl_{(aq)}$. Modelling the the solubility of $Cl_{2(g)}$ into the reactor solution has been a major difficulty in this work. This is because various first-principle approaches were followed in an effort to capture the mass transfer of Cl_2 from the gas to the solution phases. We experienced some unsatisfactory behaviour of the model as solver ode15s would often fail to integrate the model equations and prematurely stop simulations due to issues related to nonlinearity in the model.

As discussed in Section 2.3.2.1 of Chapter 2, presenting the various steps in first-principle modelling, the work of developing first-principle models can often require significant efforts of trial-and-error, as various candidate models can be suggested until satisfactory model responses are obtained.

First Approach to Modelling $Cl_{2(g)}$ Solubility:

The solubility of $Cl_{2(g)}$ into the reactor solution was initially modelled as presented in Equation 3.13, where the molar quantity of $Cl_{2(g)}$ dissolving into the reactor solution was written as follows:

$$F_{Cl_{2(l-g)}} = k_{Cl_2} \cdot (P_{Cl_{2(g)}} - P_{Cl_{2(aq)}}) \tag{3.13}$$

where
$F_{Cl_{2(l-g)}}$ = Flow rate of $Cl_{2(g)}$ dissolving into reactor solution (kmol/min)
k_{Cl_2} = Mass transfer coefficient (kmol/kPa)
$P_{Cl_{2(aq)}}$ = Vapour pressure created by evaporated solute $Cl_{2(aq)}$ from reactor solution into gaseous phase (kPa)
$P_{Cl_{2(g)}}$ = Total partial pressure of $Cl_{2(g)}$ present into reactor (kPa)

With Equation 3.13, solver ode15s failed to integrate the model equations as it stopped simulations prematurely. The variables $P_{Cl_{2(aq)}}$ and $P_{Cl_{2(g)}}$ were respectively modelled from Raoult's law (Equation 3.14), from which $P_{Cl_{2(aq)}}$ is directly proportional to a measure of concentration (mole fraction) of $Cl_{2(aq)}$ that builds up in the reactor solution during the reaction phase; and Dalton's law (Equation 3.15), which relates $P_{Cl_{2(g)}}$ to the mole fraction of $Cl_{2(g)}$ in the reactor, as described by Luyben 1990a. Those equations were written in accordance with the basic model assumptions made, that the solution and vapour phases in the model displayed ideal behaviour (see Section 3.2.2.1 of Model Assumptions).

$$P_{Cl_{2(aq)}} = x_{Cl_{2(aq)}} \cdot P^o_{Cl_{2(g)}} \tag{3.14}$$

$$P_{Cl_{2(g)}} = y_{Cl_{2(g)}} \cdot P_{(gas)} \tag{3.15}$$

$P^o_{Cl_{2(g)}}$ = Vapour pressure of pure $Cl_{2(g)}$ at standard conditions (kPa)
$x_{Cl_{2(aq)}}$ = Mole fraction of $Cl_{2(aq)}$ in reactor solution
$y_{Cl_{2(g)}}$ = Mole fraction of $Cl_{2(g)}$ in the reactor gas
$P_{(gas)}$ = Total pressure of gas in reactor (kPa)

Second Approach to Modelling $Cl_{2(g)}$ Solubility:

Alkan et al. 2005 have conducted a study on the solubility of $Cl_{2(g)}$ in aqueous hydrochloric acid solutions from which, an empirical model of the solubility of $Cl_{2(g)}$ was proposed and written in terms of the concentration of $HCl_{(aq)}$ and temperature of the solution, as presented in Equation 3.16.

$$C_{Cl_{2(aq)}} = 4.46 \cdot 10^{-8} exp\Big(\frac{2927}{T}\Big)\Big[- 10.73(C_{HCl})^{3/2} + 63.55(C_{HCl}) - \ldots \\ 89.41(C_{HCl})^{1/2} + 92.02\Big] \tag{3.16}$$

$C_{Cl_{2(aq)}}$ = Solubility of $Cl_{2(g)}$ in $HCl_{(aq)}$ solution (kmol/m^3)
C_{HCl} = Concentration of $HCl_{(aq)}$ solution (kmol/m^3)
T = Temperature of solution (K)

Their experimentation was conducted at constant atmospheric pressure of 81.33 kPa in Erzurum (Turkey), for concentrations of $HCl_{(aq)}$ varying from 0 kmol/m^3 to 7 kmol/m^3 and temperatures varying from 20 $^{\circ}C$ to 70 $^{\circ}C$. Though an interresting study, the conditions at which it was conducted did not quite match those of our reactions which took place at a $HCl_{(aq)}$ concentration of 11.5 kmol/m^3, and especially at a much higher pressure of 300 kPa (gauge). Because of those considerable differences in process conditions, we could not effectively make use of their empirical model as a reliable estimate for the solubility of $Cl_{2(g)}$ in our reactor solution of $HCl_{(aq)}$. However, we still attempted to run our reactor model with Equation 3.16, but no simulated results could be obtained as the simulation ran for about 2 hours and the MATLAB session froze to the point where we had to abort it. We believe that this behaviour was due to numerical problems arising from the occurence of possible modelling errors, inapropriate options settings of the FSOLVE numerical optimization routine, and difficulties encountered by FSOLVE to converge to consistent initial conditions of the model state variables.

No further attempt was then made to troubleshoot the reactor model such that it could work with Equation 3.16. Instead, we kept looking for alternative methods of modelling the solubility of $Cl_{2(g)}$ that would enable the model to run with little to no complications.

Third Approach to Modelling $Cl_{2(g)}$ Solubility:

Another approach followed was that described by Henry's law, discussed in section 2.5 of Chapter 2, from which it is known that the solubility of a gas into a solution is affected by the pressure exerted by the gas onto the solution. Therefore, the solubility of $Cl_{2(g)}$ in the reactor solution of $HCl_{(aq)}$, to generate a concentration of $Cl_{2(aq)}$, can be derived as a fucntion of the partial pressure of $Cl_{2(g)}$ and its corresponding Henry's law solubility constant (Equation 3.17):

$$C_{Cl_{2(aq)}} = H^{CP} \cdot P_{Cl_{2(g)}} \tag{3.17}$$

where
H^{CP} = Henry's law solubility constant (kmol/(m^3.kPa))
$C_{Cl_{2(aq)}}$ = Concentration of $Cl_{2(g)}$ dissolved into $HCl_{(aq)}$ solution (kmol/m^3)
$P_{Cl_{2(g)}}$ = Partial pressure of $Cl_{2(g)}$ into reactor (kPa)

However, the issue with Equation 3.17 was that an estimate of the Henry's law solubility constant (H^{CP}) of $Cl_{2(g)}$ dissolving into the $HCl_{(aq)}$ solution must have been evaluated at similar conditions to our reactions processes. This constant H^{CP} was not available to us since we could not obtain information of an estimate of it

from litterature, and did not conduct any laboratory experiments to estimate it.

Some trial runs of the model were done with Equations 3.17, using the Henry's law solubility constant of $Cl_{2(g)}$ in water, but the simulations stopped as solver ode15s failed to integrate the model. An example of warning messages we obtained read as follows:

"Warning: Failure at t = 4.110822. Unable to meet integration tolerances without reducing the step size below the smallest value allowed (1.421085e-014) at t."

The simulation time for this particular batch was only 4 minutes instead of the normal 191 minutes (about 3 hours and 18 minutes). The warning message above informed us that solver ode15s could not integrate certain differential equations of the model, which we could not clearly identify, beyond the simulation time step of 4 minutes. The numerical integration failed because some equations had fast nonlinear dynamics within infinitesimal integration step sizes. The solver step size tolerance of 1.421085×10^{-14} was reached and could not be violated during the numerical integration of the model.

Fourth Approach to Modelling $Cl_{2(g)}$ Solubility:

After numerous trial-and-error efforts to adjust the solubility equation of $Cl_{2(g)}$ and to find good consistent initial conditions of model equations, we successfully estimated the solubility of $Cl_{2(g)}$ into the reactor solution. This was achieved by modelling the molar flowrate of $Cl_{2(g)}$ dissolving into solution as the difference between the molar quantities of $Cl_{2(g)}$ and $Cl_{2(aq)}$ inside the reactor, as shown in Equation 3.18.

$$F_{\mathrm{Cl}_{2(\mathrm{l-g})}} = C_{\mathrm{Cl}_{2(\mathrm{g})}} \cdot V_{gas} - C_{\mathrm{Cl}_{2(\mathrm{aq})}} \cdot V_{sol} \tag{3.18}$$

where
$F_{Cl_{2(l-g)}}$ = Flowrate of $Cl_{2(g)}$ dissolving into reactor solution (kmol/min)
$C_{Cl_{2(aq)}}$ = Molar concentration of $Cl_{2(aq)}$ in solution (kmol/m^3)
$C_{Cl_{2(g)}}$ = Molar concentration of $Cl_{2(g)}$ in gas phase (kmol/m^3)
V_{gas} = Total volume of gas in reactor (m^3)
V_{sol} = Total volume of solution in reactor (m^3)

Equation 3.18 worked well for model simulations and the benefits of implementing it were the following:

- The numerical solver ode15s could integrate the model equations and generate simulated responses over the full simulation time span of every batch,

without the solver failing and prematurely stopping the simulations due to numerical problems and nonlinearity in the model.

- The equation could be directly used as an additional term to the molar differential equations of Cl_2 in both gaseous and solution phases, as given in Equations 3.19 and 3.20:

$$\frac{dN_{\mathrm{Cl}_{2(\mathrm{g})}}}{dt} = F^{In}_{\mathrm{Cl}_{2(\mathrm{g})}} - F_{\mathrm{Cl}_{2(\mathrm{l-g})}} \tag{3.19}$$

$$\frac{dN_{\mathrm{Cl}_{2(\mathrm{aq})}}}{dt} = -\frac{1}{2} r_2 V_{\mathrm{sol}} + F_{\mathrm{Cl}_{2(\mathrm{l-g})}} \tag{3.20}$$

where
$F^{In}_{Cl_{2(g)}}$ = Input data of $Cl_{2(g)}$ flow rate pumped into reactor (kmol/min)
r_2 = Rate of reaction of $Cl_{2(aq)}$ with $H_2O_{(l)}$ (kmol/(m^3.min))
N = Moles of chemical species (kmol)

- The modelled concenrations of the Cl_2 in the gas and solution phases were affected by the solubility of $Cl_{2(g)}$ in the reactor solution (Equation 3.18).

- At last, model simuations generated sensible responses for most states and algebraic variables of the system, since they displayed such dynamic trends that were consistent with the input variables of utilities and $Cl_{2(g)}$ flow rates the model was subjected to.

3.2.2.5 Accuracy of Model Responses

When simulating the model, it was necessary to verify the consistency of its responses. The model had to demonstrate good qualitative and quantitative responses, following the dynamics of the various input variables to which it was subjected. An important part of verifying the model's consistency was to ensure that solver ode15s converged towards correct solutions of the equations. This was done through validation, by qualitatively observing how well the model simulated responses compared to the real plant data. The more stable and closer the model responses were to plant data, the more accurate the integrated solutions of model equations were deduced.

An estimate of the overall model performance, the mean absolute error of model responses was used as an index to quantify the accuracy of the model responses in comparison to plant data. This was computed as shown in Equations 3.21 and 3.22, where the latter was calculated by subtracting the mean absolute error of Equation 3.21 from the point of perfect accuracy of 100 percent.

$$Mean\ Absolute\ Error = \frac{100\ \%}{N} \sum_{t=1}^{N} \frac{|Data(t) - Model\ Response(t)|}{|Data(t)|} \tag{3.21}$$

$$Model\ Accuracy = 100\ \% \ - Mean\ Absolute\ Error \tag{3.22}$$

Where
N = Length of the simulation time span
t = Time steps
Data = Batch measurements

3.2.2.6 Model Validation

The model was validated by comparing the simulated response of temperature of reactor and that of pressure of gas, to some plant data sets covering 45 batches of the real reactor's operation. The concentrations of all chemical species in the model could not be confronted with real plant data because they were not available to that effect. However, consistent and reasonable simulated responses of the moles of all chemical species present in the reactor solution were obtained, as shown in the next chapter.

Chapter 4

Results and Discussion

This chapter covers the results obtained from the various simulation runs of the model, along with their discussion. It presents two cases of some of the good model responses that were generated, where the simulation responses compared well to the data sets of two batch runs of the real reactor. The chapter also gives an example of a batch which generated poor simulation responses. This is to give an account of the model limitations as seen through its performance.

4.1 Model of Explicit ODEs

This section discusses the performance of the model in terms of stability of the temperature and pressure responses, as well as how well they tracked the sets of real plant measurements they were compared to during validation. The quality of the model responses was used to deduce the correctness of the numerically integrated solutions of all differential equations. The concentrations of the chemical species in the reactor were not validated, since no data was available to that effect.

Since the full set of results for all 45 batches of plant data at our disposal could not be presented in this report, this section only covers the results for two cases of the good simulations obtained. In those simulations, the model demonstrated good prediction of temperature and pressure data. The section also presents a case of a poor simulation obtained, in which the model responses (especially pressure) showed large deviations from the batch data. However, in order to account for the model performance with the full set of 45 batches of data used to validate it, the chapter lastly presents the percentage accuracy of the model temperature and pressure responses for all simulations done.

4.1.1 Good Simulation Responses

Amongst all simulation runs, the two cases of batches 33 and 34 were selected to present and discuss the good performance of the model responses. The simulations were run on a computer, with processor specifications of Intel(R) Core(TM) i5-3337U CPU, 1.80 GHz and an installed memory (RAM) of 6 GB.

The dynamic responses of the main variables (temperature and pressure) of interest for validation are given. Also presented are: an evaluation of the consistent initial conditions of the model derivative (state) variables; the dynamics of the two reaction rates of the chemical process; the molar dynamics of all chemical species interacting in the reactor (reactants and products); the thermodynamic contribution of the exothermic reactions to the reactor temperature dynamics; and finally a measure of the absolute error, resulting from the model temperature and pressure responses, together with their accuracies as compared to plant data.

4.1.1.1 Case 1

This case presents the validation of model temperature and pressure responses, covering about four hours of operation. In this run, the model was simulated with the same input plant data of steam, cooling water and chlorine gas flow rates as that of batch 33, which generated the plant output data of temperature and

pressure, which the model responses were compared to. The simulation ran for about 4 minutes on computer, throughout the full simulation time span of 236 minutes of this batch, without solver ode15s stopping the simulation run.

Consistent Initial Conditions

Initial values of the model states variables determine the starting points of the dynamic behaviour of these variables, as discussed in Section 3.2.2.4 of Chapter 3. Table 4.1 below shows a comparison of 3 sets of the initial values of the states variables in the reactor compartment of the system.

Table 4.1: Initial Conditions of Reactor State Variables

State Variables	**Values of Initial Conditions**		
	Guessed	**Consistent**	**Integrated**
moles of $Rh_{(s)}$ (kmol)	0.2693	0.2693	0.2334
moles of $HCl_{(aq)}$	6.2790	0.0000415	0.0000337
moles of $H_2O_{(l)}$	2.0930	2.0930	1.9457
moles of $Cl_{2(aq)}$	1.0465	0.5432	0.5170
$RhCl_3(H_2O)_{(aq)}$	0.0010	0.0010	0.0370
moles of $H_2O_{(g)}$	0.0001	0.0010	0.0010
moles of $Cl_{2(g)}$	0.0398	0.5433	0.5172
$T_{reactor}$ (K)	290.9189	290.8944	290.9156

The first column of values shows guessed values assigned to the model states variables based on information known of the process. The moles of $Rh_{(s)}$ were calculated from the amount of Rhodium sponge that was loaded into the reactor (29 kg), as well as the moles of $HCl_{(aq)}$ (546 L at a concentration of 11.5 kmol/m^3), the moles of $Cl_{2(g)}$ read from its flowrate plant data and the reactor temperature read from data. The values of these 4 variables were calculated from information of the process and were known to be correct, the remaining variables were all estimated.

The second column shows the consistent initial values of the state variables, as computed from the FSOLVE routine of MATLAB. During this task, FSOLVE converged to values that were correct solutions to the differential equations, as it can be seen from Figure 4.1, in which the system being at steady state at the initial time step (t_0), all differential equations became zero when evaluated at those values. However, from the columns of guessed to consistent values, considerable differences could be seen in the molar values of $HCl_{(aq)}$ which dropped from 6.27 kmol (actual amount loaded into the reactor) to a very small value.

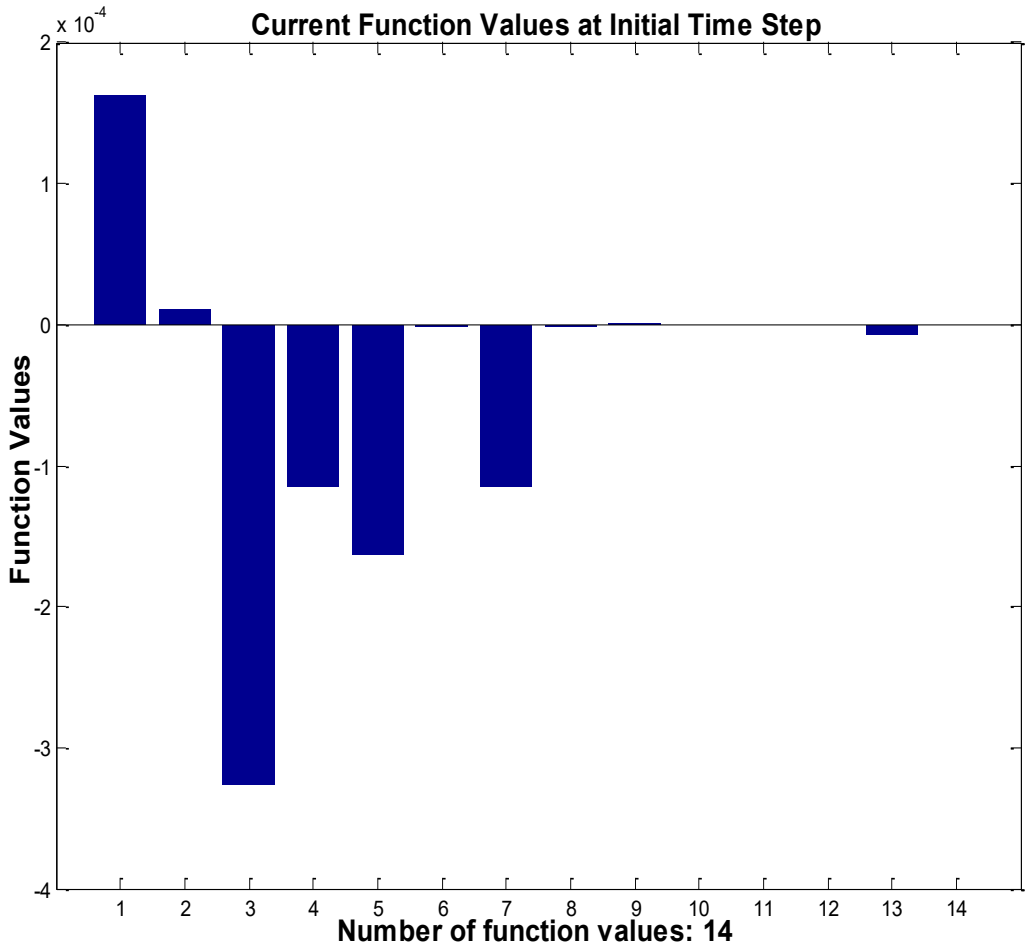

Figure 4.1: Function Evaluation at Initial Conditions

The moles of $Cl_{2(g)}$ significantly inceased from 0.0398 kmol (read from data) to 0.533 kmol. It will be seen in the model responses that those changes which occurred during simulations have affected the dynamics of the model responses. An attempt was made to run the model with the initial guessed values from the first column of values in Table 4.1, but solver ode15s stopped the simulation as it could not integrate the equations due to the occurence of large derivatives at certain simulation time steps, which were believed to be caused by the nonlinearities in the model equations. This was a reccuring numerical difficulty that we had experienced in this work.

The third column shows solver ode15s numerically integrated solutions of the model equations at t_0. They were seen to be much closer to those of the second column. This proves that the integrated solutions of model equations were

greatly affected by the consistent intial values (conditions) of the state variables of a system, expected to be true solutions to the model equations. A possible interpretation of the significant changes seen in the molar values of $HCl_{(aq)}$ and $Cl_{2(g)}$ accross the three columns of values could be that, the mathematical equations describing the dynamics of those two chemical species might be incomplete for the real system they are trying to mimic. This effectively means that their equations, as written in the model, might not be the correct ones for which the actual molar amounts of $HCl_{(aq)}$ (6.279 kmol) and $Cl_{2(g)}$ (0.0398 kmol), calculated from the amounts of reactants known to have been loaded into the reactor, could be true solutions of. This could also result from the fact that we did not know the exact chemistry of this process as already discussed in Section 3.1 of Chapter 3.

Rates of Reactions

The reaction rates r_1 and r_2 of the two chemical reactions taking place in the reactor, namely the dissolution of the crude rhodium sponge ($Rh_{(s)}$) in the solution of $HCl_{(aq)}$ and the reaction of $Cl_{2(aq)}$ with $H_2O_{(aq)}$ to produce $HCl_{(aq)}$, were modelled as given by Equations A.22 and A.23 respectively, in Section A of Model Equations in Appendix A. The reaction rate constants (k_{r1}, k_{r2}), used in both reaction rates equations were modelled according to the Arrhenius Law given by Equation A.20. Values for the reaction kinetics parameters of activation energies (E_{a1}, E_{a2}) and frequency factors (k_1, k_2), used in the Arrhenius Law, were all assumed as we could not get information about their estimated values in litterature. They are presented in Table B.3 of Section B.3 in Appendix B. Figure 4.2 presents the dynamics of the reaction rates that were generated during this simulation run. Both reaction rates were seen to display similar dynamics over time, with the rate of $HCl_{(aq)}$ formation (r_2) being almost three times that of the rate of $Rh_{(s)}$ dissolution (r_1).

Molar Dynamics of Chemical Species

Figure 4.3 displays the molar dynamics of all the chemical species interacting in the reactor solution. The model demonstrated stable molar responses, for which no negative values of moles were generated, and the simulated moles of reactants and products showed consistent and realistic dynamic trends. The moles of $H_2O_{(l)}$ and $Rh_{(s)}$ decreased over time as $H_2O_{(l)}$ reacted with $Cl_{2(aq)}$ to produce more $HCl_{(aq)}$ and $Rh_{(s)}$ dissolved into the reactor solution of $HCl_{(aq)}$. However, the moles of $HCl_{(aq)}$ and $Cl_{2(aq)}$ showed increasing trends over the simulation time span, similar to those of the rates r_1 and r_2 of the two reactions of the process given in Figure 4.2. This is because, although consumed in the dissolution reaction, $HCl_{(aq)}$ was also a product of the second reaction of $Cl_{2(aq)}$ and $H_2O_{(aq)}$. The moles of

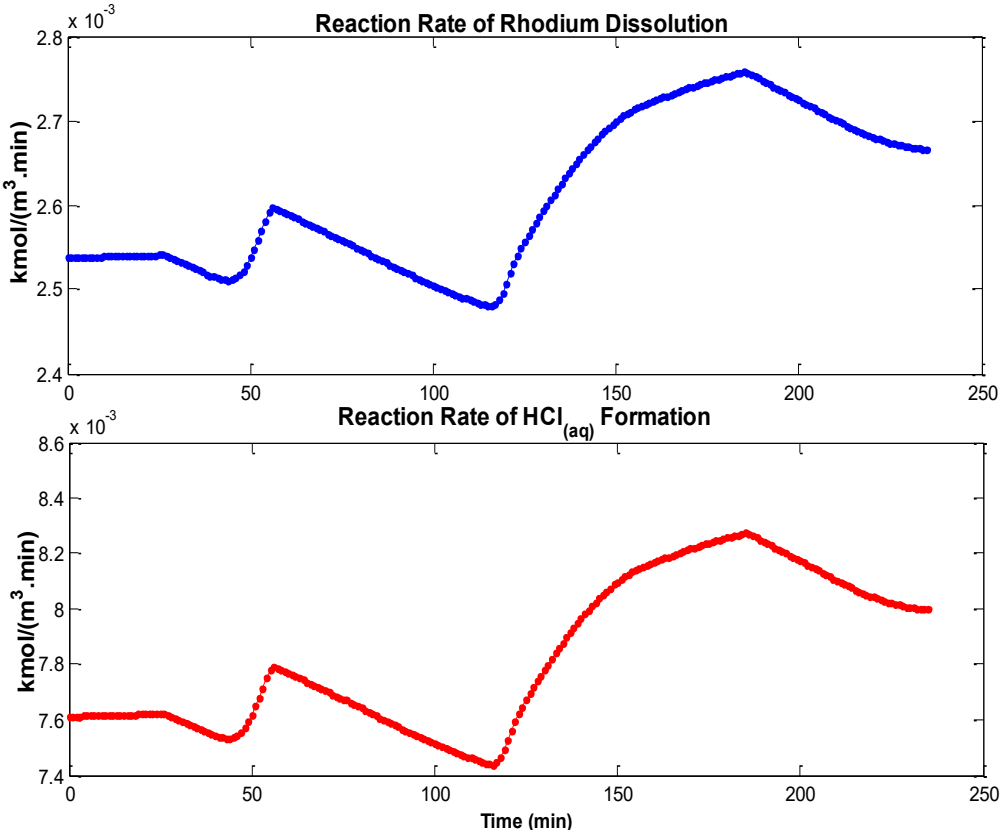

Figure 4.2: Reaction Rates

$Cl_{2(aq)}$ increased because gaseous $Cl_{2(g)}$ dissolved into the reactor solution during the reaction phase of the process. Therefore, the simulated moles of $HCl_{(aq)}$ and $Cl_{2(aq)}$ shown in Figure 4.3 were the overall amounts generated from all chemical reactions and phase transfer dynamics occuring in the reactor.

As already discussed in the section of consistent initial conditions, the plot of molar responses also showed very small amount of $HCl_{(aq)}$ (about 4.2 $\times 10^{-5}$) at the initial time step, instead of the calculated actual amount of 6.279 kmol that is known to have been loaded into the real reactor. This is because the model could not reproduce that same molar amount of $HCl_{(aq)}$ that was initially loaded into the reactor, since that value was found not to be a consistent (true) solution to the modelled differential equation of $HCl_{(aq)}$. It was written, according to the dynamics of the two chemical reactions of this process, as shown by Equation A.30 in Appendix A. Finally, Figure 4.3 also shows the molar dynamics of rhodium(III) chloride ($RhCl_3(H_2O)_{(aq)}$) to increase over the simulation time span as expected. This species was the main product of the dissolution reaction of crude rhodium

sponge ($Rh_{(s)}$) in $HCl_{(aq)}$.

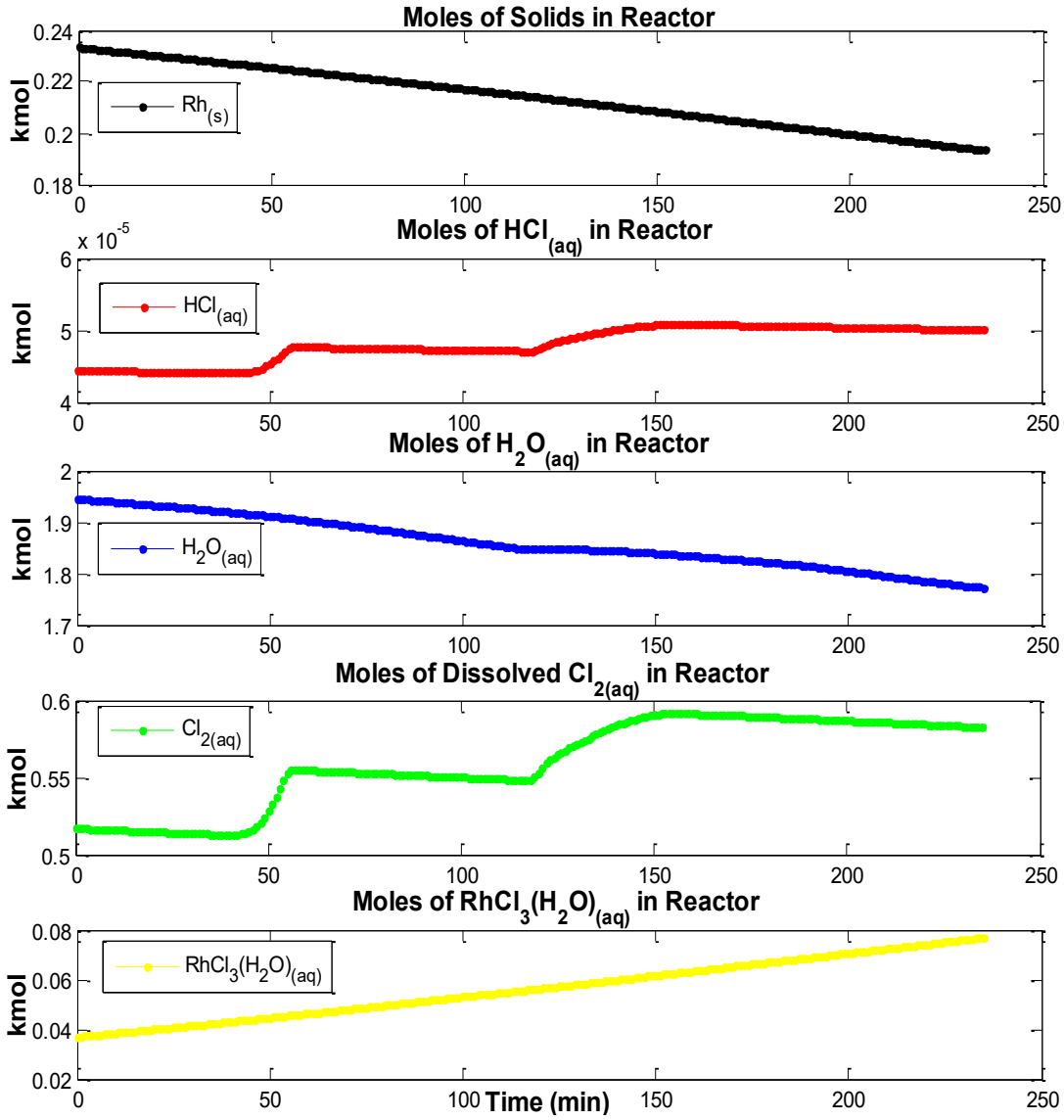

Figure 4.3: Moles of Chemical Species in Reactor Solution

Temperature Response

The simulated responses of the reactor and jacket temperatures are seen in Figure 4.4. The plant data of steam and cooling water flowrates was passed as inputs variables into the model during simulations. Steam was kept at a fixed temperature of 115 $°C$ (388 K), whereas the temperature of cooling water was read from

the data and passed to the model as an additional input variable. The values of supplied cooling water temperature varied between 19 to 22 $^{\circ}C$ for this batch.

A few observations can be made from the temperature responses obtained. The reactor temperature showed a good qualitative response as compared to its plant data. The simulated temperature increased when steam was added into the jacket and dropped when cooling water was pumped in order to cool the reactor. Those temperature dynamics occurred within almost similar time intervals as the plant temperature data. Figure 4.4 also shows that the dynamics of the jacket and reactor temperatures were faster than those of the temperature data. This is seen from the fact that unlike temprature data, the modelled temperatures showed no dead time in their responses as utilities were pumped into the jacket. This result could be due to the fact that the thermal dynamics of the reactor wall were neglected, in an effort to reduce the size of the model to a simpler system of fewer equations, which we could easilly solve numerically and had already managed to run succesfully without solver ode15s prematurely stopping the simulation.

Another possible explaination to the responses observed could be that there may have been some mathematical limitation in the modelled equation of jacket temperature, which we have formulated to the best of our understanding of the process. Because the modelled reactor temperature has shown to be quite responsive to the dynamics of the jacket temperature, we believe that a more realistic numerical implimentation (modelling and integration) of the jacket temperature differential equation, could possibly generate a reactor temperature response that would demonstrate better prediction of the temperature data of the real reactor. Finally, the reactor temperature was also seen to show noticeable deviation from the plant temperature data, from the time step of about 180 minutes. This was due to the effect of heat generated from the reactions, as seen in the next section.

Thermodynamic Contribution of Reactions

The detailed thermodynamic contribution of the exothermic reactions of the process is given in Figure 4.5. The figure shows two subfigures: in the first, Figure 4.5a, gives the overall thermodynamic contributions of both the exothermic chemical reactions (heat generated) and the utility inputs to the reactor temperature dynamics; the second, Figure 4.5b, gives the heat generated by each chemical species interacting in the reactions, which all contributed to the total heat generated by the reactions (seen in the second bottom subplot of Figure 4.5a). Figure 4.5a shows that the reactions have generated significant energy during the reaction phase. This can explain the observation made earlier about the simulated reactor

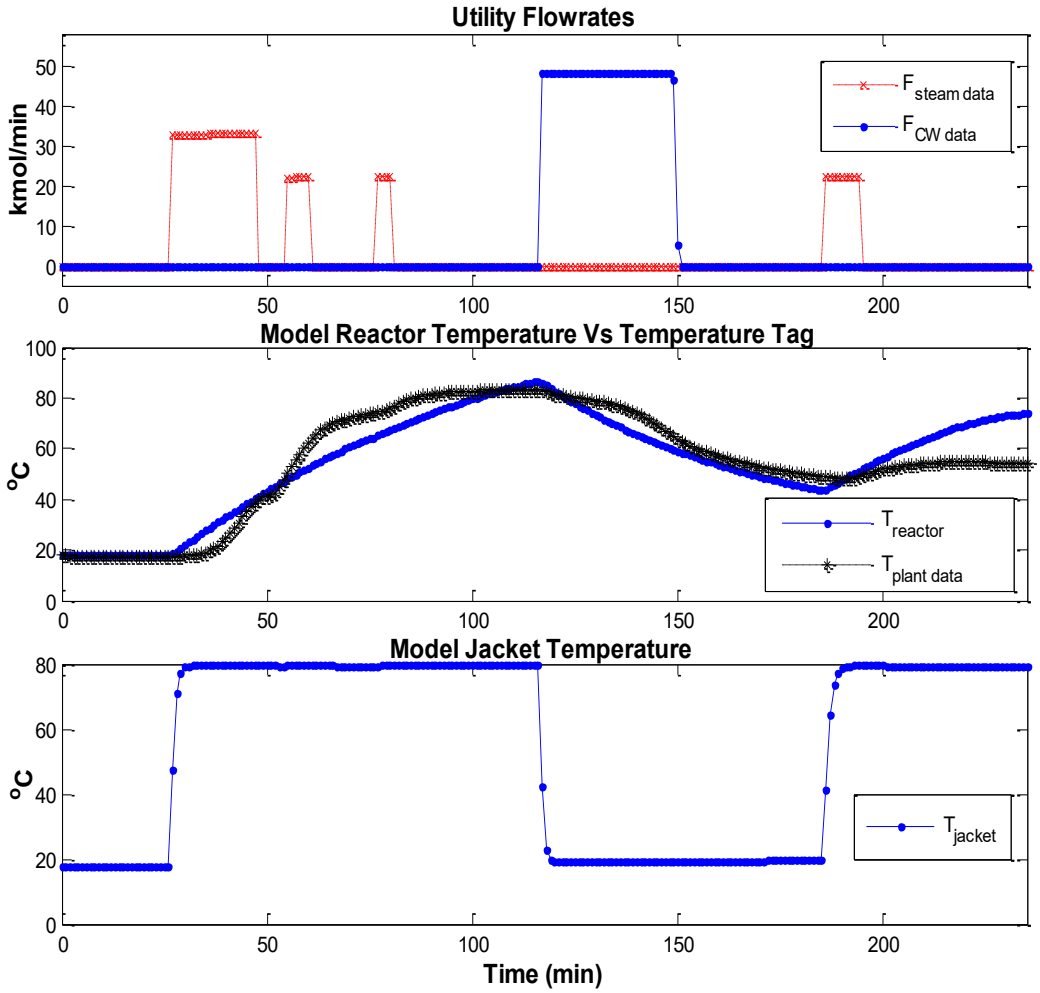

Figure 4.4: Dynamics of Jacket and Reactor Temperatures

temperature deviating from its plant data at the time step of about 180 minutes. The utilities in the second subplot of Figure 4.5a showed realistic dynamics as heat transferred from the jacket to the reactor compartment of the reactor decreased over time as steam was pumped into the jacket. The cooling water cold utility absorbed more heat over time as it cooled the reactor. A closer look at Figure 4.5b revealed that the chemical species of $Cl_{2(aq)}$, $RhCl_3(H_2O)_{(aq)}$ and $Rh_{(s)}$ generated the most energy in the process. Whereas, the species of $H_2O_{(aq)}$ and $HCl_{(aq)}$, as well as the vaporized water made the smallest contributions to the process overall heat of reactions.

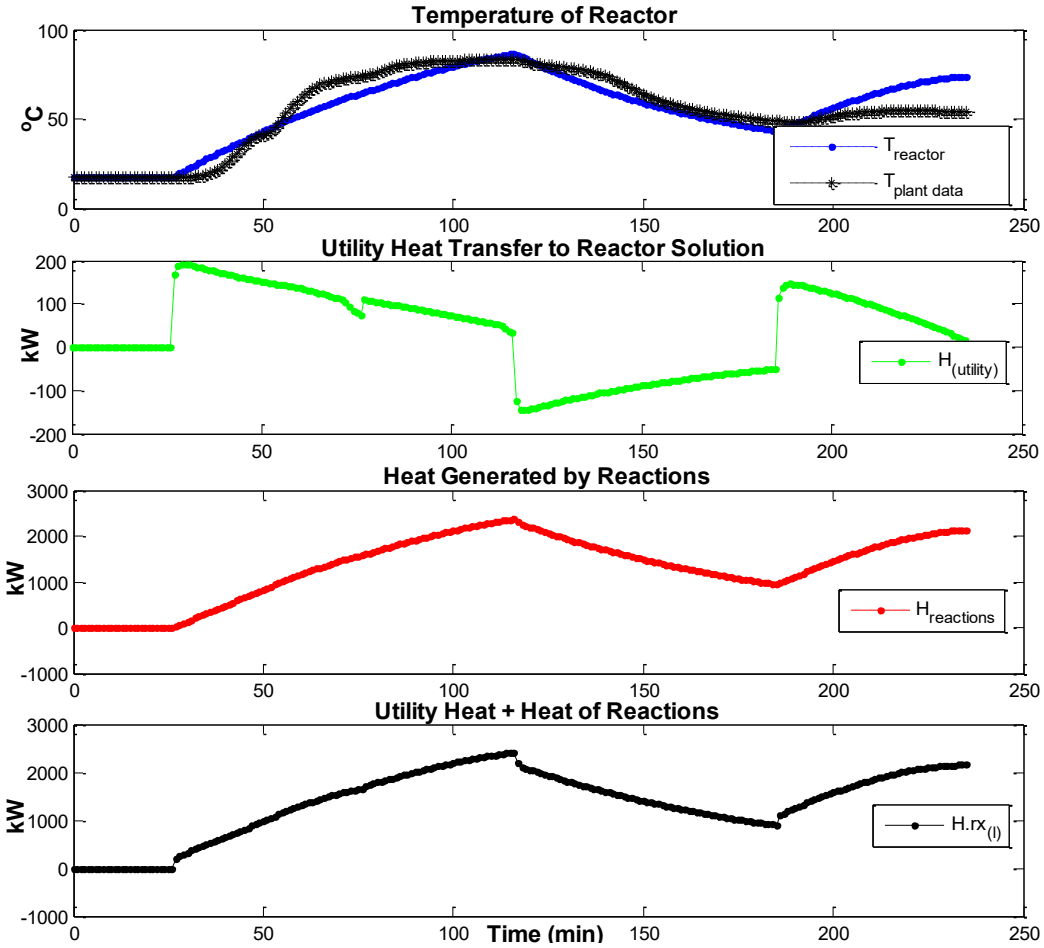

(a) Overall Heat of Reactions

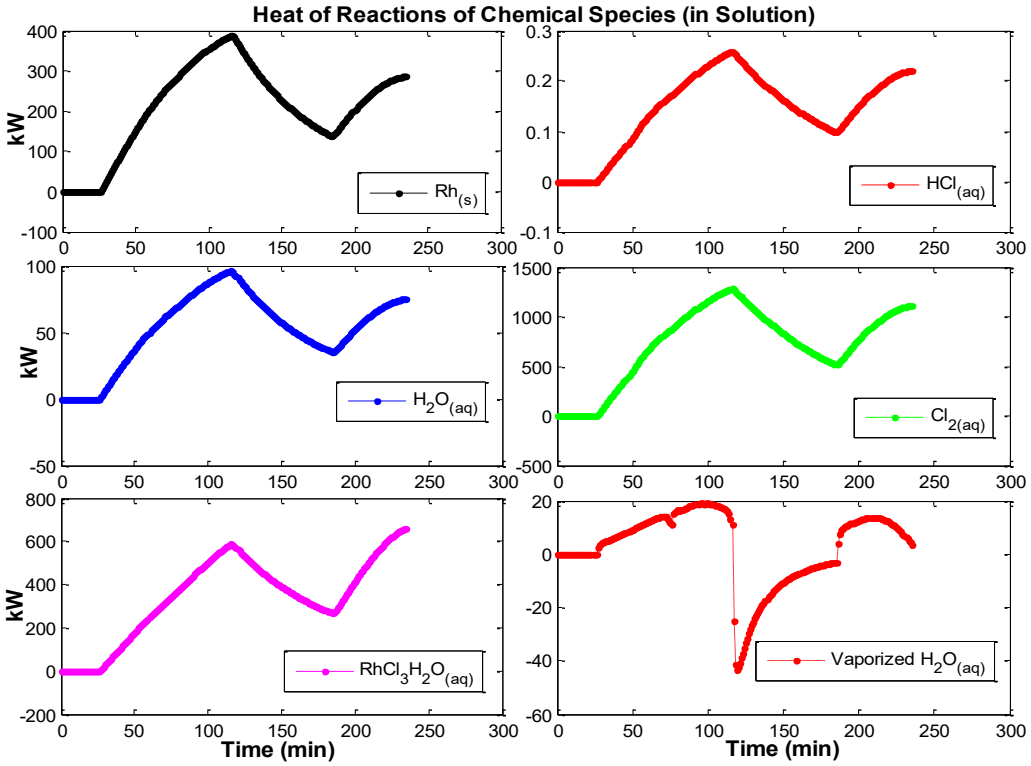

(b) Species Heat of Reactions

Figure 4.5: Contributions of Process Heat of Reactions

Pressure Response

Figure 4.6 shows in two subfigures the detailed dynamics of all the variables that affected the simulated pressure response of the reactor model. The first subfigure, Figure 4.6a, gives the molar dynamics of the gaseous species of $Cl_{2(g)}$ and $H_2O_{(g)}$ in the reactor; the second subfigure, Figure 4.6b, presents three subplots of simulated dynamics, from which the top subplot shows the dynamics of the flowrate data of $Cl_{2(g)}$ passed into the model as an input variable, as well as the modelled solubility of $Cl_{2(g)}$ as it dissolved into the reactor solution during the reaction phase. The middle subplot from the top, displays the model pressure response plotted against the pressure plant data of this batch. And the bottom subplot displays the simulated dynamics of the pressure equation, derived from the Ideal Gas Law equation, without the effect of the simulated reactor temperature.

It should be emphasized that since the reactor pressure was modelled according to the Ideal Gas Law equation, the pressure response was directly affected by the dynamics of the model temperature as well as those of the total moles of gaseous species ($Cl_{2(g)}$ and $H_2O_{(g)}$) in the reactor. Furthermore, in all our simulations with the full set of 45 batches of plant data available to us, the model generated such values of consistent initial conditions of the moles of $Cl_{2(g)}$ that were different from the actual values read from plant data. As already discussed in the section of consistent initial conditions, the value of 0.5433 kmol was found to be the solution to the differential equation describing the moles of $Cl_{2(g)}$ in the reactor, instead of the actual value of 0.0398 kmol read from the flowrate data of $Cl_{2(g)}$ at the inital time step (t_0). The consequence of this change in the moles of $Cl_{2(g)}$ at t_0 was that, the pressure response was generated with an offset value of about 700 kPa in this simulation. This means that the simulated pressure response actually started from 800 kPa, with an offset value of 700 kPa above the pressure data. However, we did not succeed to correct this offset from the simulated pressure, as it was directly created by the computed consistent initial molar value of 0.5433 kmol of $Cl_{2(g)}$. In the end, in order to be able to compare the dynamics of the model pressure response to the plant data more efficiently, the offset value was manually subtracted from the simulated pressure response, as an attempt to align it to the same starting value of 100 kPa as the data it was compared to.

The middle subplot of Figure 4.6b shows that the model has demonstrated good qualitative response of the reactor pressure. However, some quantitative deviations could be noticed between the simulated pressure and the pressure data. The model pressure showed to be quite affected by the dynamics of the simulated temperature. This can be seen from the fact that the simulated pressure started

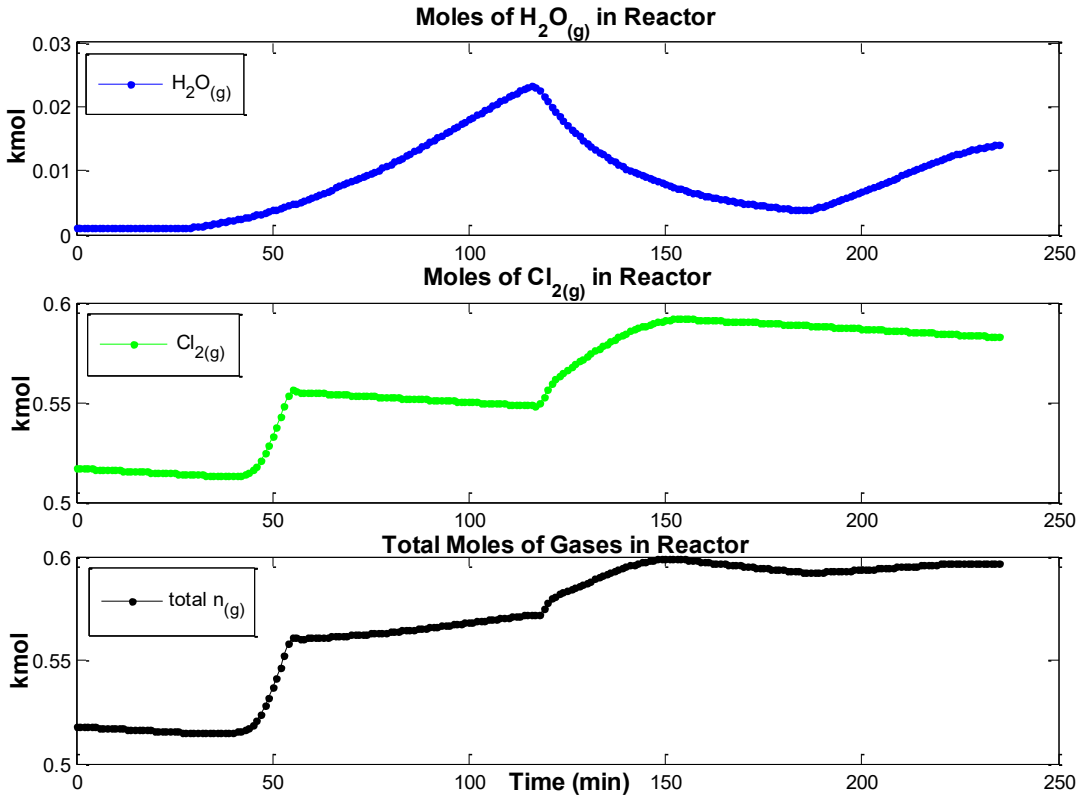

(a) Molar Responses of Gaseous Species

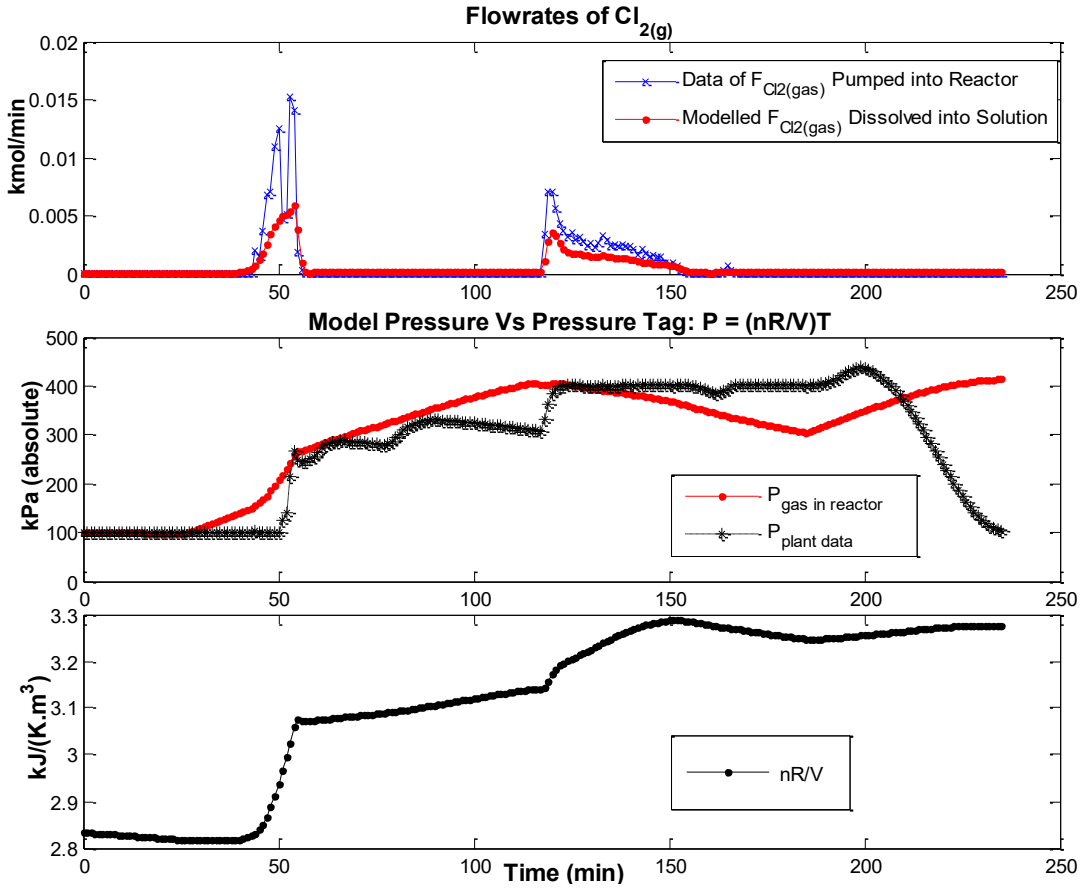

(b) Dynamics of Reactor Pressure Response

Figure 4.6: Pressure Simulation

rising at the simulation time step of 30 minutes, similar to the simulated temperature, where no flowrate of $Cl_{2(g)}$ was even introduced into the model. It also showed similar dynamics as temperature at time steps of 180 minutes and beyond. This behaviour was quite remarquable and we believed it to be expected because of the assumption made, that the pressure of the reactor model obeyed the Ideal Gas Law, which describes that the pressure of a gas is directly proportional to its temperature. However, this assumption was not applicable to the temperature and pressure dynamics of the real reactor, for which deviation from ideal behaviour of the real reactor gas content could be expected, as seen from the plant data of both temperature and pressure.

In order to further support the argument that the assupmtion of ideal gas behaviour has affected the simulated pressure of the reactor, the third subplot of Figure 4.6b shows the dynamics of the pressure equation without the effect of the simulated temperature. Its trend clearly reveals some noticeable differences to the simulated pressure response of the middle subplot, and is seen to display similar dynamics to the total moles of gas inside of the reactor model (seen in the bottom subplot of Figure 4.6a).

Finally, of particular importance to the pressure response was the depressurization of the reactor. The plant data of pressure shows depressurization of the reactor from the time step of 200 minutes, as the reactions reached completion. This drop in pressure could not be due to $Cl_{2(g)}$ dissolving into the reactor solution at the end of the batch, since the input data of $Cl_{2(g)}$ flowrate showed no evidence of such a possibility. Therefore, the pressure drop seen in the plant data of reactor pressure was probably due to some plant air that was sparged into the reactor in order to depressurize it. We did not have data for this plant air available in order to reproduce the depressurization phase of the reactor.

Absolute Error and Model Accuracy

Figure 4.7 gives a quantitative indication of the model performance by displaying the dynamics of generated errors and accuracy of the model simulated temperature and pressure responses, with respect to their plant data. It contains two subfigures, Figure 4.7a displays the errors generated from the simulated temperature and pressure responses, and Figure 4.7b displays the resulting accuracy achieved in those responses. They were calculated at every time step (t) of the simulation time span.

Successful validation of the model was determined by how well the model simulated responses of pressure and temperature tracked their respective plant data.

The absolute error of the model is the idex that we have used to measure the model performance, in terms of the percentage deviation of its simulated temperature and pressure responses from their data. The absolute error is a consequence of the model performance, in terms of stability of its responses and accuracy of the numerically integrated solutions of all equations. Equation 4.1 below gives the method we used to compute it.

$$Model\ Absolute\ Error = 100\ \% \times \frac{\Big|\big|Data(t)\big| - \big|Model\ Response(t)\big|\Big|}{\Big|Data(t)\Big|} \tag{4.1}$$

Figure 4.7a displaying the dynamics of the model errors, reveals that the model generated better tracking of temperature data than pressure data. This can be seen from the fact that, the simulated temperature response has generated smaller errors, on average, than the pressure response. The model temperature never reached the point of maximum error that was fixed at 100 %, with its maximum error reaching the value of only about 46 %, in comparison to the pressure response that reached the limit of maximum error of 100 % at various time steps.

In addition to the absolute error, the percentage accuracy of the model responses was computed as the numerical index representing the overall accuracy of the model. Equation 4.3 shows the method followed to estimate that index. It was calculated by subtracting the mean absolute error of Equation 4.2 from the point of perfect accuracy of 100 percent. The interpretation of this index was that the smaller the mean absolute error the more accurate the model responses.

$$Mean\ Absolute\ Error = \frac{100\ \%}{N} \sum_{t=1}^{N} \frac{|Data(t) - Model\ Response(t)|}{|Data(t)|} \tag{4.2}$$

$$Model\ Accuracy = 100\ \% \quad - Mean\ Absolute\ Error \tag{4.3}$$

Where
N = Length of the simulation time span
t = Time step
Data = Plant measurements

The model responses of this simulation run achieved on average, 89% accuracy in the reactor temperature response and 79% accuracy in the reactor pressure response.

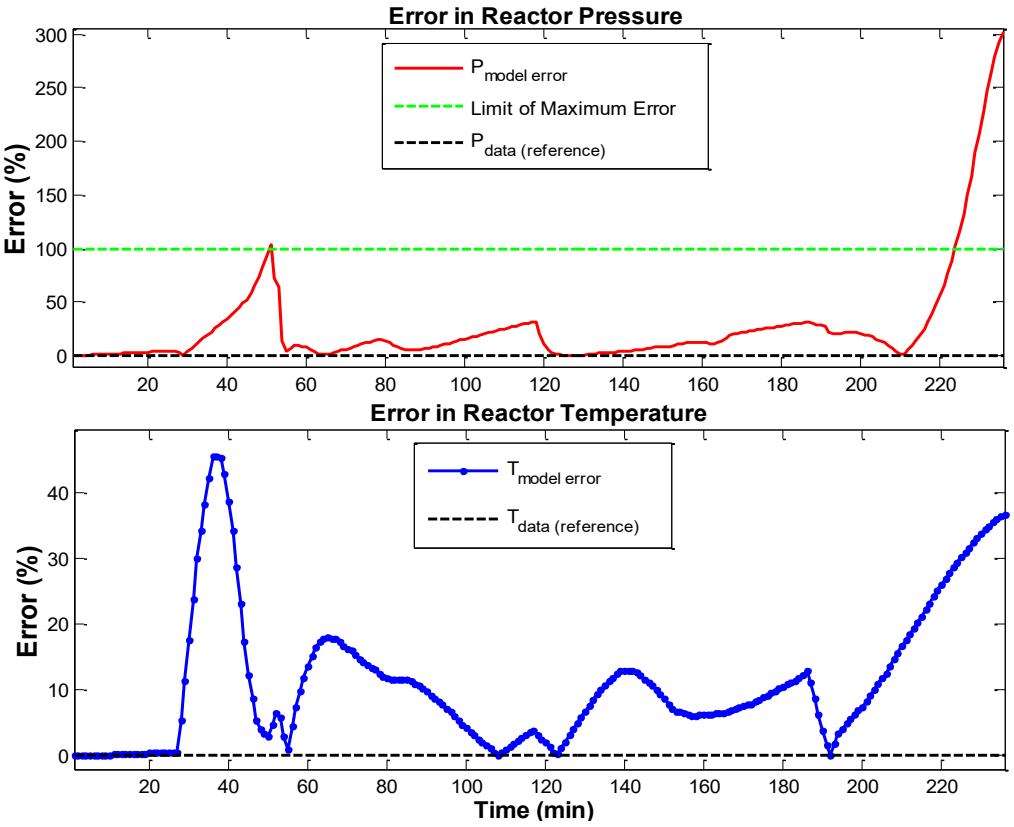

(a) Dynamics of Model Error

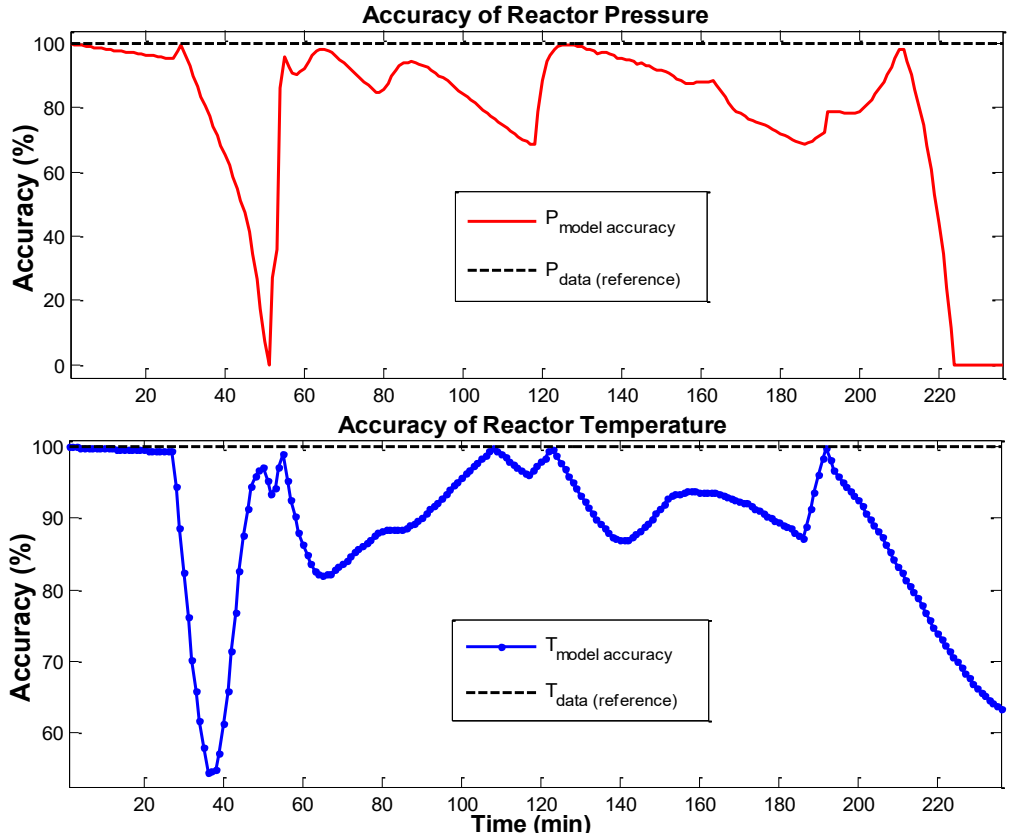

(b) Dynamics of Model Accuracy

Figure 4.7: Model Error and Accuracy

4.1.1.2 Case 2

This section presents the validation of the model temperature and pressure responses with batch 34 input and output data of the real process. This simulation was run with this batch input data of steam, cooling water and chlorine gas flow rates, which generated the temperature and pressure output data that the model responses were compared to. The simulation ran for about 3 minutes on computer, covering the full simulation time span of 181 minutes (about 3 hours), without solver ode15s stopping the simulation run. This batch is presented in this section in order to observe how the model performed with a batch that displayed different dynamics of the plant's real input and output data from those presented in the results of batch 33.

Consistent Initial Conditions

Table 4.2 gives the selected (or guessed) initial values, the computed consistent initial conditions and the integrated solutions, at the initial simulation time step (t_0), of the states variables of the reactor temperature, and moles of all chemical species contained in the reactor compartment of the model.

Table 4.2: Initial Conditions of Reactor State Variables

State Variables	**Values of Initial Conditions**		
	Guessed	**Consistent**	**Integrated**
moles of $Rh_{(s)}$ (kmol)	0.2693	0.2693	0.2419
moles of $HCl_{(aq)}$	6.2790	0.000042	0.000023
moles of $H_2O_{(l)}$	2.0930	2.0930	1.9799
moles of $Cl_{2(aq)}$	1.0465	0.5432	0.5241
$RhCl_3(H_2O)_{(aq)}$	0.0010	0.0010	0.0284
moles of $H_2O_{(g)}$	0.0001	0.0011	0.0010
moles of $Cl_{2(g)}$	0.0398	0.5433	0.5242
$T_{reactor}$ (K)	291.6684	291.6440	291.6640

The same observation made with the initial conditions of batch 33 can also be made with this batch. The computed consistent initial conditions of $HCl_{(aq)}$ (0.000042 kmol) and $Cl_{2(g)}$ (0.5433 kmol), which FSOLVE converged to as true solutions to their differential equations, were found to be very different from the actual amounts known to have been loaded into the reactor at the beginning of the batch (seen in the column of guessed values). As it was already seen in Case 1,

this will result in the simulated model responses to start at those consistent initial conditions of the model which FSOLVE converged to.

Evaluating the model at the computed consistent initial conditions given in Table 4.2 generated near zero function values to the magnitude of 10^{-4}, as seen in Figure 4.8. It is important to evaluate the model at t_0 in order to verify the correctness of the computed solutions, when the reactor model is at steady state and no dynamic changes to its input variables are applied to it.

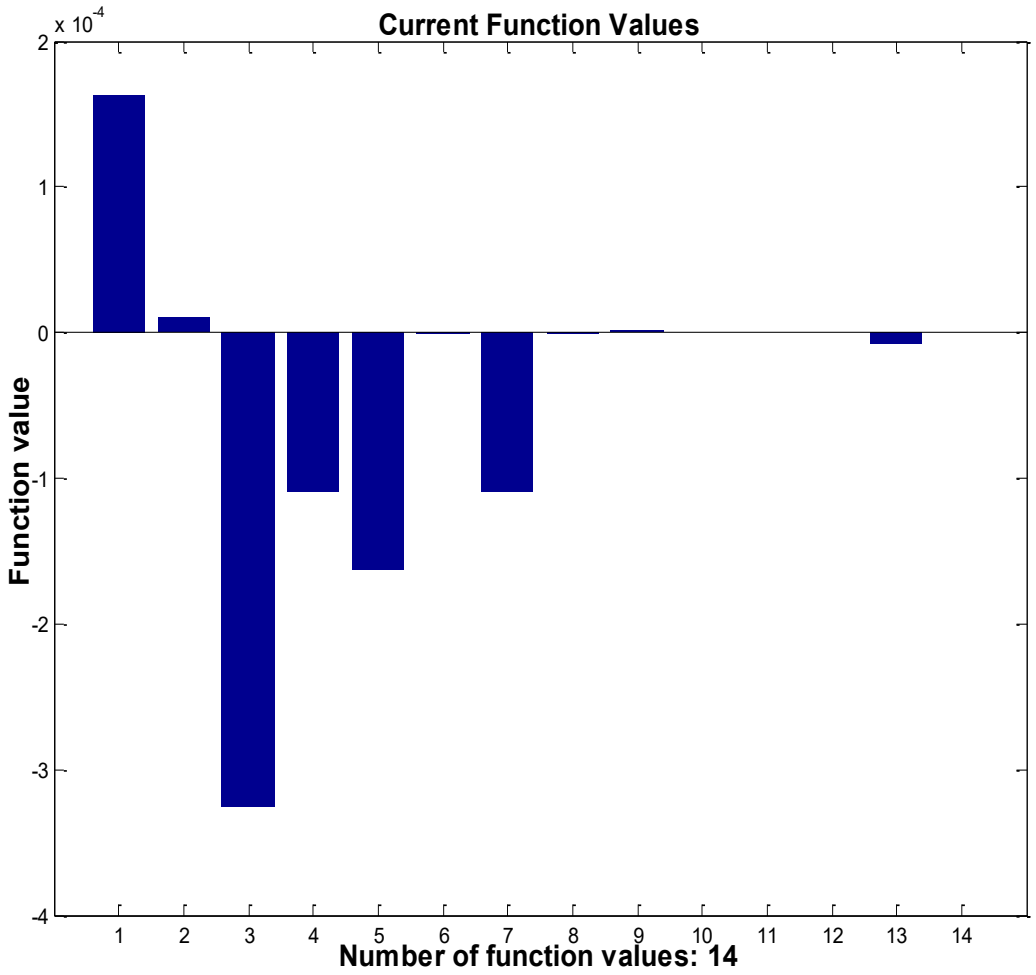

Figure 4.8: Function Evaluation at Initial Conditions

The small maginute of those function values confirm that the computed initial consistent values of the model states variables were all solutions to their respective differential equations. The negative values of function evaluations seen can be interpreted, as being the result of minor numerical instability that has occurred in the evaluation of the model equations, at the computed consistent initial conditions of model states variables.

Rates of Reactions

Figure 4.9 below displays the simulated dynamics of the rates of the rhodium dissolution reaction (r_1) and that of $HCl_{(aq)}$ formation (r_2). As with all other simulations that we have run, the reaction rate constants (k_{r1}, k_{r2}), used in both reaction rates equations were modelled according to the Arrhenius Law.

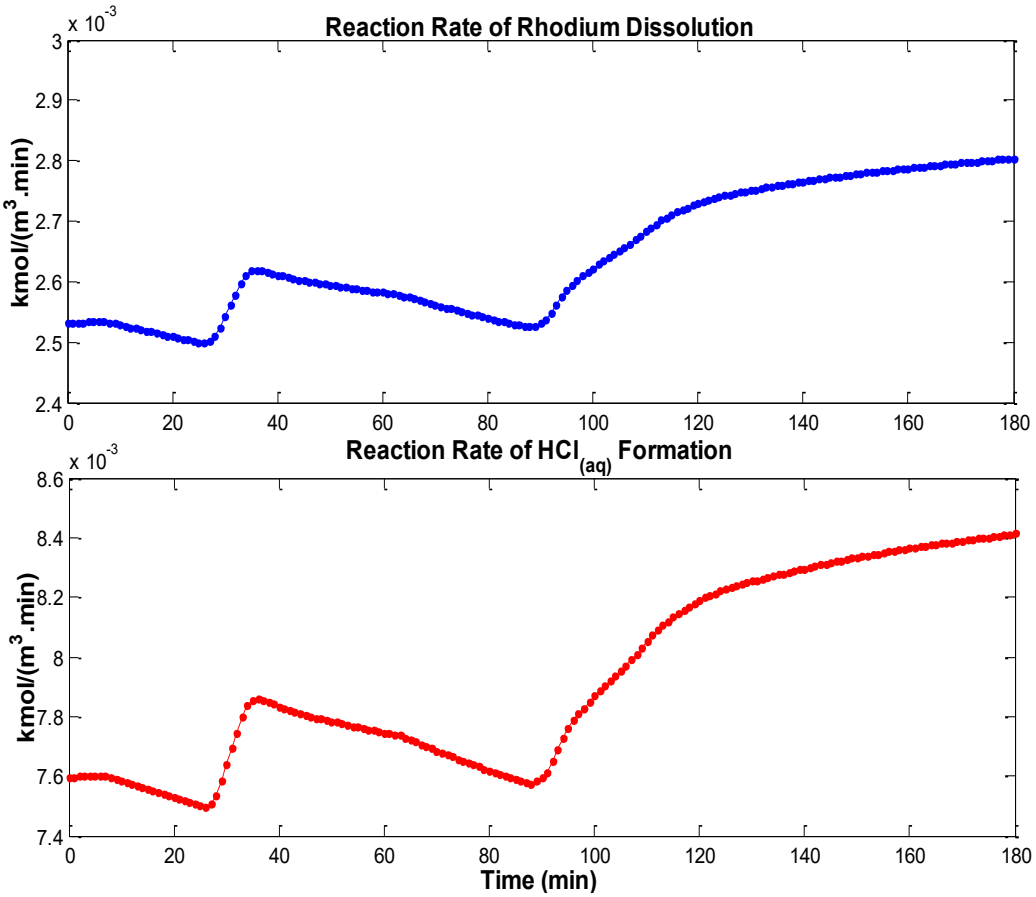

Figure 4.9: Reaction Rates

Both reaction rates demonstrated similar dynamics over time, with the rate of $HCl_{(aq)}$ formation (r_2) being almost three times larger than the rate r_1, of the rhodium dissolution reaction.

Molar Dynamics of Chemical Species

The molar dynamics of all chemical species interacting, as reactants and products, in the reactor system of the model are given in Figure 4.10 below:

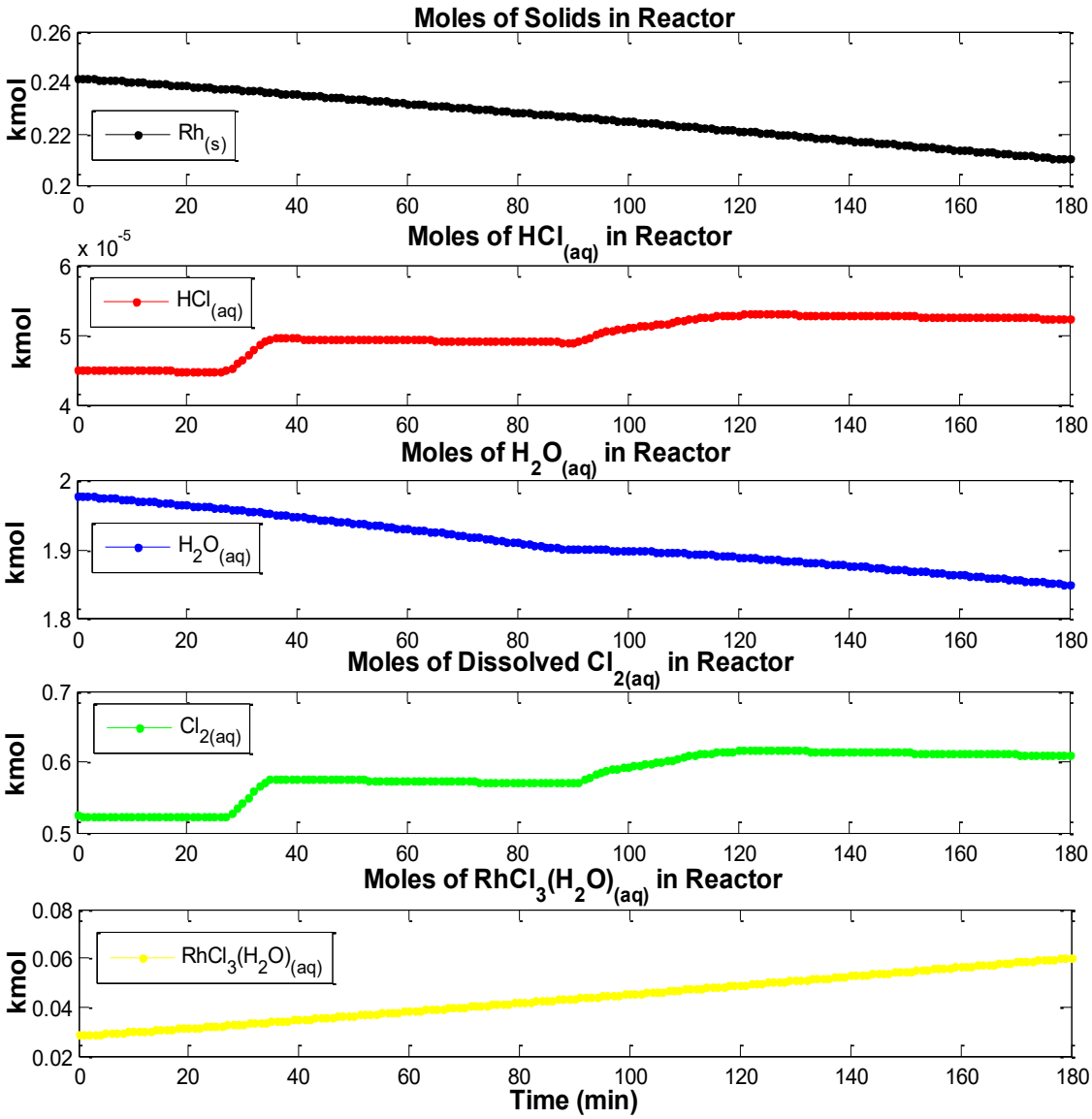

Figure 4.10: Moles of Chemical Species in Reactor Solution

The model has demonstrated stable behaviour of all chemical species presented in Figure 4.10. This is because no negative values could be seen in those responses. Furthermore, the model has generated such responses that were seen to be consistent with the dynamics of the reaction processes, whereby the molar amounts of reactants species $Rh_{(s)}$ and $H_2O_{(l)}$ decreased over time, as they were consumed during the reaction phase. Whilst the molar amounts of product species of $HCl_{(aq)}$ and $RhCl_3(H_2O)_{(aq)}$ increased over time. The moles of $Cl_{2(aq)}$ presented were the

net molar amounts which remained into the reactor solution after $Cl_{2(g)}$ had dissolved into solution and the $HCl_{(aq)}$ formation reaction had occurred.

Temperature Response

Figure 4.11 showing the simulated response of the model temperature reveals that, although the model demonstrated a good qualitative response of temperature, as compared to the temperature plant data of this batch, some noticeable deviations from data could still be seen. This is because the model temperature dynamics responsed accordingly to the jacket temperature, which demonstrated very fast dynamics. This has resulted in the model reactor temperature displaying faster dynamics than the plant temperature data.

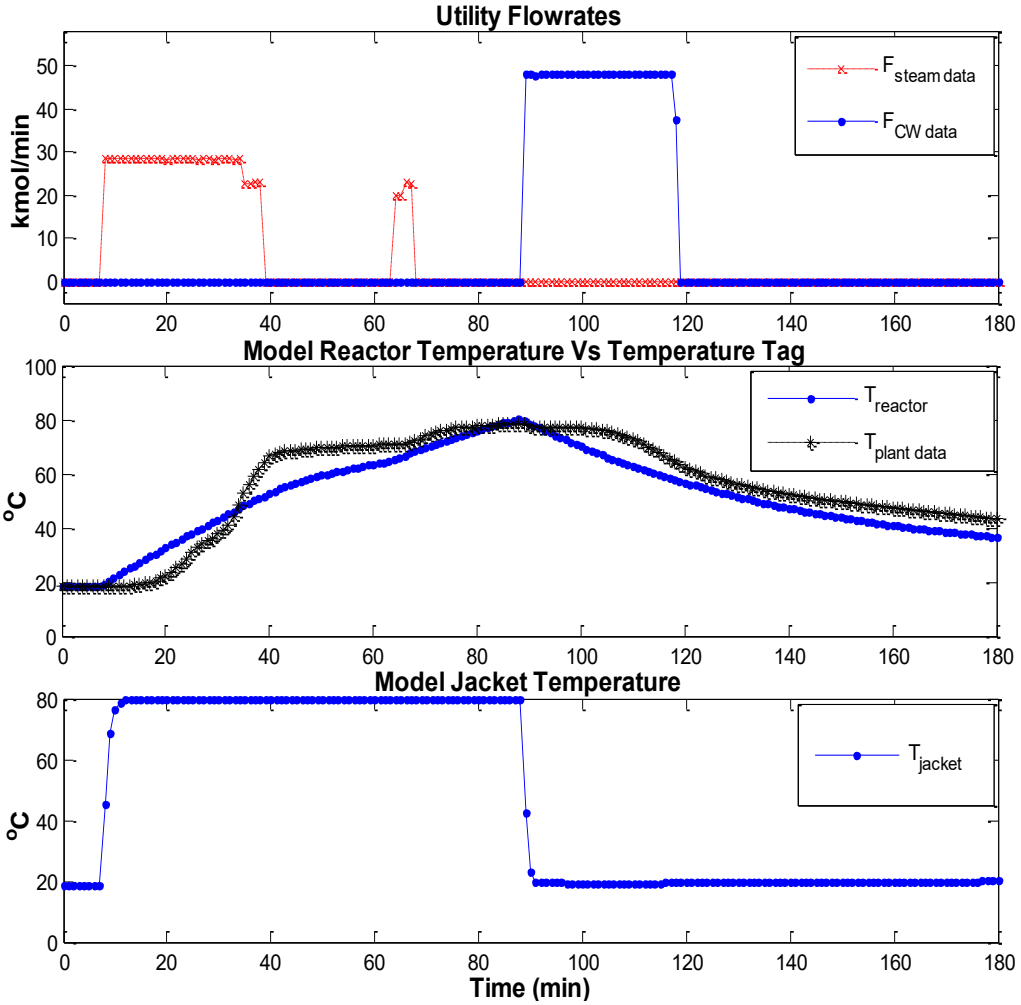

Figure 4.11: Dynamics of Jacket and Reactor Temperatures

Thermodynamic Contribution of Reactions

Figure 4.12 gives the thermodynamic contributions of the heat of reactions to the dynamics of the modelled reactor temperature. The overall energy contributions of the steam and cooling water utilities, as well as that of the two reactions are given in Figure 4.12a. The reactions showed to have generated sufficient energy which had a significant effect on the dynamic trend of the reactor temperature. The simulated energy dynamics of the cooling phase were also seen to be quite adequate, since the reactor temperature dropped upon addition of cooling water fluid into the jacket compartment of the reactor model.

Figure 4.12b gives the individual contributions of each of the chemical species reacting in the system, from which the species of $Rh_{(s)}$, $Cl_{2(aq)}$ and $RhCl_3(H_2O)_{(aq)}$ generated the most energy in the process, whereas $H_2O_{(aq)}$ and $HCl_{(aq)}$ generated the least amount of energy.

Pressure Response

The reactor pressure response is given by Figure 4.13, which displays two subfigures, namely Figure 4.13a and Figure 4.13b. The former gives the simulated molar dynamics of the gaseous species affecting the reactor pressure dynamics ($H_2O_{(g)}$ and $Cl_{2(g)}$); and the latter gives the simulated pressure response, as derived from the Ideal Gas Law, together with the dynamics of the same pressure equation without the effect of temperature to it. It could be clearly seen from Figure 4.13 that the dynamics of all gaseous species, together with the modelled temperature, had some considerable effect to the dynamics of the pressure response.

The middle subplot of Figure 4.13b shows a good qualitative response of the simulated pressure, with a similar order of magnitude as the pressure data. However, it also reveals some clear quantitave deviations of the pressure response from the plant data, at certain time steps. This is because, the dynamics of the reactor pressure were directly affected by those of both the temperature response and the total moles of gaseous species in the reactor. The deviations observed partly resulted from the assumption of ideal behaviour of the total gas in the reactor, as decribed by the Ideal Gas Law. The pressure started increasing from the time step of 10 minutes (similar to the temperature response), and continued rising between the simulation time steps of 40 minutes up to about 90 minutes. This was in clear contrast to the plant data, which showed a decrease within the same time span. Furthermore, by observing the pressure response without the effect of temperature to it (bottom subplot of Figure 4.13b), and that of the moles of $Cl_{2(g)}$

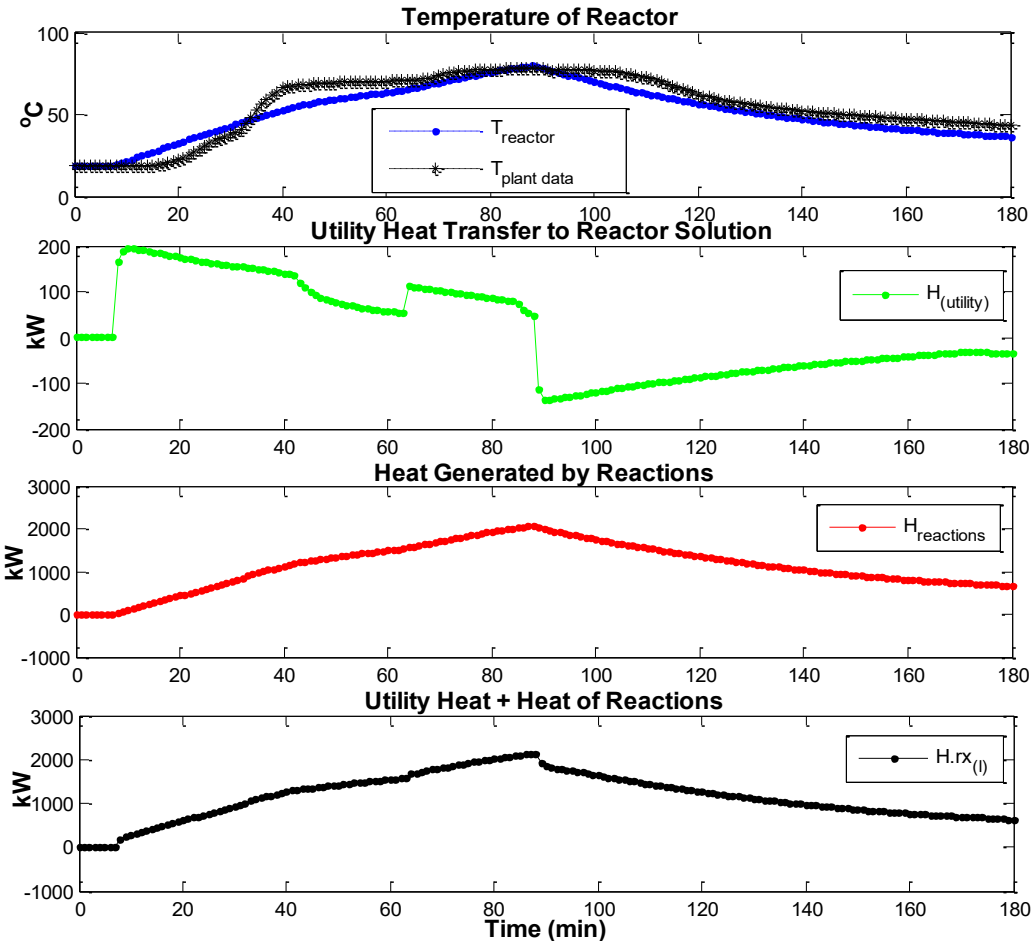

(a) Overall Heat of Reactions

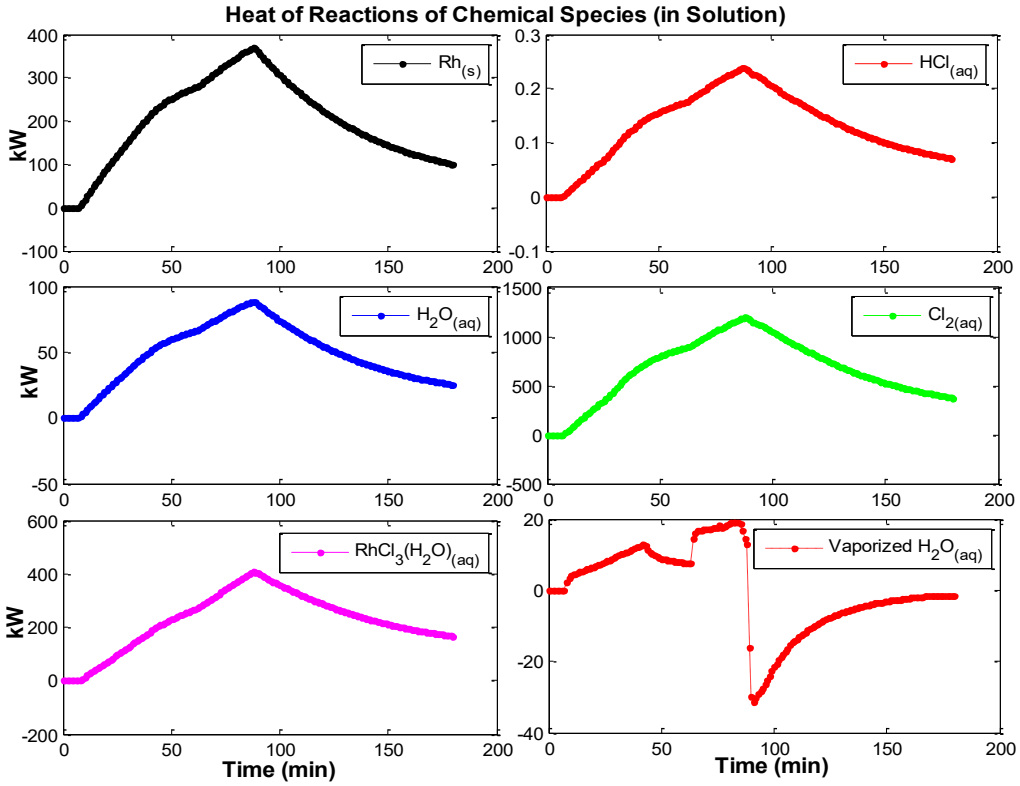

(b) Species Heat of Reactions

Figure 4.12: Contributions of Process Heat of Reactions

(middle subplot of Figure 4.13a), we could clearly notice the effect that the moles of gaseous species in the reactor had on the pressure response. This effect suggests that, there may be a limitation to the equation we have used to mathematically describe the dissolution of $Cl_{2(g)}$ into the system. Finally, the reactor was depressurized at the time step of 150 minutes, as seen from plant data, in contrast to the model response which did not display similar depressurisation. This is because no data of the plant air flowrate that was used to that effect was available to us, such that we could attempt to mimic the depressurization of the reactor.

Absolute Error and Model Accuracy

Figure 4.14 displays the errors (in Figure 4.14a) and accuracies (in Figure 4.14b) of the simulated temperature and pressure responses of the model, with respect to their respective plant data, at every time step of the simulation time span of 180 minutes.

The displayed dynamics of model errors and accuracies at every time steps, were found to be quite satisfactory, since they were consistent and correlated well to the dynamics of the simulated temperature and pressure responses observed in Figure 4.11 and Figure 4.13b. The model generated, on average, a smaller error in the temperature response in comparison to the pressure response. For this simulation, the model demonstrated a better performance in temperature than pressure, for which the simulated temperature response achieved an average accuracy of 87 % against 73 % for the pressure response.

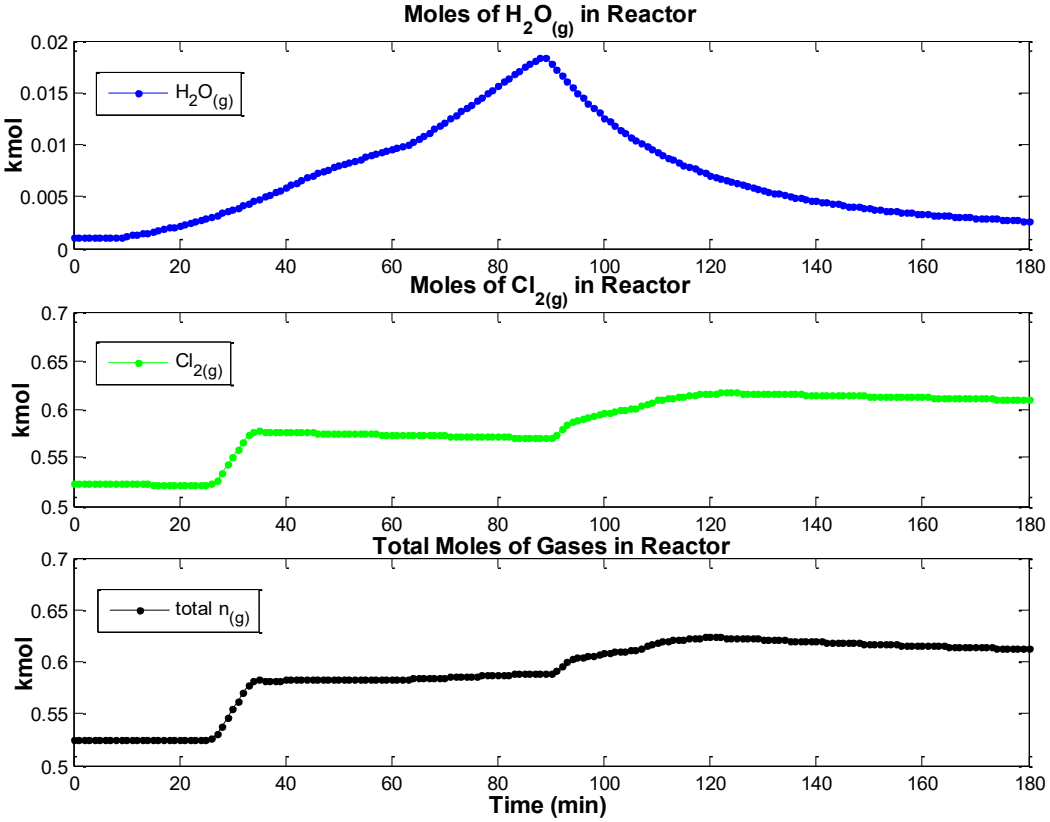

(a) Molar Responses of Gaseous Species

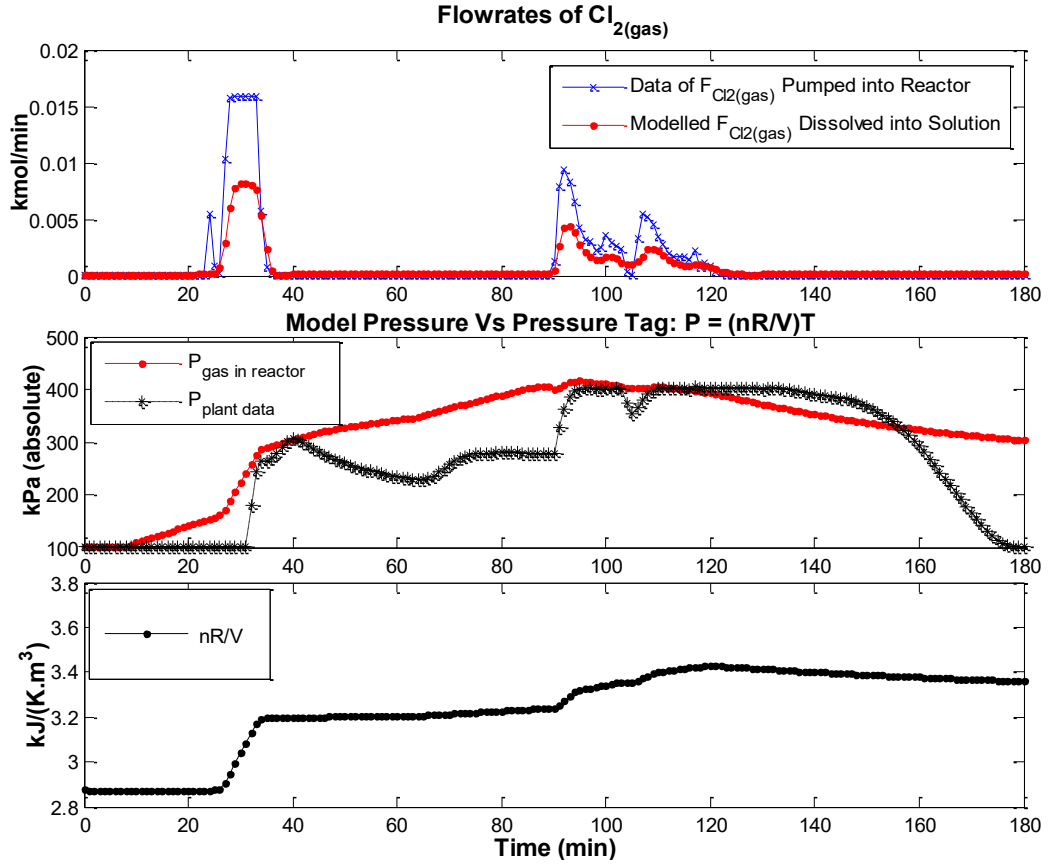

(b) Dynamics of Reactor Pressure Response

Figure 4.13: Pressure Simulation

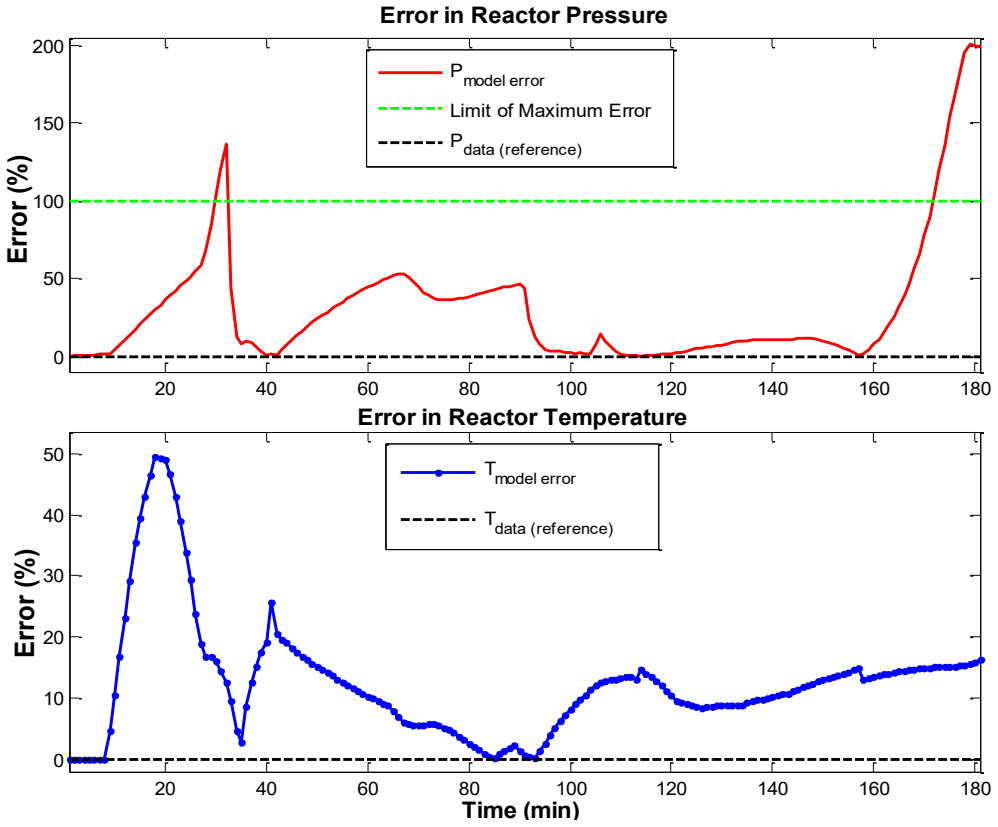

(a) Dynamics of Model Error

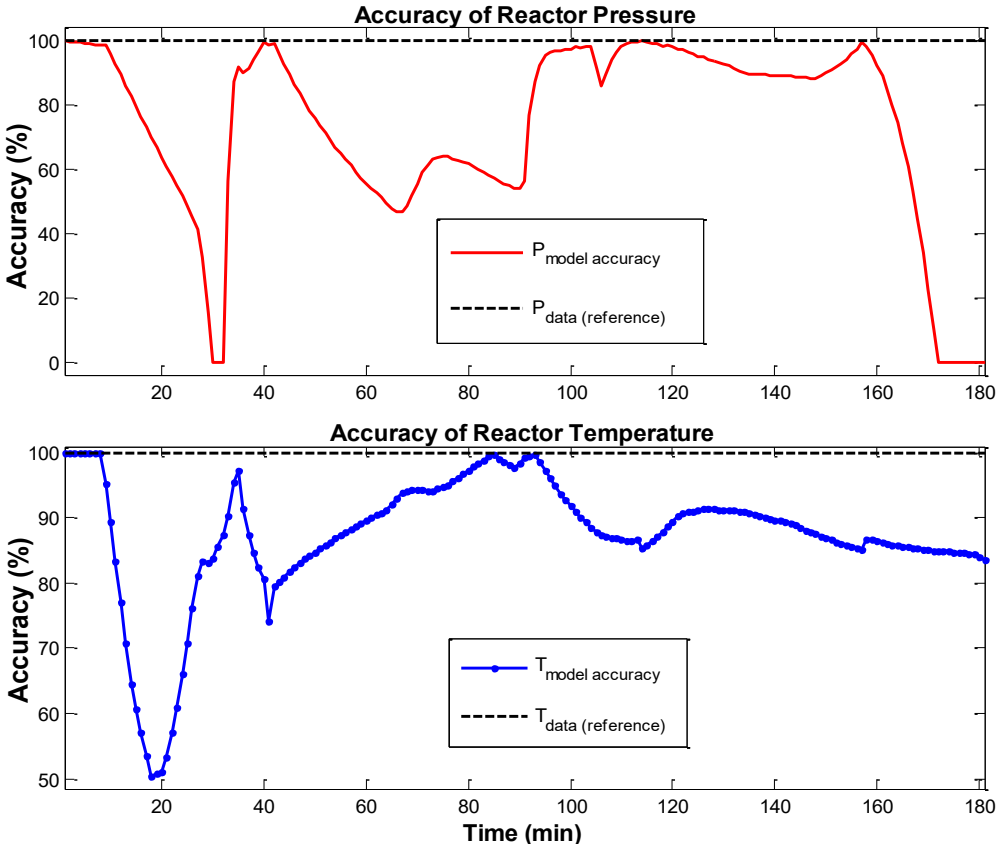

(b) Dynamics of Model Accuracy

Figure 4.14: Model Error and Accuracy

4.1.2 Poor Simulation Response

Although on average, the model has generated such responses of temperature and pressure, which demonstrated good tracking of their respective plant data with many batches, some poor performance was also observed with a few batches. Model simulations with 10 batches of plant data generated incorrect model responses of temperature and pressure, as large deviations were seen from their respective plant data. This was due to the combined effects of possible limitations in some model equations, the FSOLVE solver failing to converge to consistent initial conditions of the model variables, and solver ode15s failing to converge to correct solutions of the model equations.

This section presents the responses obtained from simulating the model with the plant data of batch 12 from the data set of 45 batches that was available to us. Similarly to previous simulations, the plant input data of utility flowrates, as well as $Cl_{2(g)}$ flowrate of this batch were also passed as input variables to the model in this simulation.

Consistent Initial Conditions

Similarly to the previous two cases of simulation results already presented, Table 4.2 below gives the initial values of the model variables, describing the quantities of chemical species present in the reactor compartment of the system.

Table 4.3: Initial Conditions of Reactor State Variables

State Variables	**Values of Initial Conditions**		
	Guessed	**Consistent**	**Integrated**
moles of $Rh_{(s)}$ (kmol)	0.2693	0.2693	0.2231
moles of $HCl_{(aq)}$	6.2790	0.000031	0.000044
moles of $H_2O_{(l)}$	2.0930	2.0930	1.9047
moles of $Cl_{2(aq)}$	1.0465	0.5441	0.5111
$RhCl_3(H_2O)_{(aq)}$	0.0010	0.0010	0.0473
moles of $H_2O_{(g)}$	0.0001	0.0013	0.0014
moles of $Cl_{2(g)}$	0.0398	0.5445	0.5113
$T_{reactor}$ (K)	294.5565	294.5413	296.2631

As already seen and discussed in the previous two cases of results presented, the same observation can be made about the noticeable difference between the actual (guessed) initial molar values of $HCl_{(aq)}$ and $Cl_{2(g)}$, known to have been

loaded into the real reactor during this batch at the initial time step (t_0), and the computed initial values that were consistent (true solutions) to the differential equations, describing their dynamics. Those differences in the initial values will have the same results of the model displaying a very small amount of $HCl_{(aq)}$ in the reactor solution, and a much higher quantity of $Cl_{2(g)}$ in the reactor, than was actually pumped into it at t_0. The evaluation of the model differential equations at every computed consistent initial values of the model 14 differential equations are given in Figure 4.15.

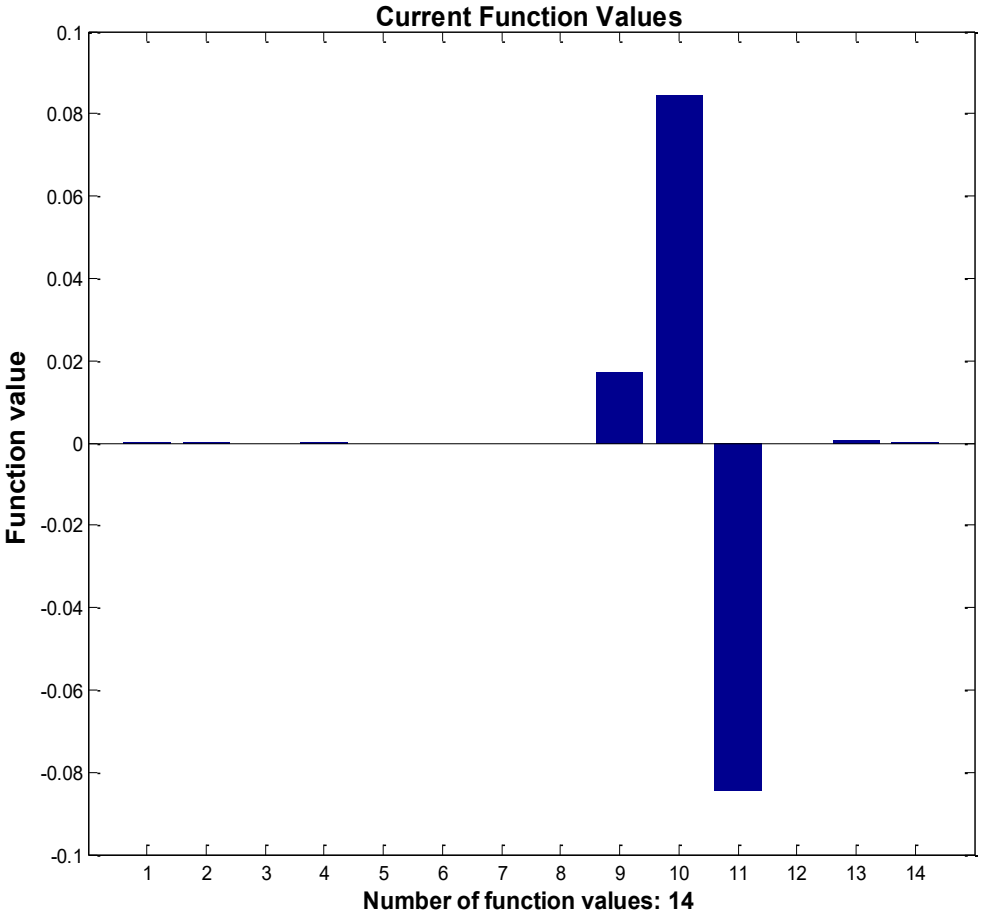

Figure 4.15: Function Evaluation at Initial Conditions

Although the function values were seen to be zero, which is an indication that they were solutions to the model equations, their magnitude evaluated to an accuracy of only 2 decimal figures (10^{-2}) was noticeably larger than those of the previous 2 simulations presented, which were evaluated to an accuracy of 4 decimal figures (10^{-4}). This result suggests that some inconsistencies or difficulties could arise during simulations. That is, convergence towards incorrect solutions of the

model equations could possibly occur, during numerical integration of the model equations. This was seen in the model responses that follow.

Rates of Reactions

The rates of the two reactions (seen in Figure 4.16) displayed such dynamic trends that were similar to one another. Again in this simulation, the rate of the dissolution reaction was about 3 times smaller than that of the $HCl_{(aq)}$ formation. However, unlike the previous cases of simulation results discussed, the dynamics of these reaction rates did not display a sequential, gradual increase over the simulation time span. Instead, the rates were seen to decrease during about the first 180 minutes of the simulation. The simulated responses of the moles of $HCl_{(aq)}$ and $Cl_{2(aq)}$ will better explain this behaviour, since the equations describing the rates of the two reactions were written in terms of the concentrations, hence the moles of those chemical species.

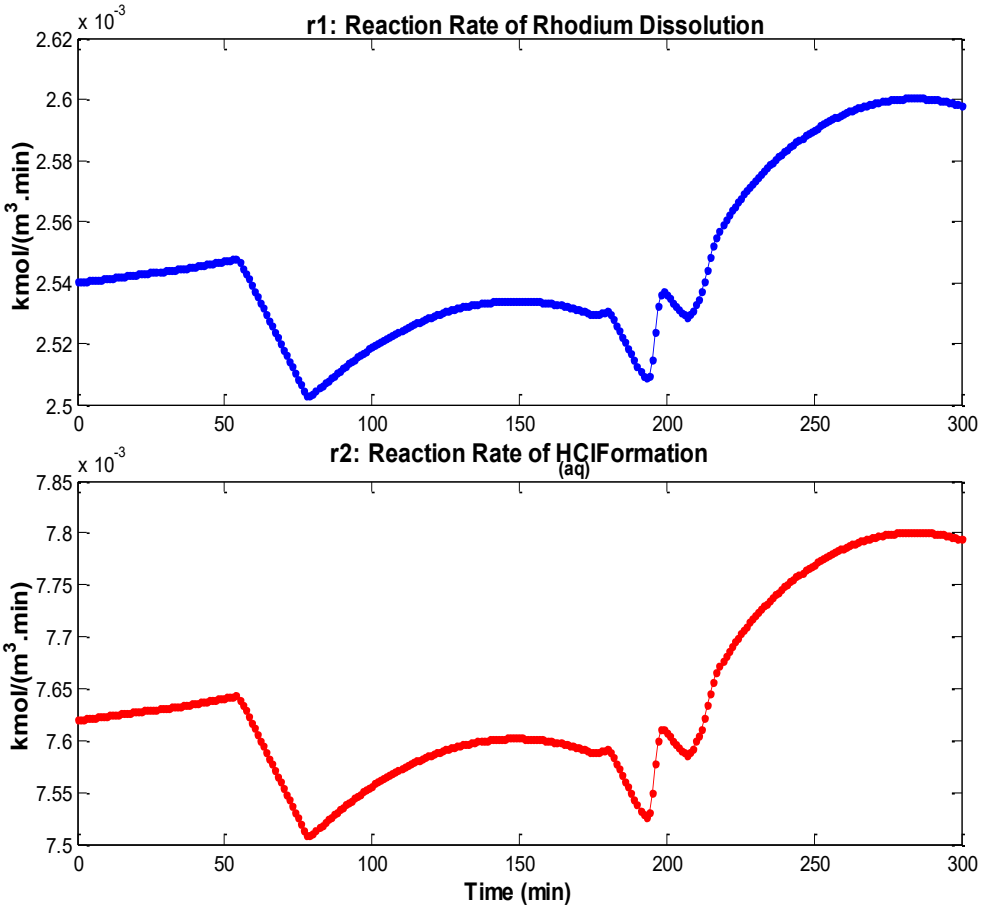

Figure 4.16: Reaction Rates

Molar Dynamics of Chemical Species

The molar dynamics of $HCl_{(aq)}$ and $Cl_{2(aq)}$, seen in Figure 4.17, revealed that the concentrations of those chemical species decreased continuously over the simulation time until about 190 minutes. Those trends were seen to be quite different from those of the previous 2 cases of simulations results already discussed, for which the molar amounts of $HCl_{(aq)}$ and $Cl_{2(aq)}$ increased sequentially over time. These decreasing trends correlate well with the fact that the dynamics of reactions rates in Figure 4.16 decreased over the first 180 minutes of simulation time.

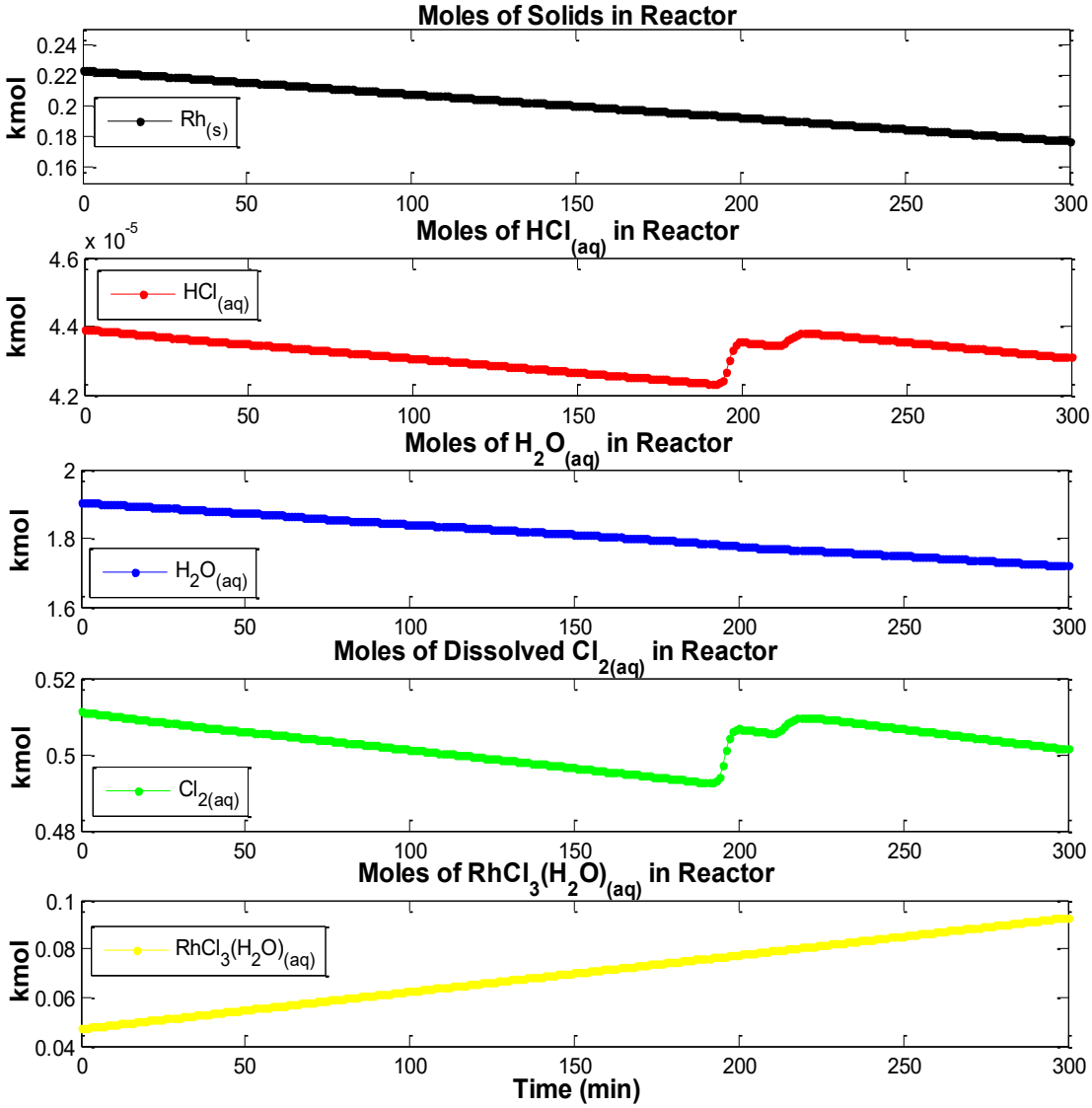

Figure 4.17: Moles of Chemical Species in Reactor Solution

Besides $HCl_{(aq)}$ and $Cl_{2(aq)}$, the remaining chemical species in the reactor solution displayed such dynamics that were consistent to the way they were understood to interact in the reaction processes. The reactants species of $Rh_{(s)}$ and $H_2O_{(aq)}$ decreased, whereas the main product species of $RhCl_3(H_2O)_{(aq)}$ increased over time, as reactions took place. Futhermore, no species showed such unstable dynamics for which negative values of moles were generated.

Temperature Response

Figure 4.18 shows the temperature response of this simulation run. The model response shows faster response than the plant data it was plotted against. The middle plot of Figure 4.18 shows a significant deviation of the simulated temperature response from the temperature data.

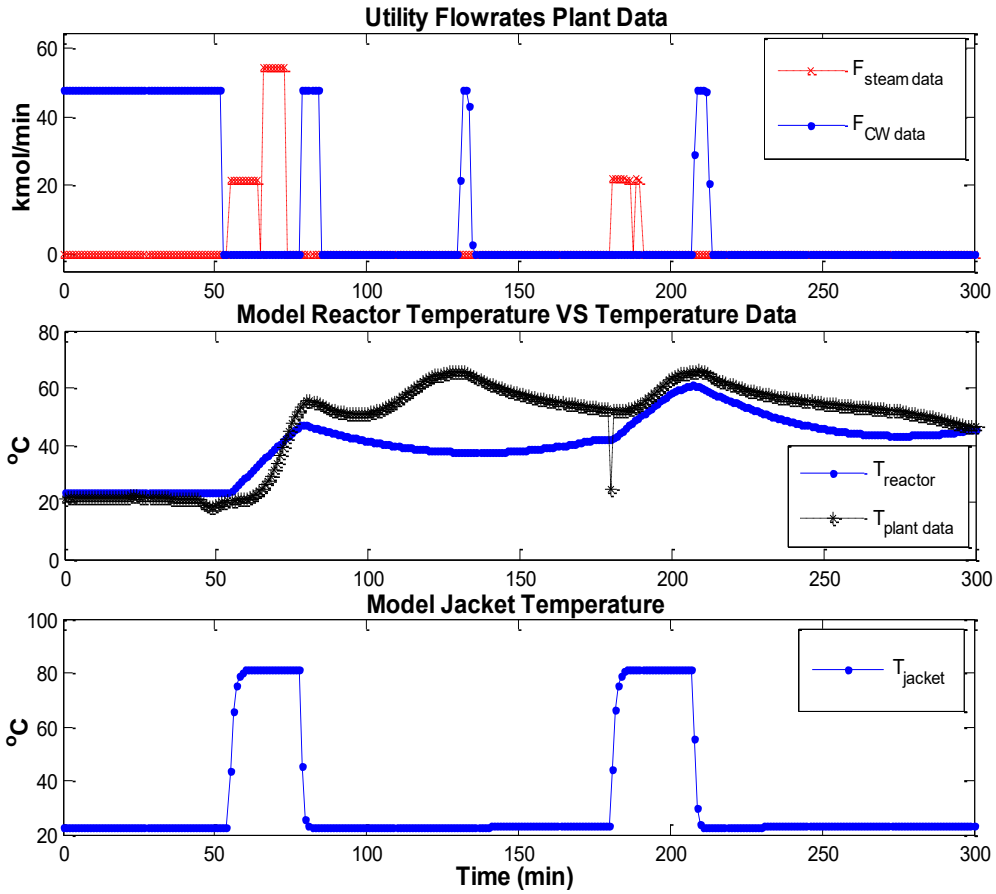

Figure 4.18: Dynamics of Jacket and Reactor Temperatures

This is because the reactions have not reproduced such energy production that would achieve a similar temperature rise as that seen in the plant data between the

time steps of 100 and 150 minutes. Such a behaviour could be attributed to the facts that, either the numerical solver ode15s used to integrate the model differential equations converged to incorrect solutions, or there was some considerable limitations to the differential equation of the reactor temperature, or a combination of both. It was already observed in the previous cases of results presented that, the model temperature was very responsive to the dynamics of the jacket temperature and hence, to the flowrates of utility inputs. This result show once again that the dynamics of the hot and cold utilities have had a considerable impact on the energy generated by the reactions, hence the reactor temperature.

Thermodynamic Contribution of Reactions

The overall energy generated by the reactions is given in Figure 4.19.

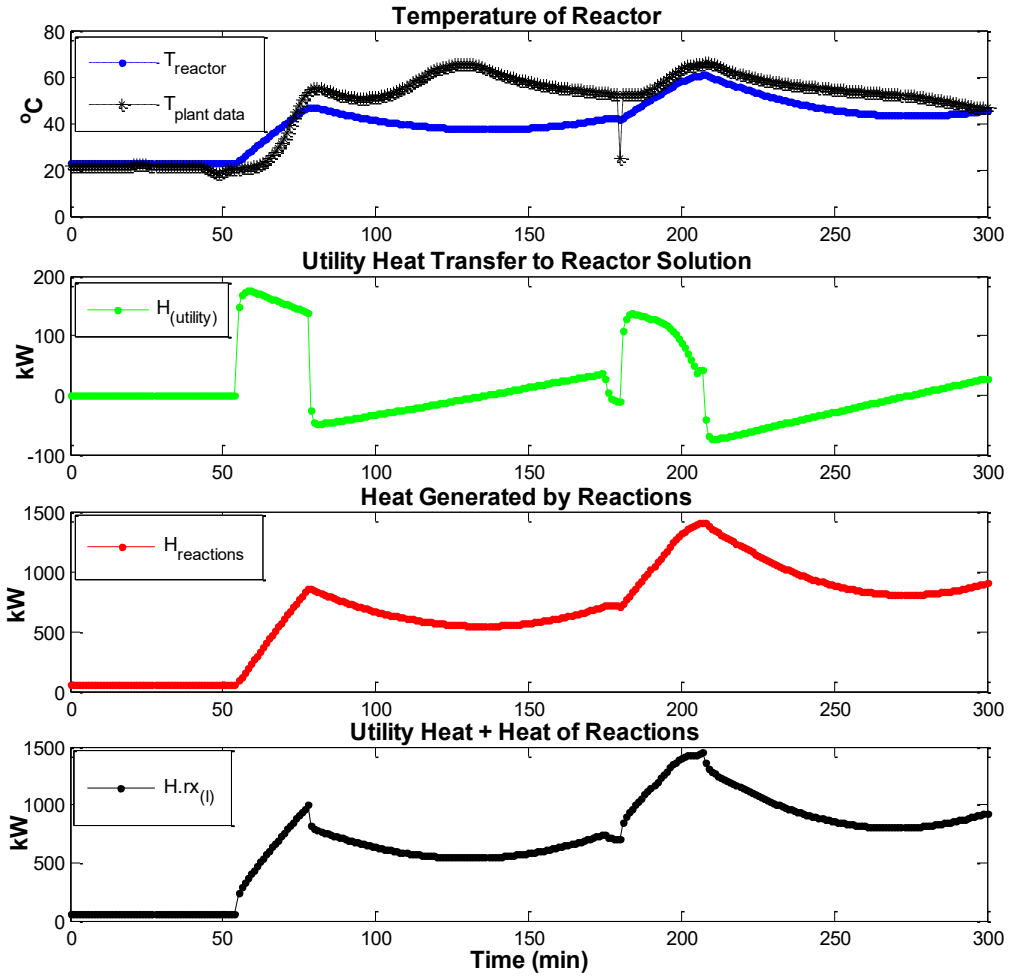

Figure 4.19: Overall Heat of Reactions

The simulated energy dynamics of the process cold and holt utilities (in the second subplot from the top), together with those of the heat generated by the reactions further explain the dynamics seen in the simulated temperature. The model failed to replicate the temperature rise seen in the plant data, between the simulation time steps of 100 and 150 minutes. This behaviour could also well be a limitation inherent to the way the temperature equation was modelled, whereby the energies generated by each of the reacting chemical species and that of the phase transfers of $H_2O_{(aq)}$ and $Cl_{2(g)}$, in the reactor solution, were summed up as the overall energy of reactions, together with the heat of utilities transferred from the jacket into the reactor compartment (see Equation A.10 in Appendix A).

Pressure Response

The pressure response of this simulation run can be seen in Figure 4.20, which contains 2 subfigures. At the top, Figure 4.20a gives the molar dynamics of the gaseous species of $H_2O_{(g)}$ and $Cl_{2(g)}$ contained in the reactor. The total amount of moles of those gaseous species (in the bottom subplot of Figure 4.20a) showed a dynamic trend that was not similar to that of pressure data. This is unlike the trends of total moles of gases that were seen in the previous cases of simulation results presented. At the bottom of Figure 4.20 is Figure 4.20b, which displays the simulated pressure response, plotted against the pressure data of the real reactor.

In this simulation run, the pressure of the reactor model has demonstrated very poor qualitative and quantitative responses with respect to plant data. This is because large deviations of the simulated pressure from pressure data could be seen in the middle subplot of Figure 4.20. This behaviour was greatly due to the fact that the model had failed to reproduce the dissolution of $Cl_{2(g)}$ into the reactor solution at the time span ranging from about 48 to 51 minutes, although significant dissolution of $Cl_{2(g)}$ was achieved at the time steps of 200 and 223 minutes (as seen in the top subplot of Figure 4.20b). This in turn had affected the dynamics of $Cl_{2(g)}$ moles in the model, which was understood to have a considerable effect on the dynamics of the reactor pressure, as $Cl_{2(g)}$ was pumped into the system in order to maintain the reactor pressure. This result suggests that the integration solver ode15s converged to such values that were incorrect solutions to the differential equation, describing the moles of $Cl_{2(g)}$, as well as the algebraic equation describing the pressure in the reactor.

The pressure response in this simulation run has shown to be a typical example of failure of the numerical solver to correctly integrate the model equations.

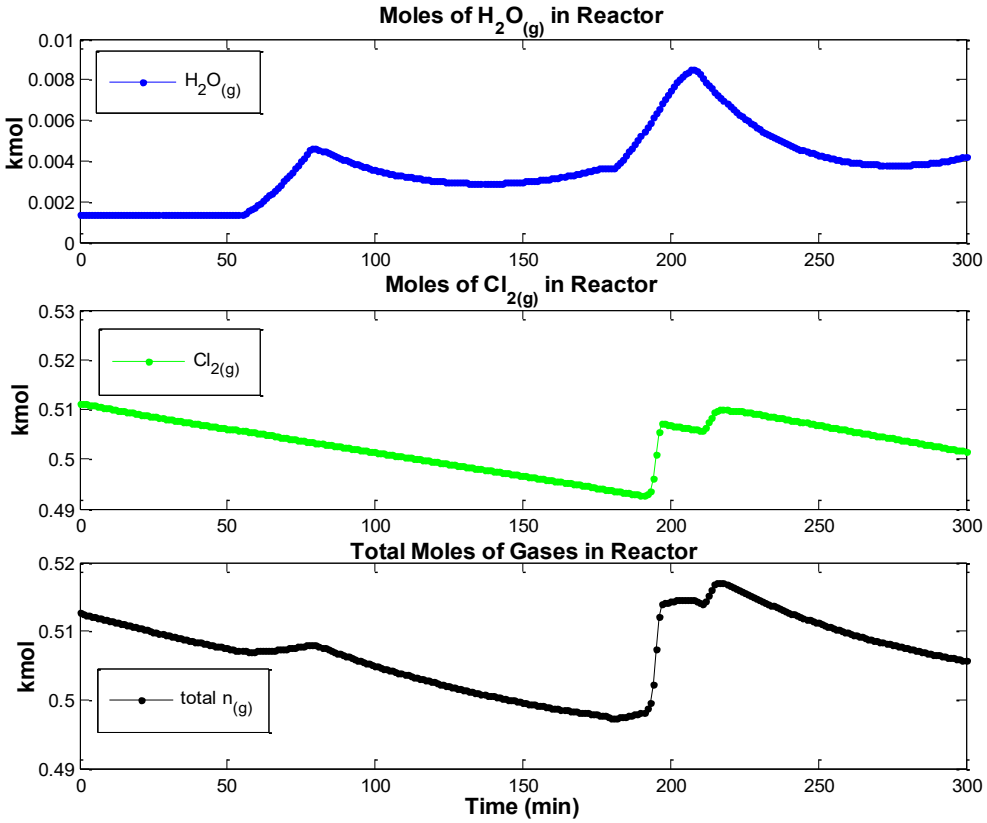

(a) Molar Responses of Gaseous Species

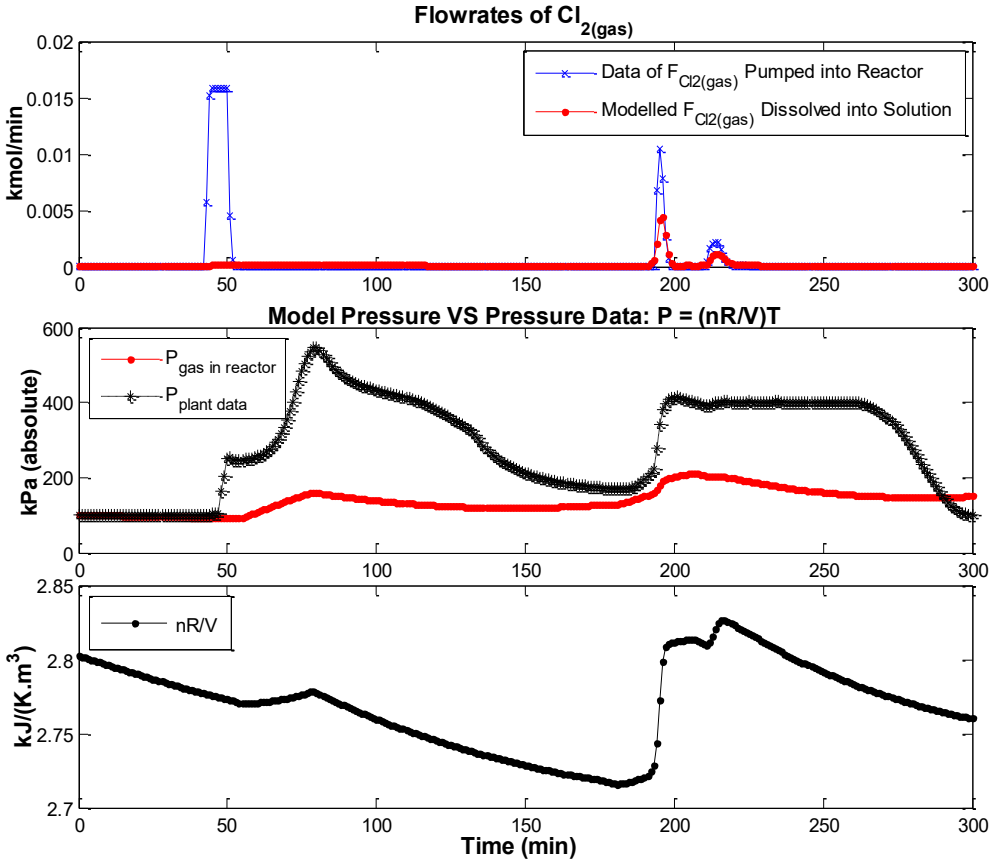

(b) Dynamics of Reactor Pressure Response

Figure 4.20: Pressure Simulation

Absolute Error and Model Accuracy

The errors generated from the simulated responses of temperature and pressure of the reactor model are shown in Figure 4.21. As seen in the simulated pressure and temperature responses of the previous section, the pressure response generated large errors as it deviated from the plant data it was compared to, hence reducing the overall accuracy of the model in its pressure response (see Figure 4.21b). The magnitudes of errors and accuracies seen in Figure 4.21a and Figure 4.21b were found to be consistent with the dynamics seen in the temperature and pressure responses discussed earlier.

The model achieved an overall accuracy of 76 % in temperature response, and an overall accuracy of 32 % in pressure response.

4.1.3 Model Accuracy for Full Set of Batches

The performance of the model in tracking the full set of 45 batches of data that was available to us, for model validation could not be entirely presented in this report. As a result of that, only the overall model performance for all batch simulations done are presented in this section. The average accuracies of the model simulated responses of reactor temperature and reactor pressure were evaluated as shown by Equation 4.4 and Equation 4.5.

$$Mean\ Absolute\ Error = \frac{100\ \%}{N} \sum_{t=1}^{N} \frac{|Data(t) - Model\ Response(t)|}{|Data(t)|} \tag{4.4}$$

$$Model\ Accuracy = 100\ \% \ - Mean\ Absolute\ Error \tag{4.5}$$

Where
N = Length of the simulation time span
t = Time steps
Data = Batch measurements

Figure 4.22 gives the statistics of the model performance of reactor temperature and pressure responses, with 44 batches of the full set of 45 batches available. This is because solver ode15s failed to integrate the model equations, when simulated with the input plant data of one of the batches. It can be seen from Figure 4.22 that the model has achieved a better performance of temperature responses than pressure responses. A total of 35 batch simulations achieved a percentage accuracy of at least 80 % in temperature responses, against only 7 batch simulations which generated pressure responses in a similar accuracy range. The pressure responses

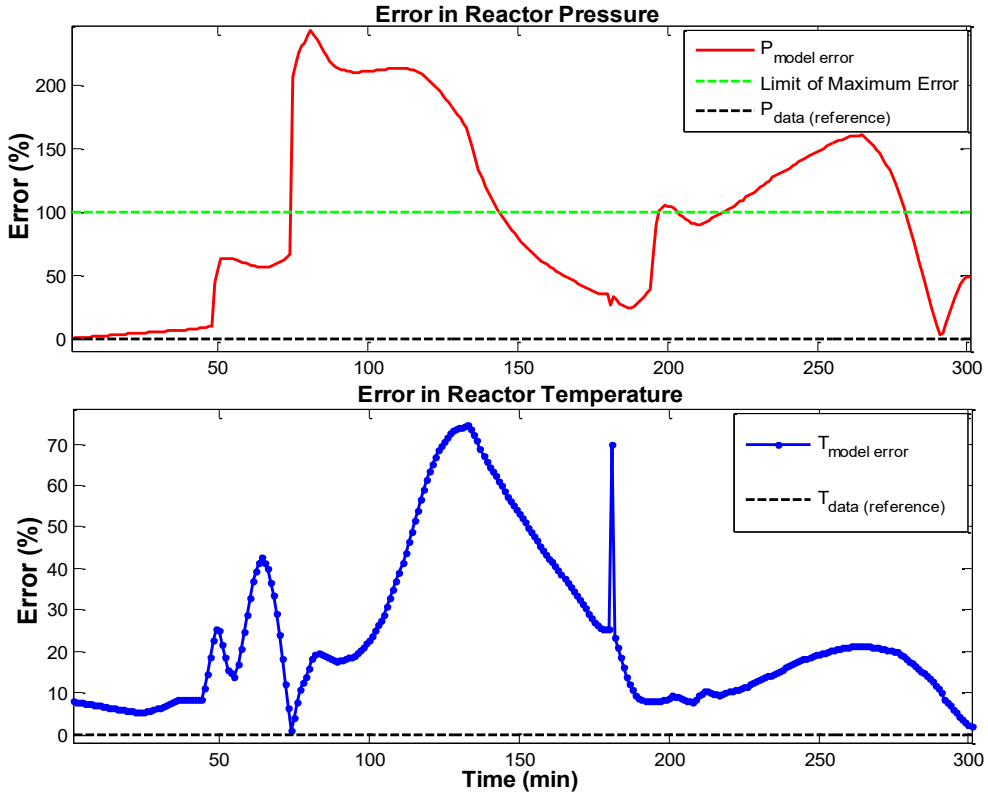

(a) Dynamics of Model Error

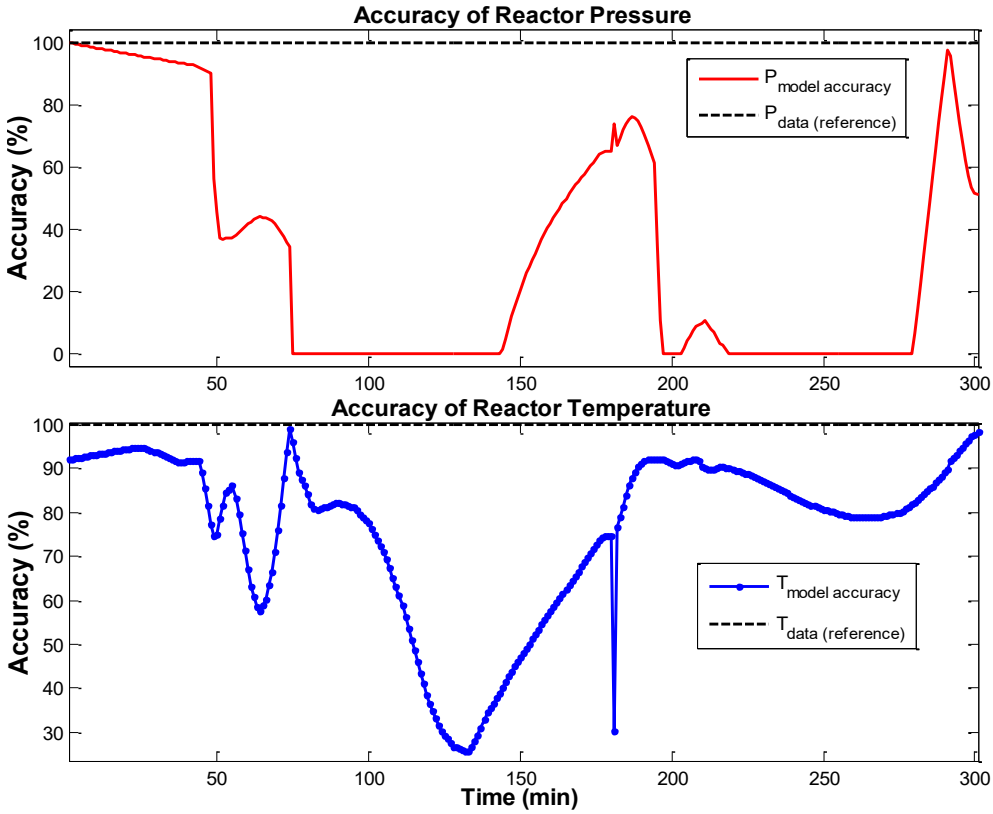

(b) Dynamics of Model Accuracy

Figure 4.21: Model Error and Accuracy

of the remaining 37 batches achieved such percentage accuracies that ranged from 10 % to 78 % , against 9 batches with temperature responses in the same accuracy range. Out of the 44 batches of plant data the simulated responses were compared to, the model has achieved an avarage temperature accuracy of 80 % against an avarage pressure accuracy of 60 %.

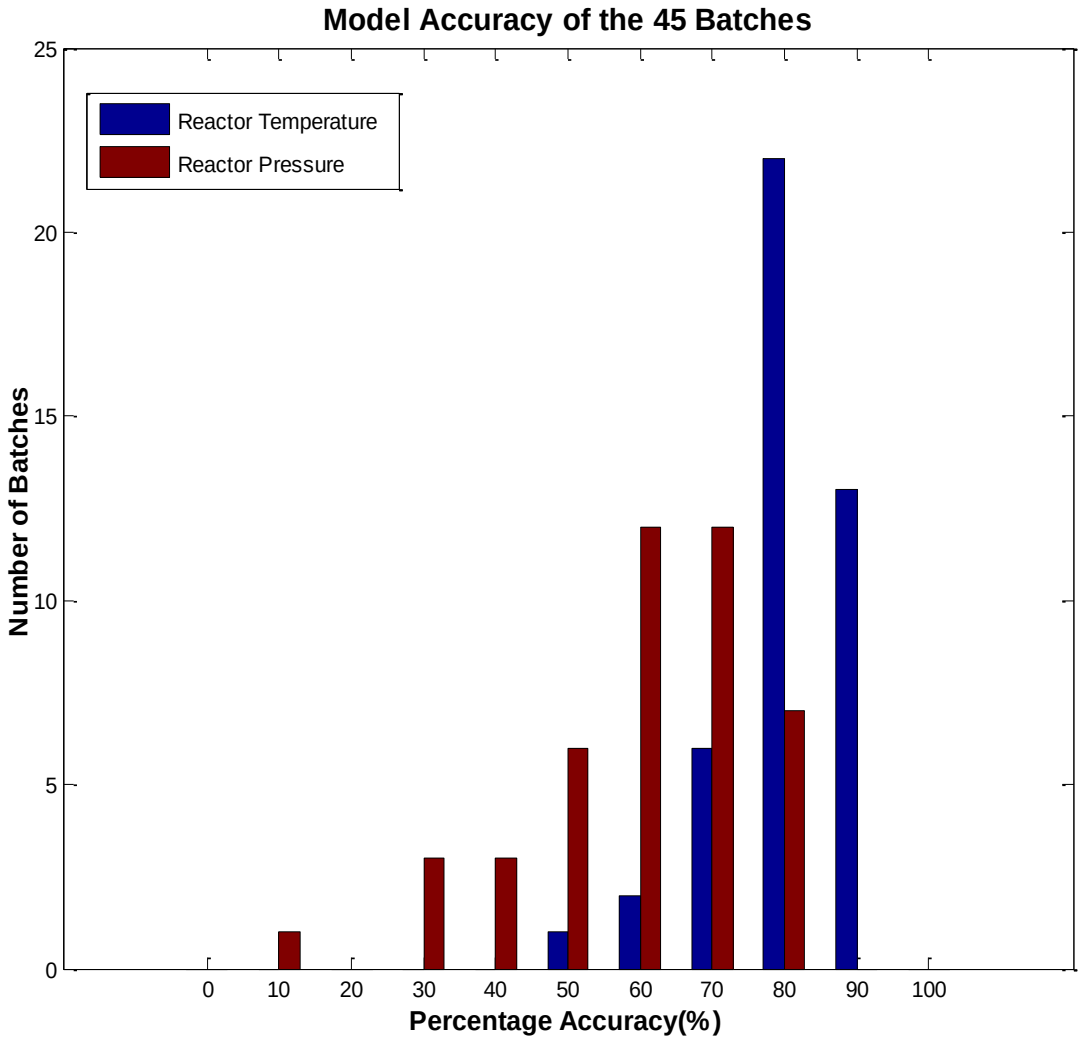

Figure 4.22: Overall Model Accuracy

Chapter 5

Conclusions and Recommendations

The following conclusions can be drawn from the work presented in this dissertation, based on the development of a first-principle model of a rhodium dissolution process taking place in a semi-batch reactor.

5.1 Model Equations and parameters

The first-principle model of the rhodium dissolution process was developed by capturing the dynamic behaviour of the transport phenomena of mass and energy transfers, occuring in the semi-batch reactor system. The model was mathematically formulated as a system of explicit ordinary differential equations (ODEs), which was entirely solved in the MATLAB computational environment. It has been quite challenging to get this first-principle model to, at least, simulate correctly throughout the simulation time spans of various batches, without solver ode15s failing. This is because this modelling work has required continuous trial-and-error adjustments of some model equations and solvers options, in search for stable and consistent simulation responses.

The differential and algebraic equations describing the dynamics of the temperature and pressure of the reactor have demonstrated good qualitative responses of the model. Simulations with 35 data set of plant input data, from the set of 45 batches of data available to us, showed some good tracking of the plant temperature data with a percentage accuracy of at least 80 %, whereas simulations with the plant input data of only 7 batches showed similar percentage accuracy in the pressure response of the model. Some noticeable deviations were still seen between plant data and model responses of temperature and pressure, since the model responses did not perfectly track their respective plant data. This was attributed

to the fact that there was always the possibility of some conceptual limitations in the temperature and pressure equations, as written in the model. For instance, the simulated temperature always showed faster responses than temperature data, possibly due to the fact that some real deadtime element of the system had not been captured, since the dynamics of the reactor wall separating the jacket and reactor compartments of the system were neglected, in order to simplify the model. In addition to that, when comparing the dynamics of the simulated pressure to those of the plant data, it was seen that the assumption made about the modelled reactor pressure, for which the gaseous species in the reactor model were to assume ideal behaviour, showed to be inconsistent with the pressure dynamics of the real reactor system. This is because the dynamics of the modelled reactor pressure were seen to be greatly affected by those of the total moles of gases in the model, as well as the modelled temperature. This behaviour was not seen between both the plant data of temperature and pressure of the real reactor.

Of particular concern was the modelling of the phase transfer equations describing the dissolution of $Cl_{2(g)}$ into the reactor solution and the evaporation of $H_2O_{(l)}$ from the reactor solution into the gas phase. Various possible models of those phase transfer equations were investigated through numerous runs of the model by trial-and-error, until the model could eventually run successfully throughout the full simulation time spans of each batch, without solver ode15s stopping simulations. During numerical integration of the model, solver ode15s would often prematurely stop simulations due to the appearance of large derivatives in the model differential equations at certain time steps. Those large derivatives were believed to be due to the presence of nonlinearities in the model equations. Furthermore, it was important to achieve stable computations of consistent initial conditions of the model states (derivative) variables, which were correct solutions to the model differential equations. This was achieved in most batches by adjusting some key options (discussed in section 3.2.2.4) of the MATLAB built-in FSOLVE solver, such as the maximum number of iterations allowed, the termination tolerance of the function values and the solver's optimization algorythm, amongst others. The model showed that the moles of $HCl_{(aq)}$ and $Cl_{2(g)}$ had such computed initial values that were different from the actual amounts known to have been initially loaded into the reactor. This inconsistency was believed to be due to the possibility that the differential equations describing those dynamics were incomplete. This was another limitation to the model since the exact chemistry of the reactions occurring in the process was not fully known in order to be captured more rigorously.

The key parameters of heat and mass transfer coefficients, namely Arrhenius reaction constants and activation energies of the two reactions, were all estimated

by trial-and-error because no estimates resulting from similar works could be obtained from literature. They were further tuned until the model temperature and pressure responses achieved some good fits of plant data. Those parameters were not optimised because we had already obtained good enough responses of temperature and pressure with the values used, which undoubtedly could still be improved through parameter estimation using various optimization algorithms. This task would require more time to develop and implement since it would have to be written as a computer programme and tested for the full data set of 45 batches at our disposal.

5.2 Numerical Integration

Although the numerical integration solver ode15s managed to integrate the model differential equations throughout the full simulation time span for most batches of plant data, some significant deviations and inconsistencies could still be seen with some simulated responses, especially those that demonstrated poor model performance. This was particularly seen in the simulated pressure response of batch 12 (in Figure 4.20b), which was presented as part of the case of results accounting for poor model performance. The responses presented in Figure 4.20b clearly showed that the model failed to correctly simulate the dissolution of $Cl_{2(g)}$ into the reactor solution at an earlier simulation time span ranging from 48 to 51 minutes, after which, it eventually showed some $Cl_{2(g)}$ dissolution at the later time steps of 200 and 223 minutes. That result had illustrated a typical example of failure in the numerical integration of the differential equations describing the molar species of $Cl_{2(g)}$ and $Cl_{2(aq)}$.

It was then believed that the difficulties encountered during numerical integrations of the model could very much have been due to the presence of nonlinearities in the model equations which, at certain time steps during simulations, could have led to solver ode15s compute large derivative values (equation evaluations), which may have been incorrect solutions to certain equations, or could simply have caused the solver to stop numerical integrations. For instance, no simulation of the model could be done with the plant input data of batch 32. This is because solver ode15s failed to integrate the model equations as it prematurely stopped the simulation at the initial integration time step of that simulation.

5.3 Model Validation

The model responses of temperature and pressure in the reactor were validated against their respective sets of plant data. The model has shown to be more successful in predicting the dynamics of reactor temperature than those of reactor pressure, from first-principle. The mass balance of the process was seen to be stable since no unreal (negative) values in the molar responses of all chemical species interacting in the process were obtained. Furthermore their simulated dynamics were mostly consistent with the description of the process, whereby amounts of reactants species decreased over the simulation time span, and those of products species increased. However, no plant data of those variables were available for comparison with model responses.

The temperature responses of the model, as simulated with input plant data of 44 batches, tracked the plant data of reactor temperature with an average percentage accuracy of 80%. Whereas the simulated pressure responses achieved an average accuracy of 60 % in tracking their corresponding plant data of reactor pressure. Those average figures of model performance have revealed that there are still considerable opportunities for performance improvement of this model, which set the basis for further work going forward.

5.4 Recommendations

Following the various limitations experienced in this study, it is believed that more work should be done to the model in order to achieve better results, from which the model could demonstrate more accurate predictions of the reactor temperature and pressure dynamics. To that end, the following recommendations can be made:

For all practical purposes, because the work of first-principle modelling can be time-consuming and somewhat difficult to achieve correctly, as it has been experienced in this work, a more systematic and realistic approach should be followed in order to correctly capture the dynamics of the dissolution of $Cl_{2(g)}$ into the reactor solution, or merely the dynamics of the reactor pressure. This could be achieved by developing an empirical model, describing the exact dynamic relationship between the flowrate of $Cl_{2(g)}$ pumped into the reactor (input variable) and the resulting pressure that builds up in the reactor (output variable). This empirical equation may then have to conveniently be massaged into a mathematical formulation that would make it easier to add to the system of first-principle equations to be solved altogether.

A thorough investigation should be conducted that would help establish a more stable and accurate method to correctly compute the consistent initial conditions of the states (derivative) variables of the model equations. In this work, this task has proved to be fundamental in the numerical integration of our system of equations, hence simulations of the model, since it has computed the initial amounts of material from which simulations started. Those initial values should ideally be solutions to the model differential equations, and consistent with the exact description of the system, from which all amounts of reactants and variables initially set to the real system are known.

Also, some more effort should be invested towards rigorously describing the exact chemistry of the process, with the full set of chemical reactions and the possible side reactions known to be taking place in the process.

Lastly, estimation of the key parameters of the model, by means of nonlinear optimisation techniques could also be done. This would help assess how much immediate improvement could be achieved in the model performance, as presented in this dissertation. More precisely, this could help investigate the effect that optimised parameters might have on the accuracy of the numerical integrations, and correctness of the computed solutions.

Appendix A

Model Equations

The model was written to describe the dynamic behaviour of some of the chemical species present in the system. The crude rhodium sponge (Rh) was the solid element; the species of H_2O, Cl_2, $RhCl_3(H_2O)$ and HCl, made up the aqueous solution in the reactor; and the species of H_2O and Cl_2 were in the gas phase. For simplicity sake, Hypochlorous acid ($HClO_{(aq)}$) was not taken into account when modelling the system because it was considered to be a by-product of the reactions.

The following equations describe the exothermic chemical reactions of dissolution of crude rhodium sponge ($Rh_{(s)}$) and formation of $HCl_{(aq)}$, taking place simultaneously in the reactor:

Reaction of Dissolution

$$Rh_{(s)} + 3HCl_{(aq)} + H_2O_{(l)} \rightarrow RhCl_3(H_2O)_{(aq)} + 3H^+_{(aq)} + 3e^- \tag{A.1}$$

Reaction of HCl Formation

$$Cl_{2(aq)} + H_2O_{(l)} \rightarrow HCl_{(aq)} + HClO_{(aq)} \tag{A.2}$$

To model the reactions, a total of 92 equations were used, of which 78 algebraic equations and 14 differential equations.

A.1 Algebraic Equations

A total of 78 algebraic equations were solved simultaneously, with the 14 differential equations. The equations were written for each of the reactor and jacket compartments of the system.

A.1.1 Reactor Side

Total Moles

$$N^{tot}_{\mathrm{rx}_{(s)}} = N_{\mathrm{Rh}_{(s)}} \tag{A.3}$$

$$N^{tot}_{\mathrm{rx}_{(aq)}} = N_{\mathrm{H_2O}_{(aq)}} + N_{\mathrm{Cl}_{2(aq)}} + N_{\mathrm{RhCl_3{\cdot}H_2O}_{(aq)}} + N_{\mathrm{HCl}_{(aq)}} \tag{A.4}$$

$$N^{tot}_{\mathrm{rx}_{(g)}} = N_{\mathrm{H_2O}_{(g)}} + N_{\mathrm{Cl}_{2(g)}} \tag{A.5}$$

Mole Fractions

$$x_{\mathrm{Rh}_{(s)}} = \frac{N_{\mathrm{Rh}_{(s)}}}{N^{tot}_{\mathrm{rx}_{(s)}}} \tag{A.6}$$

The mole fractions of $H_2O_{(aq)}$, $Cl_{2(aq)}$, $RhCl_3.H_2O_{(aq)}$, $HCl_{(aq)}$ as well as those of the gas species of $H_2O_{(g)}$ and $Cl_{2(g)}$ were calculated as Equation A.6.

Mass

$$m_{\mathrm{Rh}_{(s)}} = N_{\mathrm{Rh}_{(s)}} \cdot M_{\mathrm{Rh}_{(s)}} \tag{A.7}$$

The masses of all other aqueous and gas species in the system were calculated in a similar way as Equation A.7.

Heat Capacity

$$\begin{aligned} Cp^{rx}_{\mathrm{l}} = {} & x_{\mathrm{H_2O}_{(aq)}} \cdot Cp^{H_2O_{(aq)}}\Big|_{T_{\mathrm{rx}_{(l)}}} + x_{\mathrm{Cl}_{2(aq)}} \cdot Cp^{Cl_{2(aq)}}\Big|_{T_{\mathrm{rx}_{(l)}}} \dots \\ & + x_{\mathrm{RhCl_3{\cdot}H_2O}_{(aq)}} \cdot Cp^{RhCl_3.H_2O_{(aq)}}\Big|_{T_{\mathrm{rx}_{(l)}}} + x_{\mathrm{HCl}_{(aq)}} \cdot Cp^{HCl_{(aq)}}\Big|_{T_{\mathrm{rx}_{(l)}}} \end{aligned} \tag{A.8}$$

The total heat capacities of the solid and gas species in the reactor were calculated as Equation A.9 above.

Volumes

$$\begin{aligned} V^{tot}_{\mathrm{rx}_{(aq)}} = {} & \frac{N_{\mathrm{H_2O}_{(aq)}}}{\rho_{\mathrm{H_2O}_{(aq)}}\Big|_{T_{\mathrm{rx}_{(l)}}}} + \frac{N_{\mathrm{Cl}_{2(aq)}}}{\rho_{\mathrm{Cl}_{2(aq)}}\Big|_{T_{\mathrm{rx}_{(l)}}}} + \frac{N_{\mathrm{RhCl_3{\cdot}H_2O}_{(aq)}}}{\rho_{\mathrm{RhCl_3{\cdot}H_2O}_{(aq)}}\Big|_{T_{\mathrm{rx}_{(l)}}}} \dots \\ & + \frac{N_{\mathrm{HCl}_{(aq)}}}{\rho_{\mathrm{HCl}_{(aq)}}\Big|_{T_{\mathrm{rx}_{(l)}}}} \end{aligned} \tag{A.9}$$

The total volumes of the solid and gas in the system were calculated in a similar way to that of liquid above.

Molar Densities

$$\rho_{\mathrm{rx}_{(\mathrm{aq})}} = \frac{N^{tot}_{\mathrm{rx}_{(\mathrm{aq})}}}{V^{tot}_{\mathrm{rx}_{(\mathrm{aq})}}} \tag{A.10}$$

The molar densities of all solid, aqueous and gaseous species were calculated as shown in Equation A.10.

Molar Concentrations

$$C_{\mathrm{Rh}_{(\mathrm{s})}} = \frac{N_{\mathrm{Rh}_{(\mathrm{s})}}}{V^{tot}_{\mathrm{rx}_{(\mathrm{s})}}} \tag{A.11}$$

The molar concentrations of all aqueous and gaseous species were calculated as shown in Equation A.11.

Heights

$$h_{\mathrm{rx}_{(\mathrm{s})}} = \frac{V^{tot}_{\mathrm{rx}_{(\mathrm{s})}}}{A_{\mathrm{rx}}} \tag{A.12}$$

$$h_{\mathrm{rx}_{(\mathrm{aq})}} = \frac{V^{tot}_{\mathrm{rx}_{(\mathrm{s})}} + V^{tot}_{\mathrm{rx}_{(\mathrm{aq})}}}{A_{\mathrm{rx}}} \tag{A.13}$$

$$h_{\mathrm{rx}_{(\mathrm{g})}} = \frac{V^{tot}_{\mathrm{rx}_{(\mathrm{g})}}}{A_{\mathrm{rx}}} \tag{A.14}$$

Pressures

$$P^{tot}_{\mathrm{rx}_{(\mathrm{g})}} = \frac{N^{tot}_{\mathrm{rx}_{(\mathrm{g})}} \cdot R \cdot T_{\mathrm{rx}_{(\mathrm{g})}}}{V^{tot}_{\mathrm{rx}_{(\mathrm{g})}}} \tag{A.15}$$

$$P_{\mathrm{H_2O}_{(\mathrm{g})}} = x_{\mathrm{H_2O}_{(\mathrm{g})}} \cdot P^{tot}_{\mathrm{rx}_{(\mathrm{g})}} \tag{A.16}$$

$$P^{vap}_{\mathrm{H_2O}_{(\mathrm{aq})}} = x_{\mathrm{H_2O}_{(\mathrm{aq})}} \cdot P^{vap}_{\mathrm{H_2O}}\Big|_{T_{\mathrm{rx}_{(\mathrm{l})}}} \tag{A.17}$$

Equation A.16 was used to calculate the partial pressures of all gaseous species in the system, whereas Equation A.17 was used to calculate the vapor pressure exerted by $Cl_{2(aq)}$, $RhCl_3.H_2O_{(aq)}$ and $HCl_{(aq)}$.

Flow rates of Phase Changes

$$F_{\mathrm{H_2O}_{(\mathrm{l-g})}} = k_{H_2O} \cdot (P_{\mathrm{H_2O}_{(\mathrm{aq})}} - P_{\mathrm{H_2O}_{(\mathrm{g})}}) \tag{A.18}$$

$$F_{\mathrm{Cl}_{2(\mathrm{l-g})}} = C_{\mathrm{Cl}_{2(\mathrm{g})}} \cdot V_{gas} - C_{\mathrm{Cl}_{2(\mathrm{aq})}} \cdot V_{sol} \tag{A.19}$$

Arrhenius Reaction Rate Constants

$$k_{r1} = k_1 \cdot \exp\left(\frac{E_{\mathrm{a}_1}}{R \cdot T_{\mathrm{rx}_{(\mathrm{l})}}}\right) \tag{A.20}$$

$$k_{r2} = k_2 \cdot \exp\left(\frac{E_{\mathrm{a}_2}}{R \cdot T_{\mathrm{rx}_{(\mathrm{l})}}}\right) \tag{A.21}$$

Rates of Reactions

$$r_1 = k_{r1} \cdot C_{\mathrm{HCl}_{(\mathrm{aq})}} \tag{A.22}$$

$$r_2 = k_{r2} \cdot C_{\mathrm{Cl}_{2(\mathrm{aq})}} \tag{A.23}$$

A.1.2 Jacket Side

The jacket contained the species of liquid water, as well as water vapor and air. The algebraic relations of total moles, mass, mole fractions, heat capacities, volumes, molar densities, molar concentrations, heights of liquid and gas, total and partial pressures of the liquid and gas species, in the jacket, were calculated similarly to the equations shown for the reactor compartment of the system.

Flow rates of Phase Changes

$$F_{\mathrm{H_2O}_{(\mathrm{l-g})}} = k_{H_2O} \cdot (P_{\mathrm{H_2O}_{(\mathrm{aq})}} - P_{\mathrm{H_2O}_{(\mathrm{g})}}) \tag{A.24}$$

Enthalpy Transfers

$$H_{\mathrm{rx}_{(\mathrm{l-l})}} = (h_{\mathrm{rx}_{(\mathrm{s})}} + h_{\mathrm{rx}_{(\mathrm{aq})}}) \cdot (2\pi) \cdot (r_{rx} + w_{rx}) \cdot U_{(l-l)} \cdot (T_{\mathrm{hx}_{(\mathrm{l})}} - T_{\mathrm{rx}_{(\mathrm{l})}}) \tag{A.25}$$

$$H_{\mathrm{rx}_{(\mathrm{l-g})}} = h_{\mathrm{rx}_{(\mathrm{g})}} \cdot (2\pi) \cdot (r_{rx} + w_{rx}) \cdot U_{(l-g)} \cdot (T_{\mathrm{hx}_{(\mathrm{l})}} - T_{\mathrm{rx}_{(\mathrm{g})}}) \tag{A.26}$$

$$H_{\mathrm{rx}_{(\mathrm{g-g})}} = h_{\mathrm{rx}_{(\mathrm{g})}} \cdot (2\pi) \cdot (r_{rx} + w_{rx}) \cdot U_{(g-g)} \cdot (T_{\mathrm{hx}_{(\mathrm{g})}} - T_{\mathrm{rx}_{(\mathrm{g})}}) \tag{A.27}$$

$$H_{\mathrm{rx}_{(\mathrm{g-l})}} = (h_{\mathrm{rx}_{(\mathrm{s})}} + h_{\mathrm{rx}_{(\mathrm{aq})}}) \cdot (2\pi) \cdot (r_{rx} + w_{rx}) \cdot U_{(g-l)} \cdot (T_{\mathrm{hx}_{(\mathrm{g})}} - T_{\mathrm{rx}_{(\mathrm{l})}}) \tag{A.28}$$

A.2 Differential Equations

The differential equations are as follows:

A.2.1 Reactor Side

Moles

$$\frac{dN_{\mathrm{Rh}_{(s)}}}{dt} = -r_1 V_{\mathrm{rx}_{(l)}} \tag{A.29}$$

$$\frac{dN_{\mathrm{HCl}_{(aq)}}}{dt} = -3r_1 V_{\mathrm{rx}_{(l)}} + r_2 V_{\mathrm{rx}_{(l)}} \tag{A.30}$$

$$\frac{dN_{\mathrm{H_2O}_{(l)}}}{dt} = -r_1 V_{\mathrm{rx}_{(l)}} + r_2 V_{\mathrm{rx}_{(l)}} - F_{\mathrm{H_2O}_{(l-g)}} \tag{A.31}$$

$$\frac{dN_{\mathrm{Cl}_{2(aq)}}}{dt} = -\frac{1}{2} r_2 V_{\mathrm{rx}_{(l)}} + F_{\mathrm{Cl}_{2(l-g)}} \tag{A.32}$$

$$\frac{dN_{\mathrm{RhCl_3 \cdot H_2O}_{(aq)}}}{dt} = r_1 V_{\mathrm{rx}_{(l)}} \tag{A.33}$$

$$\frac{dN_{\mathrm{H_2O}_{(g)}}}{dt} = F_{\mathrm{H_2O}_{(l-g)}} \tag{A.34}$$

$$\frac{dN_{\mathrm{Cl}_{2(g)}}}{dt} = F^{In}_{\mathrm{Cl}_{2(g)}} - F_{\mathrm{Cl}_{2(l-g)}} \tag{A.35}$$

Temperatures

$$\begin{aligned}\frac{dT_{\mathrm{rx}_{(l)}}}{dt} = \frac{1}{Cp_l^{rx} \cdot N^{tot}_{\mathrm{rx}_{(aq)}}} \cdot \Bigg(& (-r_1 V_{\mathrm{rx}_{(l)}}) \cdot (Cp^{Rh_{(s)}}\Big|_{T_{\mathrm{rx}_{(l)}}} \cdot (T_{\mathrm{rx}_{(l)}} - T_{ref})) \ldots \\ & + (-3r_1 V_{\mathrm{rx}_{(l)}} + r_2 V_{\mathrm{rx}_{(l)}}) \cdot (Cp^{HCl_{(aq)}}\Big|_{T_{\mathrm{rx}_{(l)}}} \cdot (T_{\mathrm{rx}_{(l)}} - T_{ref})) \ldots \\ & + (-r_1 V_{\mathrm{rx}_{(l)}} - r_2 V_{\mathrm{rx}_{(l)}} - F_{\mathrm{H_2O}_{(l-g)}}) \cdot (Cp^{H_2O_{(aq)}}\Big|_{T_{\mathrm{rx}_{(l)}}} \cdot (T_{\mathrm{rx}_{(l)}} - T_{ref})) \ldots \\ & + (-\frac{1}{2} r_2 V_{\mathrm{rx}_{(l)}} + F_{\mathrm{Cl}_{2(l-g)}}) \cdot (Cp^{Cl_{2(aq)}}\Big|_{T_{\mathrm{rx}_{(l)}}} \cdot (T_{\mathrm{rx}_{(l)}} - T_{ref})) \ldots \\ & + (r_1 V_{\mathrm{rx}_{(l)}}) \cdot (Cp^{RhCl_3 . H_2O_{(aq)}}\Big|_{T_{\mathrm{rx}_{(l)}}} \cdot (T_{\mathrm{rx}_{(l)}} - T_{ref})) \ldots \\ & + F_{\mathrm{H_2O}_{(l-g)}} \cdot H_v^{H_2O} + H_{\mathrm{rx}_{(l-l)}} + H_{\mathrm{rx}_{(g-l)}} \Bigg)\end{aligned} \tag{A.36}$$

$\mathrm{H}_v^{H_2O}$ = Heat of vaporization of water (J/kmol)
$\mathrm{H}_{rx_{(l-l)}}$ = Enthalpy transfer from reactor solution to jacket solution (J/kmol)
$\mathrm{H}_{rx_{(g-l)}}$ = Enthalpy transfer from reactor gas to jacket solution (J/kmol)

$$\frac{dT_{\mathrm{rx}_{(\mathrm{g})}}}{dt} = \frac{1}{Cp_{\mathrm{g}}^{rx} \cdot N_{\mathrm{rx}_{(\mathrm{g})}}^{tot}} \cdot \left(F_{Cl_{2(g)}}^{In} \cdot Cp^{Cl_{2(g)}}\Big|_{T_{\mathrm{rxg}}^{In}} \cdot (T_{\mathrm{rx}_{(\mathrm{g})}}^{In} - T_{ref}) \ldots \right. \tag{A.37}$$
$$- F_{\mathrm{Cl}_{2(\mathrm{l-g})}} \cdot Cp^{Cl_{2(g)}}\Big|_{T_{\mathrm{rx}_{(\mathrm{g})}}} \cdot (T_{\mathrm{rx}_{(\mathrm{g})}} - T_{ref}) \ldots$$
$$\left. + H_{\mathrm{rx}_{(\mathrm{g-g})}} + H_{\mathrm{rx}_{(\mathrm{l-g})}} \right)$$

A.2.2 Jacket Side

Moles

$$\frac{dN_{\mathrm{H_2O}_{(\mathrm{aq})}}}{dt} = F_{\mathrm{CW}}^{In} - F_{\mathrm{CW}}^{Out} - F_{\mathrm{H_2O}_{(\mathrm{l-g})}} \tag{A.38}$$
$$\frac{dN_{\mathrm{H_2O}_{(\mathrm{g})}}}{dt} = F_{\mathrm{Steam}}^{In} - F_{\mathrm{Steam}}^{Out} + F_{\mathrm{H_2O}_{(\mathrm{l-g})}} \tag{A.39}$$
$$\frac{dN_{\mathrm{air}}}{dt} = F_{\mathrm{air}}^{In} - F_{\mathrm{air}}^{Out} \tag{A.40}$$

Temperatures

$$\frac{dT_{\mathrm{hx}_{(\mathrm{l})}}}{dt} = \tag{A.41}$$
$$\frac{1}{Cp_{\mathrm{l}}^{hx} \cdot N_{\mathrm{hx}_{(\mathrm{aq})}}^{tot}} \cdot \left(F_{\mathrm{utility}}^{In} \cdot Cp^{H_2O_{(aq)}}\Big|_{T_{\mathrm{utility}}^{In}} \cdot (T_{\mathrm{utility}}^{In} - T_{ref}) \ldots \right.$$
$$- F_{\mathrm{utility}}^{Out} \cdot Cp_{\mathrm{l}}^{hx} \cdot (T_{\mathrm{hx}_{(\mathrm{l})}} - T_{ref}) \ldots$$
$$\left. + F_{\mathrm{H_2O}_{(\mathrm{l-g})}} \cdot H_v^{H_2O}\Big|_{T_{\mathrm{hx}_{(\mathrm{l})}}} - H_{\mathrm{rx}_{(\mathrm{l-l})}} \right)$$

$$\frac{dT_{\mathrm{hx}_{(\mathrm{g})}}}{dt} = \tag{A.42}$$
$$\frac{1}{Cp_{\mathrm{g}}^{hx} \cdot N_{\mathrm{hx}_{(\mathrm{g})}}^{tot}} \cdot \left(F_{\mathrm{utility}}^{In} \cdot Cp^{H_2O_{(g)}}\Big|_{T_{\mathrm{utility}}^{In}} \cdot (T_{\mathrm{utility}}^{In} - T_{ref}) \ldots \right.$$
$$- F_{\mathrm{utility}}^{Out} \cdot Cp_{\mathrm{g}}^{hx} \cdot (T_{\mathrm{hx}_{(\mathrm{g})}} - T_{ref}) \ldots$$
$$\left. + F_{\mathrm{H_2O}_{(\mathrm{l-g})}} \cdot H_v^{H_2O}\Big|_{T_{\mathrm{hx}_{(\mathrm{g})}}} - H_{\mathrm{rx}_{(\mathrm{g-g})}} \right)$$

Appendix B

Model Parameters and Properties

B.1 Reactor Vessel Dimensions

Table B.1: Reactor Vessel Dimensions

Reactor Dimensions		
Names	**Values**	**Units**
Reactor Side		
Reactor Inner Radius	0.6	m
Vessel Height	1.9	m
Steel Wall Thickness	0.013	m
Glass Wall Thickness	0.003	m
Total Wall Thickness	0.016	m
Reactor Inside Wall Area	7.8	m^2
Steel Wall Cross Area	0.0566	m^2
Glass Wall Cross Area	0.4481	m^2
Total Wall Cross Area	0.5047	m^2
Reactor Cross Area	1.0347	m^2
Reactor Volume	1.9	m^3

continued on the next page

Table B.1 continued from previous page		
Names	**Values**	**Units**
Total Wall Volume	0.1248	m^3
Jacket Side		
Jacket Wall Thickness	0.016	m
Jacket Cross Area	1.131	m^2
Jacket Volume	0.294	m^3

B.2 Heat and Mass Transfer Coefficients

Table B.2: Transfer Coefficients, The Engineering Toolbox 2015

Transfer Coefficients		
Names	**Values**	**Units**
Heat Transfer		
$U_{liquid\text{-}liquid}$	4000	W/m^2K
$U_{liquid\text{-}gas}$	90	W/m^2K
$U_{gas\text{-}gas}$	90	W/m^2K
$U_{gas\text{-}liquid}$	3800	W/m^2K
Mass Transfer		
k_{H2O}	1	
k_{Cl2}	1	

B.3 Reaction Kinetics Parameters

Table B.3: Arrhenius Law Constants

Arrhenius Constants *(NOTE: Assumed Values)*		
Names	**Values**	**Units**
Activation Energy		
E_{a1}	250	kJ/kmol
E_{a2}	250	kJ/kmol
Frequency Factor		
k_1	1.8791	min^{-1}
k_2	1.8791	min^{-1}

B.4 Physical Properties

The physical properties we used were taken from Perry et al. 2007. The properties presented in this section have been converted to the International System (SI) units wherever applicable, to maintain dimensional consistency in the model.

Molar Masses $(kg/kmol)$

$$M_{Rh} = 109.9 \tag{B.1}$$

$$M_{H_2O} = 18 \tag{B.2}$$

$$M_{Cl_2} = 70.9 \tag{B.3}$$

$$M_{HCl} = 36.46 \tag{B.4}$$

$$M_{RhCl_3.H_2O} = 234.27 \tag{B.5}$$

(B.6)

Molar Densities $(kmol/m^3)$

$$\rho_{\mathrm{Rh}_{(s)}} = \frac{12.41 \times 1000}{M_{Rh}} \tag{B.7}$$

$$\rho_{\mathrm{H_2O}(l)} = \frac{5.459}{0.30542^{\left(1+(1-\frac{T}{647.13})^{0.081}\right)}} \times \left(T < 333.15\right) + \ \ldots \tag{B.8}$$

$$\frac{4.9669}{\left(2.7788 \times 10^{-1}\right)^{\left(1+(1-\frac{T}{6.4713\times 10^2})^{1.8740\times 10^{-1}}\right)}} \times \left(T \geq 333.15 \ \& \ T \leq 403.15\right) + \ \ldots$$

$$\frac{4.3910}{\left(2.4871 \times 10^{-1}\right)^{\left(1+(1-\frac{T}{6.4713\times 10^2})^{2.5340\times 10^{-1}}\right)}} \times \left(T > 403.15 \ \& \ T < 647.13\right)$$

$$\rho_{\mathrm{HCl}_{(aq)}} = \frac{3.342}{0.2729^{1+(1-\frac{T}{324.65})^{0.3217}}} \tag{B.9}$$

$$\rho_{\mathrm{Cl}_{2(aq)}} = \frac{2.23}{0.27645^{1+(1-\frac{T}{417.15})^{0.2926}}} \tag{B.10}$$

$$\rho_{\mathrm{RhCl_3H_2O}(aq)} = \rho_{\mathrm{Rh}_{(s)}} + \frac{3}{2}\rho_{\mathrm{Cl}_{2(aq)}} + \rho_{\mathrm{H_2O}(l)} \tag{B.11}$$

Critical Temperature point of H_2O (K)

$$T^c_{H_2O} = 647.13 \tag{B.12}$$

Heat of Vaporisation $(J/kmol)$

$$H_v^{H_2O} = 5.2053 \times 10^7 \times \left(1 - \left(\frac{T}{T^c_{H_2O}}\right)\right)^{\left(0.3199-0.212\times(\frac{T}{T^c_{H_2O}})+0.25795\times(\frac{T}{T^c_{H_2O}})^2\right)} \tag{B.13}$$

Heat Capacity at Constant Pressure $(J/kmol.K)$

$$Cp^{Rh_{(s)}} = 240 \times M_{Rh} \tag{B.14}$$

$$Cp^{H_2O_{(l)}} = 2.7637 \times 10^5 - 2.0901 \times 10^3 \times T + 8.125 \times 10^0 \times T^2 \ldots - 1.4116 \times 10^{-2} \times T^3 + 9.3701 \times -6 \times T^4 \tag{B.15}$$

$$Cp^{HCl_{(l)}} = (4.73 \times 10^4 + 9 \times 10 \times T + 0 \times T^2 + 0 \times T^3 + 0 \times T^4) \tag{B.16}$$

$$Cp^{Cl_{2(l)}} = 480 \times M_{Rh} \tag{B.17}$$

$$Cp^{RuCl_{3(l)}} = Cp^{Rh_{(s)}} + \frac{3}{2} Cp^{Cl_{2(aq)}} + Cp^{H_2O_{(l)}} \tag{B.18}$$

Vapor Pressure (kPa)

$$P^{vap}_{H_2O} = \frac{e^{(73.649 - \frac{7258.2}{T} - 7.3037 \times \log(T) + 4.1653 \times 10^{-6} \times T^2)}}{1000} \tag{B.19}$$

$$P^{vap}_{Cl_2} = \frac{e^{(71.334 - \frac{3855}{T} - 8.5157 \times \log(T) + 1.2378 \times 10^{-2} \times T^2)}}{1000} \tag{B.20}$$

Henry Constants

$$h_{\mathrm{Cl}_2} = 9.1 \times 10^{-2} \times e^{\left(2500 \times \left(\frac{1}{\frac{T-1}{298.15}}\right)\right)} \tag{B.21}$$

$$h_{\mathrm{HCl}} = 11.9 \times 10 \times e^{\left(9000 \times \left(\frac{1}{\frac{T-1}{298.15}}\right)\right)} \tag{B.22}$$

Bibliography

Ahmed, D. F. (2012). "Self-tuning Control of Alkylation in Batch Reactor". In: *The First National Conference for Engineering Sciences FNCES*, pp. 1–5. DOI: 10.1109/NCES.2012.6740469. URL: http://ieeexplore.ieee.org/stamp/stamp.jsp?tp=&arnumber=6740469.

Alkan, Mahir, Münir Oktay, M Muhtar Kocakerim, and Mehmet Çopur (2005). "Solubility of chlorine in aqueous hydrochloric acid solutions". In: *Journal of Hazardous Materials* April, pp. 13–18. DOI: 10.1016/j.jhazmat.2004.11.001. URL: https://www.researchgate.net/publication/7981068{_}Solubility{_}of{_}chlorine{_}in{_}aqueous{_}hydrochloric{_}acid{_}solutions.

Aller, F., Kukanja D., Jovan V., and Georgiadis M. (2009). "Modelling the semi-batch vinyl acetate emulsion polymerization in a real-life industrial reactor". In: *Mathematical and Computer Modelling of Dynamical Systems* 15.2, pp. 139–161. ISSN: 1387-3954. DOI: 10.1080/13873950802666357. URL: http://www.tandfonline.com/doi/pdf/10.1080/13873950802666357.

Aller, F., Blázquez L. F., and Miguel L. J. (2014). "Online monitoring of an industrial semi-batch vinyl acetate polymerization reaction by programmable logic controllers". In: *19th IFAC World Congress*, pp. 1290–1295. URL: http://www.nt.ntnu.no/users/skoge/prost/proceedings/ifac2014/media/files/0687.pdf.

Arora, P., Jain R., Mathur K., Sharma A., and Gupta A. (2010). "Synthesis of polymethyl methacrylate (PMMA) by batch emulsion polymerization". In: *African Journal of Pure and Applied Chemistry* 4.August, pp. 152–157. URL: http://www.academicjournals.org/article/article1379499660_Aroraetal.pdf.

Arora, S., Gesthuisen R., and Engell S. (2007). "Model based operation of emulsion polymerization reactors with evaporative cooling: Application to vinyl ac-

etate homopolymerization". In: *Computer Aided Chemical Engineering* 31.5-6, pp. 552–564. ISSN: 15707946. DOI: 10.1016/j.compchemeng.2006.07.011. URL: http://www.sciencedirect.com/science/article/pii/S0098135406002079.

Basnet, C. B., Farrington P. A., Prat D. B., Kamath M., Caracal S. C., and Beaumariage T. G. (1990). "Experiences in Developing an Object-Oriented Modeling Environment for Manufacturing Systems.pdf". In: *Proceedings of the 1990 Winter Simulation Conference*. Ed. by Richard E. Nance Osman Balci, Randall P. Sadowski. URL: http://www.informs-sim.org/wsc90papers/1990_0086.pdf.

Bell, T. (2015). *Platinum Group Metals (PGMs)*. URL: http://metals.about.com/od/properties/a/Platinum-Group-Metals-Pgms.htm (visited on 07/27/2015).

Biegler, L. T. (2000). *Differential-Algebraic Equations (DAEs)*. URL: http://www.lehigh.edu/$\sim$wes1/apci/11may00.pdf (visited on 10/23/2014).

Bilbao, S. and Julius O. Smith III (2014). *Lumped vs. Distributed Systems*. URL: https://ccrma.stanford.edu/$\sim$jos/NumericalInt/Lumped_vs_Distributed_Systems.html (visited on 10/20/2014).

Brydon, D., Pearson J., and Marder M. (1998). "Solving Stiff Differential Equations with the Method of Patches". In: *Journal of Computational Physics* 144.2, pp. 280–298. ISSN: 00219991. DOI: 10.1006/jcph.1998.6008. URL: http://linkinghub.elsevier.com/retrieve/pii/S0021999198960089.

Burkard, E. (2014). *Introduction to Ordinary Differential Equations*. URL: http://www3.nd.edu/$\sim$eburkard/Teaching/ElementaryDifferentialEquationsBook.pdf (visited on 10/25/2014).

Burke, G. (1990). "The Platinum Group Metals". In: *Minerals & Energy - Raw Materials Report* 7.4, pp. 19–23. ISSN: 1404-1049. DOI: 10.1080/14041049009409959.

Caccavale, F., Iamarino M., and Pierri vincenzo F. (2011). "The Chemical Batch Reactor". In: *Control and Monitoring of Chemical Batch Reactors*. Springer. Chap. 2, pp. 185–187. ISBN: 9780857291943. DOI: 10.1007/978-0-85729-195-0. URL: file:///C:/Users/User/Downloads/9780857291943-c2(9).pdf.

College, OpenStax (2015). *Chemistry OpenStax College*. Houston, pp. 459–509. ISBN: 9781938168390. URL: http://cnx.org/content/col11760/latest/.

Crundwell, F., Moats M., Ramachandran V., Robinson T., and Davenport W. G. (2011a). "Extractive Metallurgy of Nickel, Cobalt and Platinum Group Metals". In: *Extractive Metallurgy of Nickel, Cobalt and Platinum Group Metals*. Else-

vier, pp. 457–488. ISBN: 9780080968094. DOI: 10.1016/B978-0-08-096809-4.10036-X. URL: http://www.sciencedirect.com/science/article/pii/B978008096809410036X.

Crundwell, F. K., Moats M. S., Ramachandran V., Robinson T. G., and Davenport W. G. (2011b). "Overview". In: *Extractive Metallurgy of Nickel, Cobalt and Platinum Group Metals*. Elsevier, pp. 1–18. ISBN: 9780080968094. DOI: 10.1016/B978-0-08-096809-4.10001-2. URL: http://linkinghub.elsevier.com/retrieve/pii/B9780080968094100012.

— (2011c). "Overview of the Extraction of Platinum-Group Metals". In: *Extractive Metallurgy of Nickel, Cobalt and Platinum Group Metals*, pp. 411–413. ISBN: 9780080968094. DOI: 10.1016/B978-0-08-096809-4.10032-2.

— (2011d). "Refining of Platinum-Group Metals". In: *Extractive Metallurgy of Nickel, Cobalt and Platinum Group Metals*. Elsevier Ltd., pp. 489–534. ISBN: 9780080968094. DOI: 10.1016/B978-0-08-096809-4.10032-2. URL: <GotoISI>://A1989U129600011.

Czop, P., Kost G., Stawik D., and Wszotek G. (2011). "Formulation and identification of First- Principle Data-Driven models". In: *Journal of achievements in Materials and Manufacturing Engineering* 44.2, pp. 179–186. URL: http://www.journalamme.org/papers_vol44_2/4427.pdf.

Donati, G. (1999a). "Batch and semibatch catalytic reactors (from theory to practice)". In: *Catalysis Today* 52.2-3, pp. 183–195. ISSN: 09205861. DOI: 10.1016/S0920-5861(99)00075-9. URL: http://www.aidic.it/italiano/divisioni/process/processpublications/CT_1999-52-1831.pdf.

— (1999b). "Batch and semibatch catalytic reactors (from theory to practice)". In: *Catalysis Today* 52.2-3, pp. 183–195. ISSN: 09205861. DOI: 10.1016/S0920-5861(99)00075-9. URL: http://www.aidic.it/italiano/divisioni/process/processpublications/CT_1999-52-1831.pdf.

Edwards, J. E. (2000). "Process Modeling and Control of Batch Reactors in the Fine Chemicals Industry". In: *UK ChemCAD Seminar*. Vol. 44. October. URL: http://www.chemstations.com/content/documents/Technical_Articles/batchrx.pdf.

Gouldsmith, F. S. and Wilson B. (1963). "Extraction and Refining of the Platinum Metals". In: *Platinum Metals Reviews*, pp. 136–143. URL: file:///C:/Users/User/Downloads/pmr-v7-i4-136-143(2).pdf.

Grigorian, A. (2008). *Ordinary Differential Equation*. URL: https://www.math.uni-bielefeld.de/$\sim$grigor/odelec2008.pdf (visited on 10/22/2015).

Hairer, E. and Wanner G. (1999). "Stiff differential equations solved by Radau methods". In: *Journal of Computational and Applied Mathematics* 111.1-2, pp. 93–111. ISSN: 03770427. DOI: 10.1016/S0377-0427(99)00134-X. URL: http://www.sciencedirect.com/science/article/pii/S037704279900134X.

Heinzle, E. (2009). *Introduction to Ideal Reactors: Basic description and design*. URL: http://sistemas.eel.usp.br/docentes/arquivos/5817712/326/IntroductionReactor.pdf (visited on 10/10/2014).

Hsia, J. (2015). *Chemistry of Chlorine*. URL: http://chem.libretexts.org/Core/Inorganic_Chemistry/Descriptive_Chemistry/Elements_Organized_by_Block/2_p-Block_Elements/Group_17\%3A_The_Halogens/Chemistry_of_Chlorine (visited on 11/05/2016).

Hvala, N. and Kukanja D. (Apr. 2013). "Modelling and simulation of semi-batch polymerisation reactor for improved reactants dosing control". In: *Simulation Modelling Practice and Theory* 33, pp. 102–114. ISSN: 1569190X. DOI: 10.1016/j.simpat.2012.10.003. URL: http://linkinghub.elsevier.com/retrieve/pii/S1569190X12001360.

International Platinum Group Metals Association (2015). *Platinum Group Metals*. URL: http://ipa-news.com/ (visited on 07/27/2015).

Ionascu, E. J. (2006). *Ordinary Differential Equations-Lecture Notes*. URL: http://www.cs.bgu.ac.il/$\sim$leonid/ode_bio_files/Ionascu_LectNotes.pdf (visited on 10/20/2014).

Johnson Matthey (2015). *About PGM - PMM*. URL: http://www.platinum.matthey.com/about-pgm (visited on 07/27/2015).

Kirk-Othmer (2008). "Platinum-Group Metals". In: *Encyclopedia of Chemical Technology* 10.Viii.

Lambers, J. (2009). *Stiff Differential Equations*.

Le Lann, M. V., Cabassud M., and Casamatta G. (1999). "Modeling, Optimization and Control of Batch Chemical Reactors in Fine Chemical Production". In: *Annual Reviews in Control* 23, pp. 25–34. ISSN: 1367-5788. DOI: 10.1016/S1367-5788(99)90053-6.

Luyben, W. L. (1990a). "Fundamentals". In: *Process Modeling, Simulation and Control for Chemical Engineers*. second. McGraw-Hill International. Chap. 2, p. 35.

— (1990b). *Process Modeling, Simulation and Control for Chemical Engineers*. second. McGraw-Hill International, pp. 15–72. ISBN: 0071007938. URL: http:

//www.unirb.edu.br/pdf/livros/process_modeling_simulation_and_control_for_chemical_engineers.pdf.

Mathworks (2015a). *Choose a Solver - MATLAB & Simulink*. URL: http://www.mathworks.com/help/simulink/ug/choosing-a-solver.html#f11-41861 (visited on 01/16/2015).

— (2015b). *ode15s*. URL: http://www.mathworks.com/help/matlab/ref/ode15s.html (visited on 01/15/2015).

Miteva, T., Alvarez R., Hvala N., and Kukanja D. (2008a). "Modeling of Polyvinyl Acetate Polymerization Process for Control Purposes". In: *18th European Symposium on Computer Aided Process Engineering – ESCAPE 18*. Elsevier. URL: http://www.cpi.umist.ac.uk/prism/IJS_MITOL_escape18.pdf.

Miteva, T. and Hvala N. (2008b). "Optimization and Control of a Semi-Batch Polymerization reactor". In: *9th International PhD Workshop on Systems and Control: Young Generation Viewpoint*. URL: file:///C:/Users/User/Downloads/Miteva_2008_PHD_Workshop(3).pdf.

Moore, W. C. (1911). "Aqua Regia: Preliminary Paper". In: *Journal of the American Chemical Society* 33.7, pp. 1091–1099. ISSN: 0002-7863. DOI: 10.1021/ja02220a009. URL: http://dx.doi.org/10.1021/ja02220a009.

Mudd, G. M. (2010). "Platinum group metals : a unique case study in the sustainability of mineral resources". In: *The 4th International Platinum Conference, Platinum in transition 'Boom or Bust'*. Sun City, South Africa, pp. 113–120. URL: http://saimm.org.za/Conferences/Pt2010/113-120_Mudd.pdf.

Nabi, M. M. and Ding-li Yu (2014). "RBF Modelling and Optimization Control for Semi-Batch Reactors". In: *International Journal of Chemical, Molecular, Nuclear, Materials and Metallurgical Engineering* 8.7, pp. 672–676. URL: http://waset.org/publications/9999040/rbf-modelling-and-optimization-control-for-semi-batch-reactors.

NC State University (2015). *Numerical Methods for ODE*. URL: http://www4.ncsu.edu/$\sim$rsmith/MA573_F14/Lecture4.pdf (visited on 01/18/2015).

Nystrom, A. (2007). "Modeling and simulation of a multi phase semi-batch reactor". In: *Optimization*, pp. 173–182. URL: http://www.ep.liu.se/ecp/027/021/ecp072721.pdf.

Oliveira, R. (2003). "Combining first principles modelling and artificial neural networks: a general framework". In: *Computer Aided Chemical Engineering* 14, pp. 821–826. ISSN: 15707946. DOI: 10.1016/S1570-7946(03)80218-3. URL:

http://ac.els-cdn.com/S0098135404000432/1-s2.0-S0098135404000432-main.pdf?_tid=73a373d0-45a0-11e5-9502-00000aab0f27&acdnat=1439899294_43a642147b0ab0a17923ff75d6aea15a.

Perry, R. H. and Green D. H. (2007). *Perry's Chemical Engineers' Handbook*. Ed. by Robert H. Perry and Don H. Green. 8th ed., p. 2640. ISBN: 0-07-142294-3.

Pierri, F. (2006). "Modeling, Control and Fault Diagnosis for Chemical Batch Reactors". PhD thesis. University of Basilicata. URL: http://www.unibas.it/automatica/docs/PhDThesis_FrancescoPierri.pdf.

Prokopova, Z. and Prokop R. (2009). "Modelling and Simulation of Chemical Industrial Reactors". In: *23rd European Conference on Modelling and Simulation*. Springer, pp. 1–6. ISBN: 978-0-9553018-8-9. URL: http://www.scs-europe.net/conf/ecms2009/ecms2009CD/ecms2009acceptedpapers/ind_0044_24232ee3.pdf.

Ritchey, T. (2012). *Outline for a Morphology of Modelling Methods*. URL: http://www.swemorph.com/pdf/amg-1-1-2012.pdf.

Sander, R (2015). "Compilation of Henry ' s law constants (version 4 . 0) for water as solvent". In: *Atmospheric Chemistry and Physics* 15, pp. 4399–4981. DOI: 10.5194/acp-15-4399-2015. URL: http://www.atmos-chem-phys.net/15/4399/2015/.

Shampine, L. F. and Thompson S. (2007). *Stiff systems*. DOI: 10.4249/scholarpedia.2855. URL: http://www.scholarpedia.org/article/Stiff_systems (visited on 01/10/2015).

Sherrill, M. S. and Izard E. F. (1931). "The solubility of chlorine in aqueous solutions of chlorides and the free energy of trichloride ion". In: *Journal of the American Chemical Society* 53.5, pp. 1667–1674. ISSN: 00027863. DOI: 10.1021/ja01356a006. URL: https://www.scopus.com/inward/record.uri?eid=2-s2.0-0042456027{\&}partnerID=40{\&}md5=bc18f154f5a7131dfaf4db3c916859a2.

Simon, L. L., Fischer U., and Hungerbuehler K. (2007). "Modeling of a three-phase industrial batch reactor using a hybrid first-principles neural-network model". In: *Computer Aided Chemical Engineering* 24, pp. 45–50. ISSN: 15707946. DOI: 10.1016/S1570-7946(07)80031-9. URL: http://www.sciencedirect.com/science/article/pii/S1570794607800319.

Singh, A., de Villiers P.G.R., Rambalee P., Gous G., de Klerk J., and Humphries G. (2010). "A Holistic Approach to the Application of Model Predictive Control to Batch Reactors". In: *Automation in Mining, Mineral and Metal Processing*.

Elsevier, pp. 127–132. DOI: 10.3182/20100802-3-ZA-2014.00030. URL: file:///C:/Users/User/Downloads/UsingAPCataPreciousMetalsRefinery.pdf.

Soetaert, K., Meysman F., and Petzoldt T. (2010). "Solving differential equations in R". In: *AIP Conference Proceedings*. Vol. 1281. December, pp. 31–34. ISBN: 1548-7660. DOI: 10.1063/1.3498463. URL: http://journal.r-project.org/archive/2010-2/RJournal_2010-2_Soetaert$\sim$et$\sim$al.pdf.

Soetaert, K., Cash J., and Mazzia F. (2012). *Solving Differential Equations in R*. Springer-Verlag Berlin Heidelberg, pp. 1–115. ISBN: 978-3-642-28070-2. DOI: 10.1007/978-3-642-28070-2.

Ssennis (2014). *PFD of PGM Separation*. URL: https://en.wikipedia.org/wiki/Platinum_group#/media/File:PtMetalExtraction_II.jpg (visited on 08/24/2015).

Subathra, B. and Radhakrishnan T. K. (2011). "Modeling and Predictive Control Using Hybrid Intelligent Techniques for a Nonlinear Multivariable Process". In: *Instrumentation Science & Technology* 39.2, pp. 211–230. ISSN: 1073-9149. DOI: 10.1080/10739149.2010.545853.

The Engineering Toolbox (2015). *Overall Heat Transfer Coefficient*. URL: http://www.engineeringtoolbox.com/overall-heat-transfer-coefficient-d_434.html (visited on 09/01/2015).

The Mathworks, Inc (2017). *fsolve*. URL: https://www.mathworks.com/help/optim/ug/fsolve.html (visited on 05/05/2017).

Tyner, D., Soroush M., Grady M. C., Richards J., and Congalidis J. P. (2007). "Mathematical modelling and optimization of a semibatch polymerization reactor". In: 3, pp. 983–988. URL: http://www.physics.udel.edu/$\sim$richards/ADCHEM_2000_Paper.pdf.

University of Colorado (2014a). *Overview of Solution Methods*. URL: http://www.colorado.edu/engineering/cas/courses.d/NFEM.d/NFEM.Ch20.d/NFEM.Ch20.pdf (visited on 10/25/2014).

— (2014b). *Purely Incremental Methods:Load Control*. URL: http://www.colorado.edu/engineering/Aerospace/CAS/courses.d/NFEM.d/NFEM.Ch21.d/NFEM.Ch21.pdf (visited on 10/25/2014).

U.S. Geological Survey (2015). "Mineral commodity summaries 2015". In: *U.S. Geological Survey*, p. 196. URL: http://dx.doi.org/10.3133/70140094.

van Dam, Carel and Carl Sandrock (2012). "Modelling Dynamic Systems with Known Data: An Object-oriented Modelling System". In: *Proceedings of the*

World Congress on Engineering and Computer Science. Vol. II, pp. 24–27. ISBN: 9789881925244. URL: http://www.iaeng.org/publication/WCECS2012/WCECS2012{_}pp1166-1169.pdf.

Van Lith, P. (2002). "Hybrid Fuzzy-First Principles Modeling". PhD thesis. University of Twente. ISBN: 9036517060. URL: http://doc.utwente.nl/38031/1/t0000039.pdf.

Van Lith, P. F., Betlem B. H. L., and Roffel B. (2002). "A structured modeling approach for dynamic hybrid fuzzy-first principles models". In: *Journal of Process Control* 12.5, pp. 605–615. ISSN: 09591524. DOI: 10.1016/S0959-1524(01)00054-3. URL: http://www.sciencedirect.com/science/article/pii/S0959152401000543.

Vangheluwe, H. L. M. (2001). "Multi-Formalism Modelling and Simulation". PhD thesis. University of Gent, p. 319. URL: http://www.cs.mcgill.ca/~hv/publications/00.RUG.DSc.multiform.A4.pdf.

Weierstrass Institute (1995). *Numerical Methods for Stiff Ordinary Differential Equations*. URL: https://www.wias-berlin.de/people/john/LEHRE/NUMERIK_II/ode_2.pdf (visited on 01/10/2015).

Zapata, R. B., Aída Luz Villa, De Correa C. M., Ricardez-Sandoval L., and A. Elkamel (2010). "Dynamic modeling and optimization of a batch reactor for limonene epoxidation". In: *Industrial and Engineering Chemistry Research* 49.18, pp. 8369–8378. ISSN: 08885885. DOI: 10.1021/ie100737y.

Zavala, V. M., Flores-Tlacuahuac A., and Vivaldo-Lima E. (2005). "Dynamic optimization of a semi-batch reactor for polyurethane production". In: *Chemical Engineering Science* 60.11, pp. 3061–3079. ISSN: 00092509. DOI: 10.1016/j.ces.2005.01.020. URL: http://www.mcs.anl.gov/$\sim$vzavala/dynoptpus.pdf.